YA ZHANG

# Potential Use of Polymersomes and Lipid Nanocapsules as Therapeutic Carriers in the Rat Inner Ear

■

ACADEMIC DISSERTATION
To be presented, with the permission of
the board of the School of Medicine of the University of Tampere,
for public discussion in the Main Auditorium of Building M,
Pirkanmaa Hospital District, Teiskontie 35,
Tampere, on November 24th, 2011, at 12 o'clock.

UNIVERSITY OF TAMPERE

UNIVERSITY
OF TAMPERE

ACADEMIC DISSERTATION
University of Tampere, School of Medicine
Finland

*Supervised by*
Docent Jing Zou
University of Tampere
Finland
Professor Ilmari Pyykkö
University of Tampere
Finland

*Reviewed by*
Professor Jyrki Heino
University of Turku
Finland
Docent Varpu Marjomäki
University of Jyväskylä
Finland

Distribution
Bookshop TAJU
P.O. Box 617
33014 University of Tampere
Finland

Tel. +358 40 190 9800
Fax +358 3 3551 7685
taju@uta.fi
www.uta.fi/taju
http://granum.uta.fi

Cover design by
Mikko Reinikka

Acta Universitatis Tamperensis 1685
ISBN 978-951-44-8646-3 (print)
ISSN-L 1455-1616
ISSN 1455-1616

Acta Electronica Universitatis Tamperensis 1150
ISBN 978-951-44-8647-0 (pdf)
ISSN 1456-954X
http://acta.uta.fi

Tampereen Yliopistopaino Oy – Juvenes Print
Tampere 2011

# CONTENTS

# ABSTRACT

The traditional treatment strategies for sensorineural hearing loss (SNHL) have not been very satisfied. A cure for SNHL would thus depend on new technologies such as gene or drug delivery using nanocarriers to achieve an ideal effect. Nanocarriers are used as vectors in controlling drug release, protecting gene degradation by enzymes, and targeting therapeutic delivery. Nanocarriers, such as hyperbranched polylysine, liposomes and poly(lactide-co-glycolide) (PLGA) carrying genes, drugs and fluorophores, have been investigated in the inner ear. However there is no literature report on targeted inner ear drug or gene delivery using nanocarriers. In this study, potential use of polymersomes (PMs) and lipid nanocapsules (LNCs) as nanocarriers in rat inner ear respect to the inner ear distribution, targetability and biocompatibility was investigated. Firstly, quenching effect of copper sulfate ($CuSO_4$) on autofluorescence and 1,1'-dioctadecyl-3,3,3'3'-tetramethylindocarbocyanine-perchlorate (DiI)-encapsulated PMs were investigated. Then the distribution of PMs and TAT (TAT-PMs) or Tet1 (Tet1-PMs) peptide functionalized PMs in rat inner ear was detected; the effect of delivery methods on PM entering into the inner ear was evaluated; and the distribution and biocompatibility of the LNCs in rat inner ear were investigated.

In whole mounted specimens, autofluorescence was observed in the subcuticular cytoplasm of inner hair cells (IHCs), the OHCs, the SGCs, the strial marginal cells, the spiral ligament fibrocytes, the mesothelial cells of the scala tympani below the basilar membrane, and the epithelial cells of the Reissner's membrane. This autofluorescence could be quenched by treatment of 1 mM $CuSO_4$ (pH 5.0). At the same time the $CuSO_4$ treatment did not affect the fluorescence of DiI encapsulated in the PMs ($p > 0.05$, Kruskal-Wallis test). Different delivery methods induced different distribution pattern of the PMs: cochleostomy resulted in distribution of the PMs in the spiral ligament (SL), mesothelial cells beneath Corti's organ, supporting cells in Corti's organ, and spiral ganglion cells (SGCs); transtympanic injection induced uptake of the PMs in the SL and mesothelial cells beneath Corti's organ; topical round window membrane (RWM) surface administration showed distribution of the PMs only in SL. In the vestibulum, transtympanic injection and cochleostomy induced more distribution of the PMs than did topical RWM surface delivery ($p < 0.05$, Kruskal-Wallis test). TAT-PMs exhibited more intense fluorescence signals in the RWM cells, spiral ligament fibrocytes, and mesothelial cells beneath Corti's organ than the scrTAT-PMs and the unlabelled PMs. Tet1-PMs were detected in nerve fibers identified by the fact that Tet1-PMs were co-localized with NF-200 immunostaining; however the ScrTet1-PMs and unlabelled PMs were remote from the NF-200. LNCs were shown to pass though the RWM and reached the Corti's organ, strial vascularis and spiral ligament fibrocytes. No sigh of increased toxicity was observed in the *in vivo* study.

Both PMs and LNCs can pass through the RWM and internalized by the cochlear cells. Study of PMs showed that delivery methods affect the distribution of the PMs in the inner ear cells. After transtympanic injection, more PMs were detected in the vestibulum than in the cochlea, indicating that the PMs entered the vestibulum through the oval window. Administration via cochleostomy displayed the broadest distribution of PMs in the inner ear, because this method avoids the barriers between the middle ear and the inner ear. So it is necessary to choose optimal delivery method according to the purpose of treatment. The results suggest that enhanced permeability through the RWM can also be achieved by using TAT peptide functionalized PMs. Further more specific targeting to the cochlear nerve can be achieved by functionalizing the PMs with Tet1 peptides. Both PMs and LNCs are potential nanocarriers to carry drugs and genes in the future to perform inner ear therapeutics. The study of PMs and LNCs is still in its initial stage. More investigation of the PMs and LNCs is needed in the future work.

# ABBREVIATIONS

BDNF: brain-derived neurotrophic factor
CPP: cell-penetrating peptide
CN: cochlear nerve
DAPI: 4',6-diamidino-2-phenylindole
DiI: 1,1'-Dioctadecyl-3,3,3',3'-tetramethyl-indocarbocyanine perchlorate
DMF: dimethylformamide
EDTA: ethylenediaminetetraacetic acid
FDA: US Food and Drug Administration
FITC: fluorescein isothiocyanate
Gd-DOTA: gadolinium- tetraazacyclododecanetetraacetic acid
GFP: green fluorescent protein
GT1b: trisialoganglioside clostridial toxin
IHC: inner hair cells
LNCs: lipid nanocapsules
MesothC: mesothelial cells beneath Corti's organ
MFNPs: multifunctional nanoparticles
MRI: magnetic resonance imaging
NaCl: sodium chloride
NF-200: neurofilament 200
NIH3T3: mouse embryonic fibroblast cell line
OHC: outer hair cells
OSCs: outer sulcus cells
PBS: phosphate buffered saline
PCL: poly(ε-caprolactone)
PEG: poly(ethylene glycol)
PEO-b-PCL: poly(ethylene oxide)-block-PCL
PLGA: poly(lactide-co-glycolide)
PMs: polymersomes
rAAV: recombinant adeno-associated virus
RWM: round window membrane
ScrTAT-PMs: scramble TAT conjugated PEG-*b*-PCL polymersomes
ScrTet1-PMs: scramble Tet1 conjugated PEG-*b*-PCL polymersomes
SGCs: spiral ganglion cells
SGSCs: spiral ganglion Schwann cells
SL: spiral ligament
SLF: spiral ligament fibrocytes
SNHL: sensorineural hearing loss
SP: spiral prominence

NaCl: sodium chloride
SPIONs: superparamagnetic iron oxide nanoparticles
ST: scala tympani
StrMC: strial marginal cells
StrV: stria vascularis
SV: scala vestibuli
TAT: trans-activating transcriptional activator from human immunodeficiency virus 1
TAT-PMs: TAT functionalized PEG-*b*-PCL polymersomes
Tet1-PMs: Tet1 functionalized PEG-*b*-PCL polymersomes
TRITC: tetramethylrhodamine isothiocyanate
TSF: tractus spiralis foraminosus
TUNEL: terminal deoxynucleotidyl transferase dUTP nick end labeling

# LIST OF ORIGINAL PUBLICATIONS

The thesis is based on the following original articles which are referred to in the text by Roman numerals I-V:

I. **Ya Zhang**, Weikai Zhang, Alexander. H. Johnston, Tracey. A. Newman, Ilmari Pyykkö, Jing Zou (2010). Improving the visualization of fluorescently tagged nanoparticles and fluorophore-labeled molecular probes by treatment with $CuSO_4$ to quench autofluorescence in the rat inner ear. Hearing Res. 105(4): 120-126.

II. **Ya Zhang**, Weikai Zhang, Alexander. H. Johnston, Tracey. A. Newman, Ilmari Pyykkö, Jing Zou (2011). Comparison of the distribution pattern of PEG-*b*-PCL polymersomes delivered into the rat inner ear via different methods. Acta Oto-laryngol. doi:10.3109/00016489.2011.615066 [Epub ahead of print].

III. **Ya Zhang**, Weikai Zhang, Alexander. H. Johnston, Tracey. A. Newman, Ilmari Pyykkö, Jing Zou. Modified distribution of PEG-*b*-PCL PMs in the rat cochlea through surface functionalization with TAT and Tet1 peptides. Manuscript submitted.

IV. Jing Zou, Patrick Saulnier, Thomas Perrier, **Ya Zhang**, Tommi Manninen, Esko Toppila, Ilmari Pyykkö (2008). Distribution of lipid nanocapsules in different cochlear cell populations after round window membrane permeation. J Biomed Mater Res B Appl Biomater. 87(1):10-8.

V. **Ya Zhang**, Weikai Zhang, Marian Löbler, Klaus-Peter Schmitz, Patrick Saulnier, Thomas Perrier, Ilmari Pyykkö, Jing Zou (2011). Inner ear biocompatibility of lipid nanocapsules after round window membrane application. Int J Phar. 404(1-2): 211-9.

# 1. INTRODUCTION

The human cochlea is deeply buried in the temporal bone, and access to it is limited by membranous partitions. The blood-endolymph barrier hampers systemic application, and delivered therapeutics can be cleared from the circulation by the immune system. Traditional therapeutic methods of sensorineural hearing loss (SNHL) are not satisfactory. Gene therapy and neurotrophin delivery are novel applications for the potential regeneration or restoration of cochlear hair cells or cochlear neurons for the treatment of SNHL. Multifunctional nanoparticles (MFNPs) are potential carriers of genes and neurotrophins and may target specific inner ear cells, facilitating the treatment potential of their contents. The first nanocarriers were developed in the 1950s, but they have been used for therapeutic applications only for the past two decades (Petros et al., 2010). Drugs and genes have been recently successfully encapsulated within the nanocarriers for the purpose of prolonging the circulation time of the therapeutic and to protect it from enzymatic destruction (Lamprecht et al., 2002; Song et al., 2009). Targeted delivery of nanocarriers to specific inner ear cell populations can be achieved by functionalizing the nanocarriers with peptides. For example, nerve growth factor-derived peptide-functionalized PMs can specifically target CN and SGCs (Roy et al., 2010).

Nanocarrier delivery into the inner ear has been investigated using either systemic or local delivery (Ge et al., 2007; Horie et al., 2011; Horie et al., 2010; Kopke et al., 2006; Thaler et al., 2011; Zou et al., 2010b; Zou et al., 2011; Zou et al., 2010c). Gene expression in the inner ear was detected first with liposomes and later with polymers as the delivery vector (Jero et al., 2001; Tan et al., 2008). Liposome-based gene expression systems successfully induced enhanced green fluorescent protein (eGFP) expression in mouse inner ear following round window membrane (RWM) permeation (Jero et al., 2001).

Choosing an appropriate delivery method is necessary for efficient distribution of therapeutic agents in the inner ear while minimizing adverse effects. Intracochlear delivery appears to be the most effective method for delivering nanocarriers to cochlear cells. Topical RWM surface delivery was moderately efficient, and systemic delivery has the lowest efficiency (Tamura et al., 2005). The low delivery efficacy and the associated adverse effects of systemic administration make this method not an ideal treatment for inner ear diseases (Hoarau et al., 2004; Robey et al., 2010). A cochleostomy can be performed only in certain circumstances as it can potentially result in inner ear damage. Local drug delivery is now used extensively in the clinic for treating and diagnosing diseases (Pyykkö et al., 2010; Robey et al., 2010).

There are two openings between the middle ear and the inner ear: the round window and the oval window. The physiological function of these barriers is to prevent hazardous

substances from impairing the inner ear cells. At the same time, however, they inhibit passage of the therapeutics following intratympanic administration. The transport of MFNPs across these barriers may potentially be facilitated by functionalizing nanocarriers with cell-penetrating peptides, such as trans-activating transcriptional activator from the human immunodeficiency virus 1 (TAT) peptide.

The purposes of the present study were to 1) evaluate the efficacies of different PM delivery methods into the inner ear; 2) examining the ability of the cell-penetrating peptide TAT-conjugated PMs; 3) determining the in vivo targetability of Tet1 peptide-functionalized PMs and 4) examining the distribution and biocompatibility of lipid nanocapsules LNCs the in rat inner ear.

# 2. REVIEW OF THE LITERATURE

## 2.1 Overview of nanocarriers

### 2.1.1 Current status of the nanocarriers as therapeutic agents

The first generation of nanocarriers consisted of liposomes and polymers. Liposome or polymer-drug conjugates were the foundation of advanced drug delivery using nanocarriers (Petros et al., 2010). There are many types of nanocarriers nowadays: liposome, polymersome, micelle, nanocapsule, hyperbranched polymer, nanogel and porous silica nanocarrier (Fig. 1) (Cornelissen et al., 1998; Discher et al., 1999; Huynh et al., 2009; Petros et al., 2010; Thaler et al., 2010; Yan et al., 2011; Zhang et al., 2011). Nanocarriers were successfully loaded with drugs, DNA and siRNA to prolong circulation time in the body and to protect the loaded therapeutic from enzymatic degradation (Lamprecht et al., 2002; Song et al., 2009). Different types of nanocarriers have been developed to treat different cancers, pain, and infectious, age-related and inherited diseases (Chiang et al., 2010; Dong et al., 2010; Petros et al., 2010; Tamaki, 2009). To reduce the adverse effects of treatment, the concept of specific targeting by nanocarriers was introduced. Previously, antibodies and proteins have been conjugated to nanocarriers to induce targeted delivery of drugs and genes (Manil et al., 1986; Vives et al., 1997; Zhang et al., 2004). To reduce the size of nanocarriers, short peptides have been developed for different targeting purposes (Kreuter et al., 1995). Cell-penetrating peptides have also been designed to enhance the internalization and cellular penetration of nanocarriers (Silhol et al., 2002).

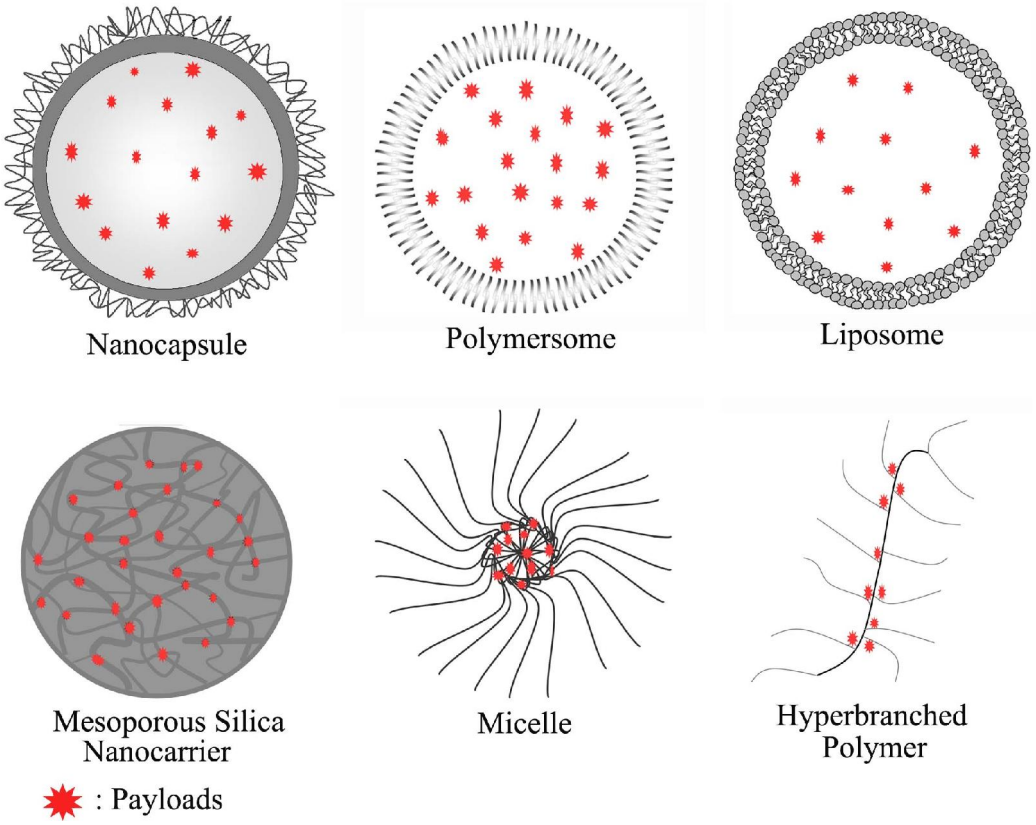


Fig. 1 Structure of nanocarriers

Higher nanocarrier internalization rates can be achieved by manipulating several aspects of the carrier themselves and the treatment protocol. Factors that increase internalization include a smaller nanocarrier size, a positive charge, higher nanocarrier concentrations, longer incubation times and higher incubation temperatures (Desai et al., 1996; Harush-Frenkel et al., 2007; Jiang et al., 2011; Panyam et al., 2002). Clathrin-mediated endocytosis, caveolae-mediated endocytosis and macropinocytosis are the primary internalization pathways of nanocarriers. The pathway by which the carrier enters the cell depends on carrier type, surface charge, and surface modifications (Harush-Frenkel et al., 2007; Jiang et al., 2011; Wadia et al., 2004). Studies of poly(ethylene oxide)-block-PCL (PEO-b-PCL) PMs demonstrated that the core/corona structure of the PMs, which is determined by the composition of the hydrophobic and hydrophilic fractions, affects the internalization pathway, whereas the PM size does not (Mahmud, 2005). Peptide-modified nanocarriers are most likely internalized via caveolae-mediated endocytosis or macropinocytosis (Del Pozo-Rodriguez, 2009; Oba, 2008; Wadia et al., 2004). When clathrin- and caveolae-mediated endocytotic pathways are inhibited, internalization via the macropinocytosis pathway is increased (Harush-Frenkel et al., 2007).

## 2.1.2 Polymersomes

PMs were first developed in late 1990s, and the proposal was made that phospholipids self-assemble into liposomes (Chiruvolu et al., 1994; Discher et al., 1999). PMs have quite stable structure compared to liposomes; they are stable for up to several months at 4 ºC and release their loaded drugs for up to 5 weeks at 37 ºC (Li et al., 2007). Unlike liposomes, which self-assemble from low-molecular weight lipids, PMs self-assemble from amphiphilic block copolymers, which consist of linked hydrophilic and hydrophobic polymer chains. Amphiphilic block copolymers have various structures: diblock (Lee et al., 2001), triblock, graft (Zheng et al., 2009) and dendritic (Jain et al., 2010) copolymers. Amphiphiles can self-assemble into spherical micelles, rod micelles (Cornelissen et al., 1998) and network phases (Jain et al., 2003). By manipulating the molecular weight of the hydrophobic chain, the size of the PMs and the thickness of the lamella can be modified (Niu et al., 2010). By manipulating the weight fraction of the hydrophilic in the amphiphilic block copolymer, the morphology of the formations can be modulated (Ahmed et al., 2004; Jain et al., 2003). The lamella of the PM is thicker than that of the liposomes, and the aqueous core of the PM can be larger than that of the liposome. One study demonstrated that the PM lamella can load up to 10 mol% of a hydrophobic substance, and the structure is quite stable at room temperature (Ghoroghchian et al., 2006a). PMs can be easily loaded with hydrophilic and hydrophobic molecules in the internal cavity and within the membrane, respectively (Ghoroghchian et al., 2006a; Liu et al., 2010).

There are three types of poly(ethylene glycol) (PEG)-based PMs based on their inner surface: poly(ethylene oxide)-b-poly(propylene oxide)-b-poly(ethylene oxide), PEG-b-poly(L-amino acid)s and PEG-b-poly(ester)s (Adams et al., 2003). Polyesters, such as poly(ethylene glycol) (PCL), poly(lactide-co-glycolide) (PLGA), poly(D,L lactide acid) (PDLLA) and poly(lactide) (PLA), are generally used as the hydrophobic core of PEG-based PMs (Adams et al., 2003; Rafat et al., 2010).

Poly(ε-caprolactone)-block-poly(ethylene glycol) (PEG-*b*-PCL) is one of several block copolymers used to produce PMs (Ghoroghchian et al., 2006b). Poly (ε-caprolactone) (PCL) forms the hydrophobic membrane of the PM, and polyethylene glycol (PEG) forms the hydrophilic corona. Both PEG and PCL are FDA (US Food and Drug Administration) approved, biodegradable polymers used in medical applications (Davidoff et al., 2011; Kim et al., 2011). Moreover, PEG is biocompatible and resistant to both protein adsorption and cell adhesion, resulting in prolonged circulation times (Halperin, 1999). Toxicity of methoxy PEG-*b*-PCL PMs loaded with indomethacin (an anti-inflammation agent) and paclitaxel (an anti-cancer agent) were investigated in the previous study. After 7 days of intraperitoneal application of the median lethal dose of the drug-loaded PMs

(which was much higher than practical effective dose), no histological changes were observed in heart, lung, liver or kidney using electron microscopy (Kim et al., 2003). A toxicity study of PEG-PCL-PDEA PMs demonstrated that this type of PM is non-toxic up to a dose of 0.5 mg/mL (Liu et al., 2010).

### 2.1.3 Lipid nanocapsules (LNCs)

LNCs are composed of 1): an oily core made of medium chain triglycerides (such as Labrafac® WL 1349); and 2): a hydrophilic and lipophilic non-ionic surfactant corona composed of hydrophilic PEGs (e.g., Solutol® HS-15) and lipophilic lecithin (e.g., Lipoïd® S75–3) (Huynh et al., 2009). LNCs are biodegradable and are stable for six months to one year in suspension (Hureaux et al., 2009; Huynh et al., 2009). Drug-loaded LNCs can release their cargo continuously over several days (Lamprecht et al., 2002). By varying the core component, concentration or viscosity of the lipid matrix, the drug release kinetics can be modulated; however, the type of the surfactant only slightly affects drug release, and the concentration of the surfactant does not affect drug release (Abdel-Mottaleb et al., 2010; Jager et al., 2009; Maupas et al., 2011). These characteristics of LNCs make them potential nanocarriers for inner ear drug delivery. Lipophilic agents and hydrophilic DNA molecules can be encapsulated in the lipid core of LNCs (Béduneau et al., 2008; Vonarbourg et al., 2009). The size of the LNC is determined by the concentration of the surfactant in the corona, which affects surface tension; lower concentrations result in larger LNCs and vice versa. The type of surfactant also slightly affects LNC size (Maupas et al., 2011).

PEGylated LNCs (i.e., coated with PEG) with PEG-660 can be rapidly cleared (with a 21-min half-life) following intravenous injection (Ballot et al., 2006; Lamprecht et al., 2002). However, LNCs PEGylated with PEG-1500, PEG-2000 or PEG-5000 exhibit a prolonged blood circulation period in vivo (Béduneau et al., 2007; Béduneau et al., 2006; Hoarau et al., 2004) (Fig. 4). PEGylation increases the stability of the LNCs (Ballot et al., 2006).

### 2.1.4 Peptide-functionalized nanocarriers

Peptide-functionalized nanocarriers were used for specific cell targeting or for enhancing cellular internalization. TrkB antibody-conjugated PEG-*b*-PCL PMs exhibited CN-specific binding, and OX26 antibody-conjugated LNCs exhibited increased blood brain barrier permeation compared with controls following systemic application (Béduneau et al., 2008; Roy et al., 2010). In the present study, the TAT peptide was used to enhance the permeation of PMs across the RWM, and the Tet1 peptide was chosen to induce targeted delivery of PMs. The biochemical properties of these two peptides are described below.

### 2.1.4.1 TAT peptide

The TAT peptide has the sequence RKKRRQRRR and belongs to the cell-penetrating peptide (CPP) family (Ruben et al., 1989). It has a strong positive charge with arginine- and lysine-rich portions. The TAT peptide penetrates cell membranes by creating a hole in the lipid membrane in an energy independent manner (Herce et al., 2007). The TAT peptide has been used to carry variable cargos in cells, including peptides, proteins, genes, and imaging agents (Baoum et al., 2009; Torchilin, 2007). The internalization rate of TAT-labeled nanocarriers can be enhanced up to 100 fold when compared to unlabeled nanocarriers (Torchilin, 2007). PMs functionalized with TAT peptide were shown internalize into cells more efficiently compared with controls without affecting cell functions (Christian et al., 2007). TAT peptide-labeled nanocarriers can cross a human epithelial monolayer (Caco-2) through a transcellular pathway (Koch et al., 2005; Lindgren et al., 2004). In contrast, it was reported that a TAT-GFP protein conjugate did not pass through an intact endothelial cell monolayer with tight junctions (bEnd.3); it did, however, cross an impaired monolayer (Simon et al., 2010a; Simon et al., 2010b).

### 2.1.4.2 Tet1 peptide

The sequence of the Tet1 peptide is ‘HLNILSTLWKYR’ and exhibits strong binding to differentiated PC12 cells, primary motor neurons, and dorsal root ganglion cells via GT1b receptors (Liu et al., 2005). Studies of GT1b receptors in the cochlea are rare. Two studies reported that GT1b receptors are expressed in the cochlea (Maguchi et al., 1991; Santi et al., 1994). This receptor was also reported to be expressed on peripheral nerve axolemma (Sheikh et al., 1999). Tet1-conjugated non-viral vectors were also found to specifically bind to neurons (Kwon et al., 2010; Park et al., 2007).

## 2.2 Investigations of nanocarriers in inner ear

Nanocarriers loaded with drug, tracers and genes have been examined in the inner ear. PEG-*b*-PCL PMs, the LNCs and silica nanocarriers loaded with fluorophores can pass through the RWM and the oval window and are detected in the cochlea and the vestibulum (Praetorius et al., 2007; Zou et al., 2008). PEG-PLA and PLGA nanocarriers can deliver drugs to the inner ear via either local RWM or systemic application (Horie et al., 2011; Horie et al., 2010). Contrast agents, such as gadolinium- tetraazacyclododecanetetraacetic acid (Gd-DOTA) and superparamagnetic iron oxide nanoparticles (SPIONs), encapsulated in liposomes, polymers and copolymers were visualized in the inner ear using magnetic resonance imaging (MRI), light microscopy and electrical microscopy. The penetration of the nanocarriers was enhanced through the use of an external magnetic field (Ge et al., 2007; Kopke et al., 2006; Thaler et al., 2011; Zou et al., 2010b; Zou et al., 2011; Zou et al., 2010c). Liposome and PEI polymers were reported to induce gene expression in the inner ear (Jero et al., 2001; Tan et al., 2008). Peptide-functionalized PMs were shown to be capable of targeting specific inner ear cell populations. For example, nerve growth factor-derived peptide-functionalized PEG-*b*-PCL PMs can specifically target the CN and SGCs (Roy et al., 2010). In the present study, the ability of Tet1-functionalized PEG-*b*-PCL PMs to specifically target the CN and of the TAT peptide to promote PEG-*b*-PCL PM passage through the RWM were investigated.

## 2.3 Delivery methods to the inner ear

Therapeutic agents for the treatment of inner ear diseases are being rapidly developed, although the delivery method can have a significant impact on the therapeutic effect. It is therefore necessary to choose an appropriate delivery method. There are two major local inner ear therapeutic agent delivery methods (Fig. 2): intact RWM delivery and intracochlear delivery (Bowe et al., 2010; Staecker et al., 2011; Swan et al., 2008). PLGA nanocarriers delivered via systemic injection through the intact RWM or intracochlearly were compared by Tamura et al. The results indicated that intracochlear delivery was the most efficient in terms of delivering the nanocarriers to the cochlea, intact RWM delivery was moderately efficient and systemic delivery exhibited the lowest efficiency (Tamura et al., 2005). The systemic delivery of viral vectors resulted in no cochlear gene delivery (Stöver et al., 2000). The low delivery efficiency and the significant side effects make systemic administration an unideal method for treating inner ear diseases (Hoarau et al., 2004; Robey et al., 2010). Local drug delivery is now extensively used for the treatment and diagnosis of inner ear diseases in the clinic (Pyykkö et al., 2010; Robey et al., 2010). Targeted drug delivery to the inner ear can be facilitated by choosing the optimal approach. For instance, intracochlear delivery via the scala media or the ST is the most efficient method for delivering gene vectors to Corti's organ (Konishi et al., 2008; Staecker et al., 2011). Alternatively, topical RWM delivery and transtympanic injection are suitable for delivering substances to the perilymph of the inner ear (Zou et al., 2003b). When substances cannot easily pass through the RWM, intracochlear delivery can be considered (Konishi et al., 2008; Lalwani et al., 1997; Luebke et al., 2001).

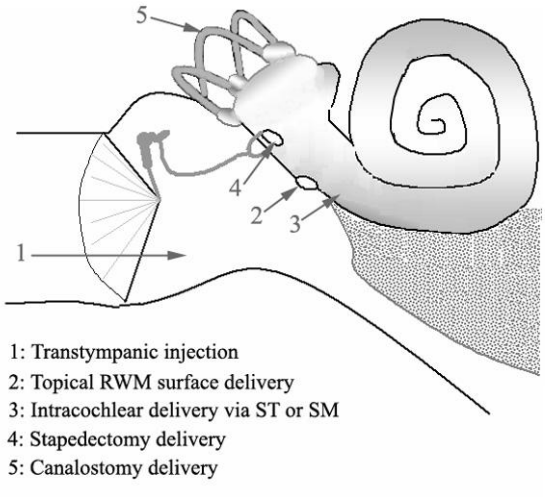


Fig. 2 Drug delivery methods to the inner ear

### 2.3.1 Topical RWM surface delivery and transtympanic injection

#### 2.3.1.1 The RWM and the oval window

There are two openings between the middle and inner ear: the RWM and the oval window. The RWM separates the ST of the inner ear from the middle ear. The oval window separates the vestibulum from the middle ear.

The RWM consists of three layers in rats: an outer epithelial layer (a single layer of cells facing the middle ear cavity); a connective tissue core; and an inner endothelial layer. The outer epithelial layer has tight junctions on the middle ear side and a continuous basement membrane beneath. The tight junction and the basement membrane protect the inner ear from hazardous substances and bacteria, but at the same time they prevent therapeutics from passing through RWM. The connective tissue core contains fibroblasts, collagen, elastic fibers, blood and lymph vessels, and 'gland-like' structures at the RWM rim. The collagen fibers are loosely arranged, and the 'gland-like' structures have openings on the middle ear mucosal surface from which they secrete mucous materials into middle ear (Goycoolea et al., 1997). The inner endothelial layer has large extracellular spaces, allowing direct contact between the connective tissue core and the perilymph (Engmer et al., 2008; Goycoolea et al., 1997). The thickness of the RWM is variable depending on the species studied. This thickness is 6-10 μm in mice (Kitamura et al., 2002), 15 μm in rat (Hellstrom et al., 1989), 10-14 μm in chinchilla (Goycoolea et al., 1997), 10 μm in guinea pig (Saber et al., 2009), and 70 μm in human (Carpenter et al., 1989). Humans have the thickest RWM, which is thicker at the rim than at the central region of the RWM.

The oval window is the barrier between the perilymph in the vestibulum and the middle ear cavity. A histological study in rats demonstrated that the annular ligament across the stapedio-vestibular joint is a porous structure composed of fibrillin, 36-kDa microfibril-associated glycoprotein (MAGP-36), and hyaluronic acid (Ohashi et al., 2006; Ohashi et al., 2008). The distance from the oval window to the saccule is 1.66 mm in humans, and the distance to the utricle is 2.25 mm (Takahashi et al., 1992). In vivo MRI studies of guinea pigs, rats, and humans indicate that the oval window is more permeable to gadolinium than the RWM (Zou et al., 2005; 2010a). Selective vestibular delivery via the oval window pathway was demonstrated by a recent MRI study (Zou et al., 2011b).

#### 2.3.1.2 Permeability of the RWM

RWM permeability to proteins, drugs, biochemical compounds, viral vectors and nanocarriers has been investigated. Following RWM surface application of antioxidants, trimethylphenylammonium and glucocorticoids, a concentration gradient was observed along the basal turn to the apex of the ST (Laurell et al., 2002; Mynatt et al., 2006; Plontke

et al., 2008). The concentration gradient was thought to be the result of a balance between the clearance and flow rates of the perilymph, but the concentration gradient decreased with time (Salt et al., 2001; Aarnisalo et al., 2006; Plontke et al., 2008).

Permeability across the RWM is influenced by several factors, including the thickness of the membrane and the size, configuration, concentration, liposolubility, and electrical charge of the delivered substance (Goycoolea et al., 1997). The permeability of the guinea pig RWM to bacteria endotoxins, dexamethasone, thiourea, methionine and trimethylphenylammonium has been investigated, and the observed concentrations in the basal turn perilymph were 0.01%, 0.01-6%, 1.4-2.4%, 1-2% and 16.5% of the original concentrations, respectively (Laurell et al., 2002; Lundman et al., 1992; Mynatt et al., 2006; Salt et al., 2001). *In vivo* and *in vitro* studies suggest that different viral vectors can pass through the RWM and can be detected in the perilymph in a time-dependent manner, except for associated adenoviruses (AAVs) (Aarnisalo et al., 2006; Jero et al., 2001; Stöver et al., 2001). Nanocarriers, such as liposomes, polymers and polymer-encapsulated SPIONs were shown to cross the RWM (Jero et al., 2001; Zou et al., 2008; Zou et al., 2010c). However, the penetration efficacy of nanocarriers is not as high as that of the viral vectors. The chosen delivery method also influences the penetration of substances through the RWM. For example, brain-derived neurotrophic factor (BDNF) administered by a single transtympanic injection or sustained RWM application in rats resulted in 0.0001% and 0.002% of the original concentration in the perilymph after 3 days, respectively (Endo et al., 2005).

Several efforts have been made to improve the permeability of the RWM. For example, disruption of the RWM epithelial layer was attempted with silver nitrate, trichloracetic acid and phenol, but these methods did not achieve satisfactory results (Aarnisalo et al., 2006; Suzuki et al., 2003). Partial digestion of the RWM using a collagenase solution increased the RWM permeability to recombinant adeno-associated virus (rAAV) vectors, resulted in elevated rAAV delivery and enhanced transfection efficacy (Wang et a., 2011). Cell-penetrating peptides were also used to improve the passage of nanocarriers through model membranes (Lindgren et al., 2004; Torchilin, 2007).

### 2.3.2 Intracochlear delivery

When a substance cannot penetrate the intact RWM or penetrates it poorly, intracochlear delivery can be considered (Bowe et al., 2010). Intracochlear delivery can substantially improve the therapeutic effect of the delivered cargo. Nanocarriers and viral vectors pass poorly through the RWM but are efficiently delivered to inner ear cells when administered via cochleostomy (Jero et al., 2001; Tamura et al., 2005). At present, intracochlear delivery is the most efficient method for gene delivery to the inner ear (Konishi et al., 2008; Staecker et al., 2011). Although hydrogel-administered BDNF to the topical RWM

surface with sustained release was reported to partially protect SGCs from degeneration, intracochlear application of BDNF resulted in full preservation of the SGCs (Agterberg et al., 2009; Endo et al., 2005). During cochlear implantation, protective therapeutic agents, such as neurotrophins and dexamethasone, can also be administered with the electrode array (Paasche et al., 2006; Shepherd et al., 2002). However, intracochlear application of a given substance is not an optimal method because it has the potential to induce inflammation (Jero et al., 2001).

### 2.3.3 Communication pathways between perilymph and inner ear cells

In vivo MRI studies on small animals, including guinea pigs, rats, and mice, demonstrated novel routes of gadolinium through the modiolus and lateral wall (Zou et al., 2005; 2009; 2010c; 2011b). Increased evidence for this novel communication route was obtained via combined scanning electron microscopy and light microscopy in the human cochlea, demonstrating that the modiolar wall of the SV and ST in the first and second turn is porous, forming a perilymphatic communication route to the peri-vascular and peri-neural spaces in the modiolus. A "peri-modiolar lymph" or fluid space can be identified in the modiolar periphery (Rask-Andersen et al., 2006). Generally, there are four perfusion pathways of substances into the inner ear (Fig. 3). The first is along the scala in the perilymph (Salt et al., 2001). The second pathway is from the perilymph to the modiolus through openings on the modiolar wall of the ST and SV; this short-cut may also be taken advantage of therapeutically given that PMs migrate to the SGCs from the ST (Rask-Andersen et al., 2006; Zou et al., 2003b; Zou et al., 2009; Zou et al., 2010c; Zou et al., 2011b). Third, perfusion can occur from the ST to the SV via either the SL or the modiolus (Salt et al., 2005; Zou et al., 2003b ; Zou et al., 2005; Zou et al., 2009; Zou et al., 2010c; Zou et al., 2011b); when substances enter the perilymph of the ST through the RWM or intracochlearly, they perfuse through fibrocytes of the SL via openings in the mesothelial sheet facing the perilymph (Laurell et al., 2002; Rask-Andersen et al., 2006; Salt et al., 1991). A fourth pathway is through Corti’s organ, which has a loose structure, and drugs applied to the perilymph of the ST can access nearly all cochlear cell populations and the nerve fibers of the peripheral processes of the SGCs (Ulfendahl et al., 2000). Lastly, perfusion can occur between the basal SV and the vestibulum (Salt et al., 2005).

Fig. 3 Arrows show the opening position in ST and SV.

# 3. AIMS OF THE PRESENT RESEARCH

The purposes of the present study were 1) to evaluate the efficacy of PM delivery into the inner ear via different methods; 2) to facilitate the outcome of the cell-penetrating peptide-TAT; 3) to determine the in vivo targetability of Tet1 peptide-functionalized PMs; and 4) to examine the distribution and biocompatibility of LNCs in the rat inner ear.

This study had the following specific aims:

I. To improve visualization of PEG-*b*-PCL polymersomes by quenching autofluorescence. (Study I).

II. To compare the distribution of PEG-*b*-PCL polymersomes administered via different methods in rat inner ear cells (Study II).

III. To evaluate the permeability of the RWM to TAT-PEG-*b*-PCL polymersomes and the axonal targeting of Tet1-PEG-*b*-PCL polymersomes in the rat inner ear. (Study III)

IV. To evaluate the distribution and toxicity of lipid nanocapsules (LNCs) in the rat inner ear following topical RWM application. (Study IV and V)

# 4. METHODS AND MATERIALS

## 4.1 Subjects

### 4.1.1 Polymersomes and lipid nanocapsules

PMs were provided by school of Biological Sciences, University of Southampton. LNCs were provided by Universite´ d'Angers-INSERM U646 Inge´ nierie de la Vectorisation Particulaire.

#### 4.1.1.1 Polymersomes

Brifly, NH2-PEG5.8K-b-PCL19K (60 mgs, Polymer Source Inc., Canada) was dissolved in 2 mL dimethylformamide (DMF, Sigma-Aldrich, UK). 4-nitrophenyl-iodoacetate (10 mg, Sigma-Aldrich, UK) was added and the reaction mixture stirred for 4 hours. Diethyl ether (50 mL, Polymer Source Inc., Canada) was added and the solution left overnight, the resulting precipitate was filtered and washed with diethyl ether to give iodoacetate-PEG5.8K-b-PCL19K functionalized polymer (45 mg, 75% yield). 15 mg of the solid was dissolved into DMF (1 mL) and then peptide (1 mg) was added. The peptide sequences (Protein Peptide research Ltd, UK) used were Tet1 (NH2-HLNILSTLWKYRC-COOH), a scrambled Tet1 sequence (ScrTet1) (NH2-LHNYTWLSLRKIC-COOH), TAT (NH2-CYGRKKRRQRRRA-COOH) and a scrambled Tat sequence (ScrTAT) (NH2-CRYRKRKGRARQR-COOH).

The carboxy cyanine dye 1,1'-Dioctadecyl-3,3,3',3'-tetramethyl-indocarbocyanine perchlorate (DiI, Invitrogen, UK) was dissolved in DMF at a concentration of 0.1 mg/mL. Tet1-PEG5.8K-b-PCL19K (6.0 mg) was added to the DiI/DMF solution (0.4 mL). The polymer solution was then added dropwise (~1 drop every 8 seconds) to rapidly stirring phosphate buffered saline (PBS, Oxoid, UK) (1.60 mL). The sample was then dialyzed. Control PMs with the scrambled ScrTet1 peptide (ScrTet1-PMs) and unlabelled PMs were made using ScrTet1/TAT-PEG5.8K-b-PCL19K and iodoacetate-PEG5.8K-b-PCL19K respectively. Diameter of the Tet1-PMs analyzed by DLS was 105.0 (+/-) 20.0 nm. Both of ScrTet1-PMs and unlabelled PMs had typical hydrodynamic diameters similar to the Tet1-PMs. The preparation of TAT-PMs was identical, however the amounts of polymer used were TAT-PEG5.8K-b-PCL19K (1 mg) and PEG5K-b-PCL5K (5 mg). For the preparation of control samples of ScrTAT-PMs and unlabelled PMs the Tat labelled polymer was replaced with ScrTAT-PEG5.8K-b-PCL5K and iodoacetate-PEG5.8K-b-PCL19K respectively. The typical hydrodynamic diameter of the TAT-PMs and the control samples were 62.6 (+/-) 9.2 nm. The zeta potential was measured on a Malvern Nanosizer. There was no difference in the zeta potential measurements for the Tet-PMs and ScrTet1-PMs, as was the case for the TAT-PMs and ScrTAT-PMs. The typical

measurements for the Tet1-PMs, the Tat-PMs and the unlabelled PMs were -0.764, -1.63 and -0.578 mV respectively. Before use in in vivo experiments the PMs were sterile filtered through a 0.2 µm cellulose acetate syringe filter.

### 4.1.1.2 Lipid nanocapsules

Emulsion of Labrafac® WL 1349 (kindly provided by Gattefossé SA. Saint-Priest, France), an oil made of capric and caprylic acid triglycerides (average molecular weight of 512); Lipoïd® S75-3 (gift from Lipoïd Gmbh, Ludwigshafen, Germany), a soybean lecithin made of 69% phosphatidylcholine and other phospholipids; Solutol® HS 15 (gift from BASF, Ludwigshafen, Germany), another surfactant; polyethylene glycol 660 hydroxystearate (C18E15); and free polyethylene glycol 660 at room temperature (oil in water). The optimal amounts of ingredients for preparation of 50 nm of LNCs were: Labrafac® (1.028 g), Lipoïd® (0.075g), Solutol® (0.846 g), NaCl (0.089 g) and pure water (2.962 g). After progressive heating at a rate of 4 ºC/min under magnetic stirring, a short interval of transparency at temperatures close to 70 ºC, and the inverted phase (water droplets in oil) was obtained at 85 ºC. Then, three cycles of cooling and heating were applied between 85 ºC and 60 ºC at the same rate of 4 ºC/min (close to the phase inversion zone). Finally, rapid dilution in cold water at a temperature close to 0 ºC produced a suspension of nanocapsules.

For pegylation, the LNCs were incubated for 90 min with DSPE-PEG-amino at 60 ºC. The suspension was vortexed every 15 min and then quenched in an ice bath for 1 min. The final DSPE-PEG concentration corresponded to 6 mol % of total surface molecules (i.e., Solutol and Lipoïd). For fluorescence labeling, 2 mg of Fluorescein-5-isothiocyanate (FITC, Fluorescéine IsoThioCyanate, France) was added to 2.95 mL of the LNC suspension, and the pH was increased to 10 by adding a few drops of 0.1M $Na_3PO_4$ solution. The sample was stirred at 35ºC for 45 min. The sample was cooled in order to stop the reaction, and size exclusion chromatography utilizing a Sephadex G-15 column was performed to separate free FITC from labeled LNCs. Fractions corresponding to the FITC-labeled LNCs were analyzed by dynamic light scattering. The hydrodynamic diameter of 52 ± 5 nm and a zeta potential of -35 ± 7 mV (for non-labeled LNCs, we obtained diameter of 48.9 nm, zeta potential of 5.0 ± 0.5 mV and concentration of 123 mg/ml). For Rhodamine B (ChemExper Inc., Belgium) labeling, FITC was replaced by 2 mg Rhodamine B.

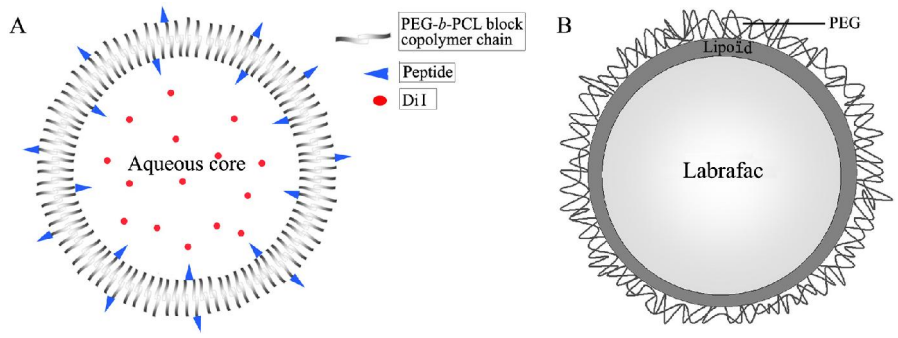


Fig. 4 Structure of polymersomes (A) and lipid nanocapsules (B). PEG: poly(ethylene glycol); PCL: poly(ε-caprolactone); DiI: 1,1'-Dioctadecyl-3,3,3',3'-tetramethyl-indocarbocyanine perchlorate.

### 4.1.2 Animals

Topical RWM surface delivery was assessed for TAT-PMs, ScrTAT-PMs and unlabeled PMs by placing gelatin sponge pledgets saturated in solutions of these nanocarriers on the RWM. The left cochlea was treated with TAT-PMs and the right cochlea was treated with ScrTAT-PMs. Unlabeled PMs were applied bilaterally to the RWM. Three days following the beginning of delivery, the animals were sacrificed and the cochleae were harvested and whole-mounted for confocal microscopy (Table 1).

One group of animals received bilateral transtympanic injections of Tet1-PMs, ScrTet1-PMs or unlabeled PMs to the middle ear cavity. Three days following injection, the cochleae were harvested. Four cochleae from each treatment group were whole-mounted. The other four cochleae were decalcified with 10% ethylenediaminetetraacetic acid (EDTA, Merck) and processed for cryosectioning (Table 1).

Another group of rats were treated with Tet1-PMs, ScrTet1-PMs or unlabeled PMs via left bulla cochleostomy unilaterally. Three days following administration, the cochleae were harvested. Two cochleae were whole-mounted and three were decalcified with 10% EDTA and processed for cryosectioning (Table 1).

Six rats were used to examine LNC distribution. Five LNC-treated rats and five sodium chloride (NaCl)-treated rats were used to test hearing thresholds. Ten untreated rats were used as controls (Table 1).

Table 1 List of cochleae numbers used in the present study

| | TAT / ScrTAT / Unlabeled-PMs | Tet1 / ScrTet1 / Unlabeled-PMs | Tet1 / ScrTet1 / Unlabeled-PMs | LNC distribution | LNC toxicity (LNC-treated / NaCl-treated / Untreated) |
|---|---|---|---|---|---|
| Number of cochleae | 7 / 7 / 6 | 8 / 8 / 8 | 5 / 5 / 5 | 12 | 5 / 5 / 10 |
| Delivery methods | Topical RWM | Transtympanic injection | Intracochlea | Topical RWM | Topical RWM |

### 4.1.3 Ethical aspects

Sprague-Dawley (SD) rats supplied by the experimental animal unit, University of Tampere were used in the study in accordance with the local ethics committee of University of Tampere standards (permission no: 985/2003).

## 4.2 Methods

### 4.2.1 Methods to administer nanocarriers to inner ear

Animals were anesthetized by 0.8 mg/kg medetomidine hydrochloride (Domitor, Orion, Finland) and 80 mg/kg ketamine hydrochloride (Ketalar, Pfizer, UK). The operation was performed under sterile conditions: surgical towels were autoclaved and operating instruments were sterilized by a bead sterilizer (STERI 250, Switzerland). The animals were placed on a thermo-regulated heated pad covered with surgical towel in a rightward lateral position.

For intact RWM application by gelatin sponge, a small piece of gelatin sponge (Gelfoam®) pledget soaked in nanocarriers (around 8 $mm^3$ soaking with 10µl nanocarriers solution) was placed near the round window niche and covered on the RWM.

For transtympanic injection to middle ear, 40µl of nanocarrier solution was injected into the middle ear cavity using a 27 gauge needle.

For sustained application of nanocarriers to the RWM using osmotic pumps (TAT-PMs, ScrTAT-PMs and the unlabeled PMs in Study III), post-auricular pathway was chosen. A hole was drilled on the bulla with a 2 mm diameter burr. After identifying the stapes artery, the RWM was identified above the artery, a small piece of gelatin sponge (Gelfoam®) pledget, around 8 $mm^3$, soaked in nanocarrier solutions was placed on the RWM. The micro-osmotic pump (ALZET®, 1003D) was filled with 100 µl PM solutions and connected to a catheter (PE60, Becton Dickinson and Company) prefilled with the same solution (Fig. 5). The catheter tip was placed onto the gelatin sponge, the catheter was fixed on the bulla with Phosphate Cement (Heraeus Kulzer GmbH, Germany), and the osmotic pump was implanted subcutaneously in the neck.

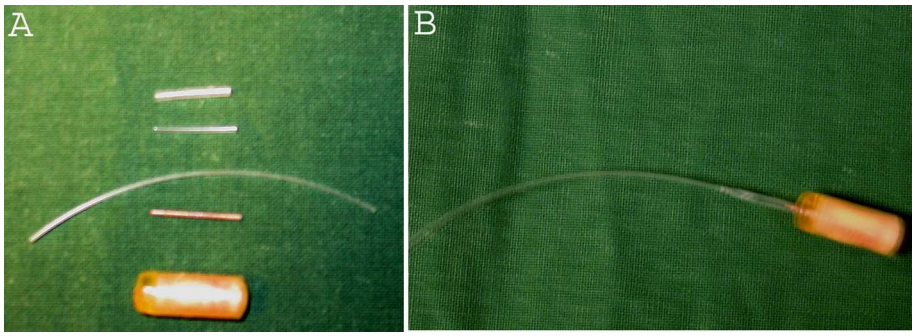


Fig. 5 Osmotic pump used in the sustained delivery.

For PMs applied to ST by osmotic pumps through cochleostomy, after visualizing the stapes artery as previously mentioned, the ST was identified below the artery. A small

hole was drilled on the bony labyrinth with a 1 mm diameter burr. The micro-osmotic pump (1003D, Alzet, Canada) was filled with 100 µl nanocarrier solutions and connected to a catheter (PE60, Becton Dickinson and Company) prefilled with the same solution (Fig. 5). The catheter tip was inserted into the hole and the surroundings sealed by a small piece of muscle. A drop of tissue adhesive (Histoacryl®, B. BRAUN, Germany) was applied to the muscle to fix the catheter. Finally the catheter was fixed on the bulla with Phosphate Cement (Heraeus Kulzer GmbH, Germany), and the osmotic pump was implanted in the neck.

After operation, Rimadyl (1.0 mg/kg, Pfizer,UK) was injected i.p to relieve pain. Baytril (10 mg/kg, Orion, Germany) was injected i.p. once a day to prevent potential middle ear infection. Antisendan (Atipamezole hydrochloride, Orion pharma, Finland) (2 mg/kg) was injected i.p. after the operation to accelerate recovery from anaesthesia of the animals.

### 4.2.2 Specimen preparation

The rats were anaesthetized using the previously described method. The bullae were fixed by cardiac perfusion with 4% Paraformaldehyde (PFA) (Merck, Germany) [0.01 M PBS containing 0.6% (v/v) heparin, pH 7.4 to remove the blood before fixation]. No inflammation was found in the middle ear cavity of all animals. The isolated cochleae were rinsed with tap water for 1 minute to remove free nanocarriers on surface, and the samples further stored in the 4% PFA solution for 2 hours.

For whole mounted samples, after washing with PBS, the basal turn, middle turn, and apex (include Corti's organ, spiral ligament, and modiolus) of the cochlea, the round window membrane, the saccule, the ultricle and the ampullae of vestibular were isolated. The tectorial membrane was removed under a stereo-microscope.

Cochleae were decalcified with 10% EDTA (ph 7.2) for 3 weeks. For paraffin sections, a standard paraffin embedding procedure was used and the samples were sectioned at 5 µm thickness (Study V). For cryosections, cochleae were incubated in 30% sucrose overnight at 4 ºC, embedded in O.C.T. compound (Tissue Tek®), sectioned with cryostat (Leica CM3050S, Germany) at 30 µm thickness (Study III).

### 4.2.3 Quenching of autofluorescence (Study I)

To investigate autofluorescence in inner ear cell populations, after stained with 4',6-diamidino-2-phenylindole (DAPI) (10 µg/ml, Sigma-Aldrich, USA) for 10 min at room temperature in the dark, the isolated cochlea tissue (Corti's organ, spiral ligament, modiolus, and the ampullae of vestibular) was washed with PBS, placed on 8-well slides (Cel-Line/Thermo scientific, USA) and mounted with Fluoromount (Sigma-Aldrich,

USA) for confocal microscopy.

To detect the quenching effect of $CuSO_4$ treatment on autofluorescence of cochlea tissue and specific labeling of the inner ear cell populations, isolated cochlea tissue were stained with FITC-conjugated phalloidin (50µg/ml, Sigma Aldrich, USA) and antibody against Neurofilament-200 (the secondary antibody was conjugated with FITC). After stained with DAPI (10 µg/ml) for 10 min at room temperature in the dark, the isolated cochlea tissue was treated with 1 mM $CuSO_4$ in 0.01 M ammonium acetate buffer (pH 5.0) for 90 min. After washing with PBS, the specimens were placed on 8-well slides and mounted with Fluoromount for confocal microscopy.

DiI encapsulated PMs were prepared with 1 mM $CuSO_4$ in 0.01 M ammonium acetate buffer (pH 5.0). The fluorescence intensity of the PMs was measured at 0 and 90 min by a spectrofluorometer (Photon Technology International, UK, serial number: 2406) equipped with FeliX32 operating software. For the untreated control, the PMs were prepared with 0.1 M PBS and measured at the same time points as the $CuSO_4$-treated samples. The fluorescence signal intensities of the $CuSO_4$-treated and untreated samples were corrected with the $CuSO_4$ and PBS references, respectively. Five trials were repeated.

### 4.2.4 Immunohistochemistry

#### 4.2.4.1 Antibodies

To investigate the quenching effect of $CuSO_4$ treatment on specific labelling, rabbit anti-NF-200 polyclonal antibody (1:200 in 0.1% BSA, Sigma Aldrich, USA) was used (Study I). In the PCL-*b*-PEG polymersome distribution study, NF-200 (1:200 in 0.1% BSA), rabbit anti-S-100 polyclonal antibody (1:200 in 0.1% BSA, Abcam, USA), and rabbit anti-Periphrin polyclonal antibody (1:100 in 0.1% BSA, Millipore, CA) were applied (Study III). In the LNC toxicity study, NF-200 antibody (1:200), S-100 antibody (1:400), purified mouse anti-CtBP2 monoclonal antibody (1:200, BD Transcription laboratorios, USA), and mouse monoclonal antibody to synaptophysin (1: 200, Sigma-Aldrich, USA) were used (Study V).

Secondary antibodies include FITC-labeled goat anti-rabbit IgG (1:200, Sigma-Aldrich, USA), FITC-labeled goat anti-mouse IgG (1:200, Sigma-Aldrich, USA), Alexa Fluor-568 labelled goat anti rabbit IgG (1:400, Invitrogen, USA) or TRITC labelled goat anti mouse IgG (1:400, Invitrogen, USA) were used depending on the host of primary antibodies.

#### 4.2.4.2 Immunostaining procedure

The paraffin sections were deparaffined. The cryosections were washed with PBS for 5

min x3. Then the samples were incubated with goat serum (1:20 with 0.1% BSA) for 1 hour at room temperature, incubated with primary antibodies as previously described over night at 4ºC, washed with PBS-T, incubated with secondary antibodies for 1 hour at room temperature, washed with PBS-T, stained with 10µg/ml DAPI for 10 minutes, and mounted with Fluoromount for confocal microscopy observation.

### 4.2.5 Apoptotic analysis

The specimens were deparaffinized, treated with 0.1% Triton-X100, incubated with 0.1% trypsin at 37ºC, irradiated with 0.1M citrate buffer (PH 6.0) at 350W microwave irradiation, and washed with PBS. For positive control, tissue was incubated with 0.2 µg /ml Proteinase K in 50 mM Tris buffer (pH 7.5). Terminal deoxynucleotidyl transferase dUTP nick end labeling (TUNEL; Roche Diagnostic GmbH, Germany) mixture (20µlEnzyme solution in 180µl lable solution) was applied on slides (50µl label solution on negtive control slides) for 60 minutes at 37ºC, washed with PBS, and whole mounted with Gel Mount TM Aqueous Mounting Medium (Sigma-Aldrich, USA) for confocal microscopy.

### 4.2.6 Confocal microscopy

The samples were observed using an Olympus microscope (Eclipse Ti) installed with ANDOR IQ software. The excitation lasers were 405 nm (blue excitation), 488 nm (green excitation), and 561 nm (red excitation) with Lambda 10-2 (Sutter instrument co.) as the excitation source. The corresponding emission filters were 525/50 (FITC), 607/45 (TRITC and Alexa 568) and 447/60 (DAPI). For 3D scanning, the inter slice thickness was 0.5 µm.

### 4.2.7 Auditory brainstem response measurement (Study V)

BioSig32 (Tucker Davis Technologies, USA) was used for ABR threshold recording .A click duration of 50 µs and a repetition rate of 21.1/s were used for stimulation. Responses from 500 sweeps were averaged with a gain of 20 at each intensity level using a filter of 0.1–3 kHz. Thresholds were judged by visible repeatable minimum response.

The latency interval between peakI and peakII ($Interval_{peakI\text{-}II}$) at 50dB were compared among groups or different time points. The time points were as follows: before surgery, 2 h post-administration, 1 week post-administration (D7), 2 weeks post-administration (D14), 3 weeks post-administration (D21), and 4 weeks post-administration (D28).

### 4.2.8 Analysis and statistics

Statistical analyses were performed using the SPSS 11.5 software package. For the spectrofluorometer study, the fluorescence signal intensities and the remaining levels of

DiI-encapsulated PMs in $CuSO_4$-treated and untreated samples were compared using Student's t-tests at different time points. The fluorescence of PMs on confocal microscopic images of the RWM, SL, and vestibulum (utricle and saccule) was measured using ImageJ 1.42q software. The fluorescence intensity was determined using pixel gray values ≥1 following subtraction of the background noise. The fluorescence intensities of the PMs delivered using the three methods were compared with the Kruskal-Wallis Test using SPSS 11.5 software. Colocalization of the Tet1-PMs, ScrTet1-PMs and unlabeled PMs with NF-200 immunostaining in confocal micrographs was analyzed using ImageJ 1.42q software. In the LNC toxicity study, ABR thresholds were compared at different time points using one-way analysis of variance (ANOVA), and a Bonferroni test was used for pairwise multiple comparisons of ABR measurements. An independent sample T-test was used to comparison compare the number of ribbon synapses between the different groups. A p-value of less than 0.05 was considered significant.

# 5. RESULTS

## 5.1 Autofluorescence in rat inner ear (Study I)

### 5.1.1 Autofluorescence

In whole-mounted specimens, autofluorescent dots were observed in the subcuticular cytoplasm of inner hair cells (IHCs). Clear autofluorescence dots were also detected in the SGCs, strial marginal cells, SLFs, mesothelial cells of the ST below the basilar membrane, and in the epithelial cells of Reissner's membrane. A sparse distribution of autofluorescence was observed in outer hair cells (OHCs). No autofluorescence was observed in the supporting cells, including Deiters' cells, Hensen or Claudius cells (Fig. 6 and Fig. 7).

### 5.1.2 Quenching of autofluorescence

Following 90 min of $CuSO_4$ treatment, no autofluorescence was visible in any of the specimens. Moreover, the specific labeling from FITC-conjugated phalloidin and NF-200 stained with a FITC-goat anti-rabbit IgG antibody were not visibly decreased following $CuSO_4$ treatment (Fig. 7 D-F).

Fluorospectrometer results indicated that 90 min of $CuSO_4$ treatment does not reduce the fluorescence intensity of DiI-tagged PMs (Table 2). The in vivo study demonstrated that visualization of DiI-tagged PMs was not affected by a 90 min of $CuSO_4$ treatment (Fig. 8 and Fig. 9).

Table 2 Fluorescence intensity of $CuSO_4$ and PBS treated DiI tagged polymersomes

| | $CuSO_4$ treatment ($x10^4$) (Mean±SEM) | PBS treatment ($x10^4$) (Mean±SEM) |
|---|---|---|
| Before | 59.2±2.4 | 58.6±5.9 |
| 90 minutes treatment | 44.5±5.5 | 44.5±1.8 |

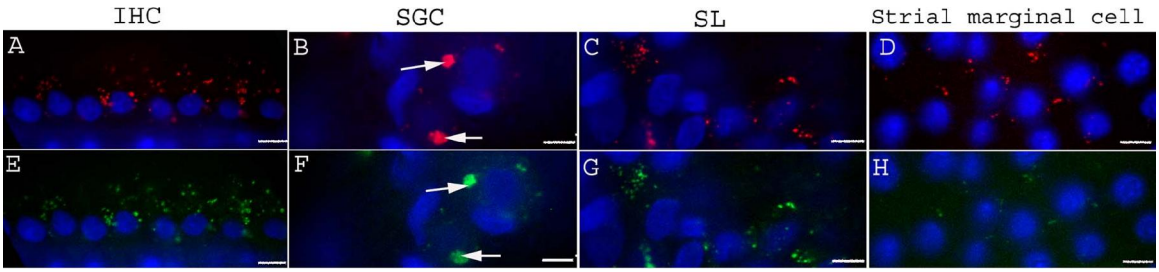


Fig. 6 Autofluorescence in inner hair cells, spiral ganglion cells, spiral ligament fibrocytes and strial marginal cells. Red: autofluorescence in red channel; Green: autofluorescence in green channel; Blue: DAPI. IHC: inner hair cell; SGC: spiral ganglion cell, SL: spiral ligament. Scale bar=10μm. (Figure 2 in Study I)

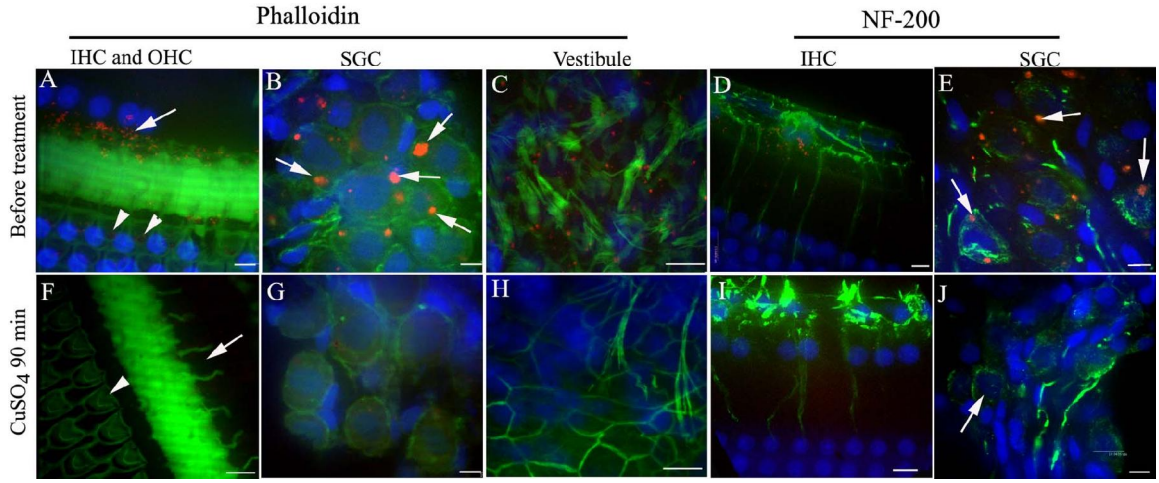


Fig. 7 Autofluorescence was detected in inner hair cells (arrows in A and F), outer hair cells (arrowheads in A and F), spiral ganglion cells (arrows in B, E and J) and vestibule (C). Autofluorescence was diminished by $CuSO_4$ treatment for 90 min (F-J). Green: Phalloidin (A-C and F-H) and NF-200 immunostaining (D, E, I and J); Red: autofluorescence; Blue: DAPI. IHC: inner hair cell; OHC: outer hair cell; SGC: spiral ganglion cell. Scale bar=10μm.

## 5.2 Polymersomes delivered via different methods (Study II)

Three methods were used to deliver PMs into the inner ear: topically on the RWM surface, transtympanic injection and intracochlear delivery.

### 5.2.1 Cochlear distribution of the polymersomes

The RWM distribution of the PMs was examined in all animals, with significantly lower fluorescence signals in the topical RWM group than in the other two groups ($p < 0.01$; Table 3). PMs delivered via topical RWM and transtympanic injection were only detected in the outer epithelial layer of the RWM, but they were detected in all three layers in the cochleostomy group (Fig. 8 A1; Fig. 9 G and H).

In the SL, PMs were detected in all animals by analysis of whole-mount specimens (Fig. 8 D, I and N). In the stria vascularis, PMs were observed in the lumens of the capillaries in the topical RWM group and in the pericytes of the capillaries in the cochleostomy group (Fig. 8 C and M). PMs were observed in Hensen and Claudius cells of Corti's organ in the cochleostomy group (Fig. 9 E). PMs delivered via cochleostomy were also detected in the spiral ganglion (Fig. 8 O and Fig. 9 F). PMs were detected in the mesothelial cells beneath Corti's organ in the transtympanic injection and cochleostomy groups (Fig. 8 G and L; Fig. 9 E).

Table 3 Quantification of polymersome uptake in rat cochlea delivered via three methods

| | RWM ($x10^4$ pixels) (Mean±SEM) | SL ($x10^4$ pixels) (Mean±SEM) | Vestibulum ($x10^4$ pixels) (Mean±SEM) |
|---|---|---|---|
| Topical RWM | 12.7±1.4** | 12.1±1.2 | 9.2±2.6* |
| Transtympanic injection | 32.8±3.2 | 11.0±0.8 | 27.8±3.3 |
| Cochleostomy | 33.3±8.9 | $20.4±2.0^{\#\#}$ | 23.1±2.8 |

**: $p < 0.01$ and *: $p < 0.05$ significantly lower than the other two delivery methods (Kruskal-Wallis Test)
##: significantly higher than the other two delivery methods, $p < 0.01$ (Kruskal-Wallis Test)
RWM: round window membrane; SL: spiral ligament.

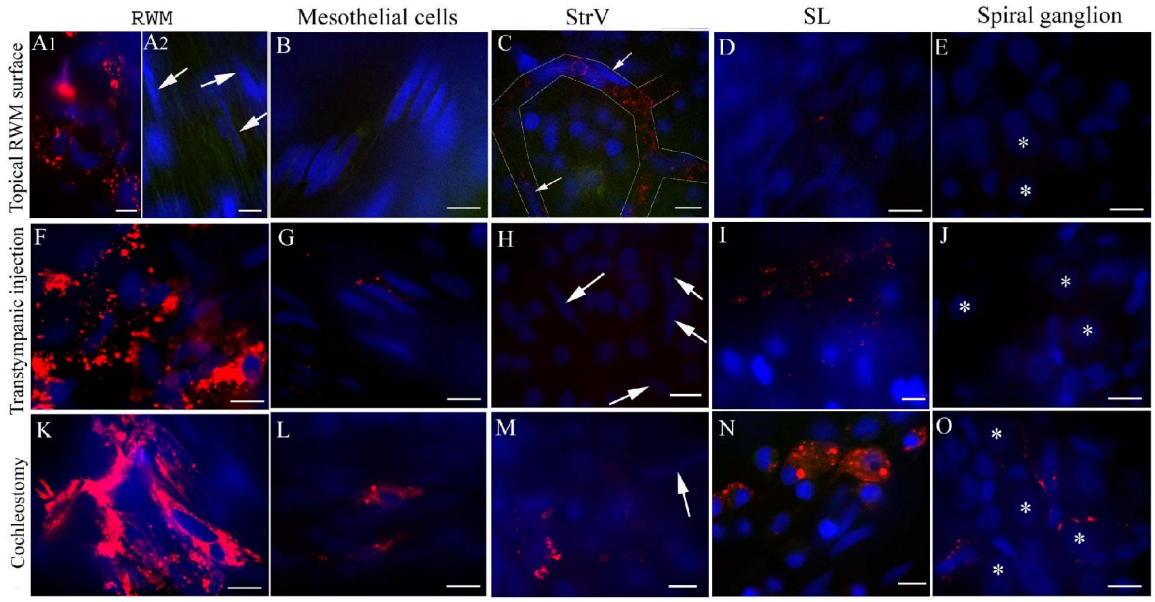


Fig. 8 Whole-mounted samples show unlabeled polymersomes administered via topical round window membrane (A-E), transtympanic injection (F-G) and cochleostomy. Arrows in A2 indicate nuclei in the connective tissue layer of the RWM. Arrows in C, H and M indicate the nuclei of the endothelial cells of the strial capillaries. Asterisks in E, J and O indicate the nuclei of spiral ganglion neurons. Red: PMs. Blue: DAPI. RWM: round window membrane; StrV: strial vascularis; SL: spiral ligament. Scale bar = 10 µm. (Figure 5 B in Study I; Figure 2 in Study II)

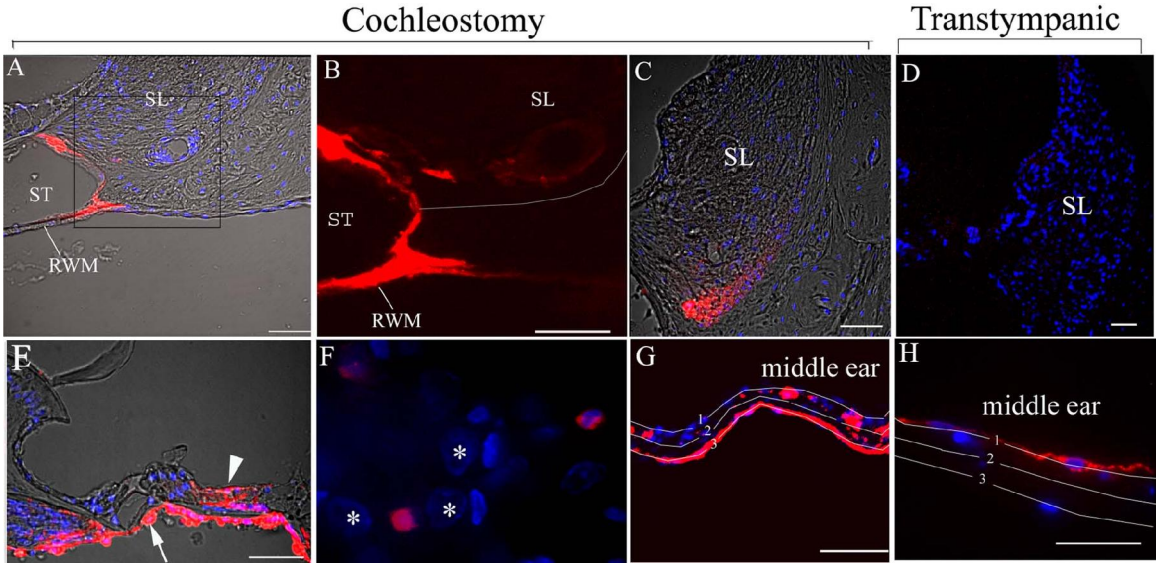


Fig. 9 Cryosections show unlabeled polymersomes delivered via cochleostomy and transtympanic injection. Panels A and B show the unlabeled PMs surrounding a blood vessel in the SL (B is a magnified image of the rectangular area in A). Panel C shows the unlabeled PMs in type III and type IV SLFs. Panel E shows unlabeled PMs in the CN within the spiral lamina canal, in mesothelial cells beneath Corti's organ (arrow), and in supporting cells in Corti's organ (arrowhead). Panel F shows unlabeled PMs in the spiral ganglion. Panels G and H show unlabeled PMs in the RWM (1: epithelial layer; 2: connective tissue layer; 3: endothelial layer). Red: PMs; Blue: DAPI. RWM: round window membrane; SL: spiral ligament; ST: scala tympani. Scale bar = 50 µm. (Figure 3 and Figure 4 in Study II)

### 5.2.2 Vestibular distribution of the polymersomes

Measurements of the fluorescence signal from confocal images of whole-mounted samples indicated that more PMs were delivered into the vestibulum via transtympanic injection and cochleostomy than by topical RWM ($p < 0.05$; Table 3). The fluorescence signals of the PMs delivered by transtympanic injection and cochleostomy were not statistically different ($p > 0.05$; Table 3). However, cryosections indicated that the PMs delivered by transtympanic injection were located in the endolymphatic and perilymphatic spaces of the vestibulum (Fig. 10 A and B). In contrast, PMs delivered via cochleostomy were present in the utricular branch of the vestibular nerve and in mesothelial cells of the SCC facing the perilymph (Fig. 10 C and D).

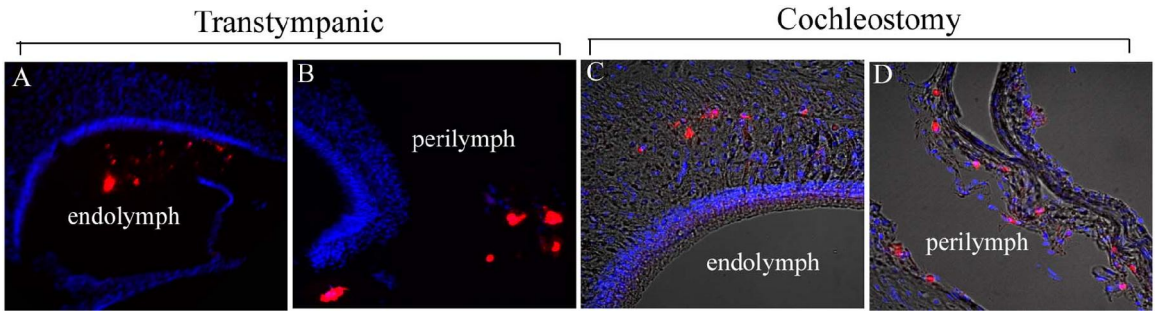


Fig. 10 Cryosections indicate that polymersomes were present in vestibulum. Red: PMs; Blue: DAPI. Scale bar=10 µm. (Figure 5 in Study II)

## 5.3 Peptide-functionalized polymersomes

### 5.3.1 TAT-functionalized polymersomes (Study III)

Uptake of TAT-PMs in RWM was significantly higher than that of ScrTAT-PMs or unlabeled PMs ($p < 0.05$). In the mesothelial cells beneath Corti's organ, the uptake of TAT-PMs was significantly higher than unlabeled PMs ($p < 0.05$) and tended to be higher than that of ScrTAT-PMs ($p = 0.065$). In the SL, the uptake of TAT-PMs was significantly higher than that of ScrTAT-PMs ($p < 0.05$) but not the unlabeled PMs ($p = 0.074$, Table 4 and Fig. 11). TAT-PMs were observed in outer sulcus cells where the ScrTAT-PMs and the unlabeled PMs were not presented. TAT-PMs were detected in SGSCs in one animal (Fig. 11).

Table 4 Quantification of polymersome uptake in the rat cochlea after topical round window membrane administration.

| | RWM (x104 pixels) (Mean±SEM) | Mesothelial cells (x104 pixels) (Mean±SEM) | SL (x104 pixels) (Mean±SEM) |
|---|---|---|---|
| TAT-PMs | 30.9±3.4 | 15.6±1.1 | 12.9±1.9 |
| ScrTAT-PMs | 11.0±0.7* | 8.9±1.0 | 9.2±2.1 |
| Unlabeled PMs | 12.7±1.4* | 9.2±1.2* | 12.1±1.5* |

*: $p < 0.05$ compared with TAT-PMs (Kruskal-Wallis test)

RWM: round window membrane; SL: spiral ligament

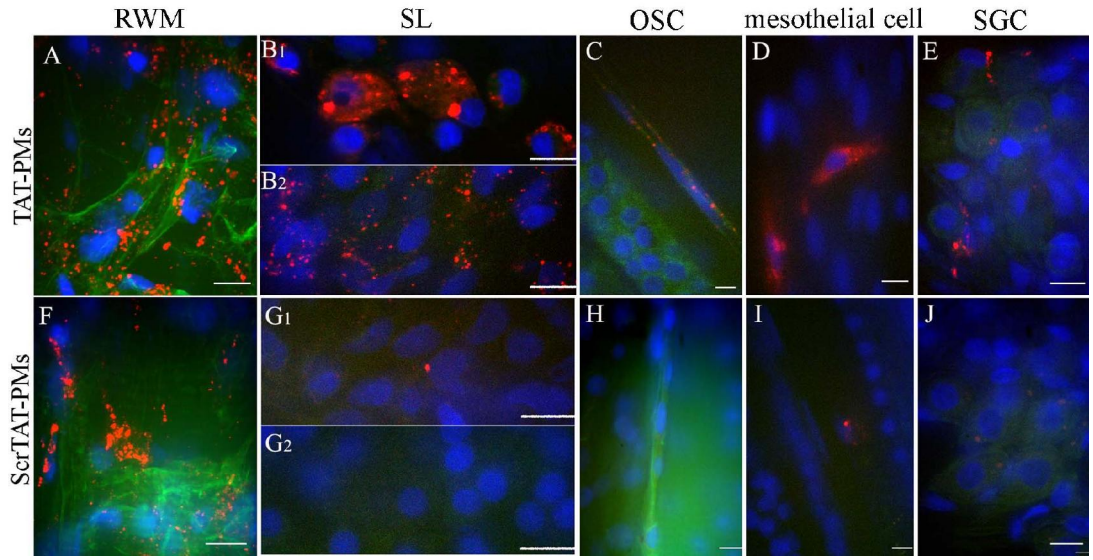


Fig. 11 Distribution pattern of TAT-PMs and ScrTAT-PMs in cochlear cells. Green in A, C, F and H: FITC-conjugated phalloidin. OSC: outer sulcus cells; PMs: polymersomes; RWM: round window membrane; SGC: spiral ganglion cell; SL: spiral ligament. Red: PMs. Blue: DAPI. Scale bar=10 μm. (Figure 3 in Study III)

### 5.3.2 Tet1-functionalized polymersomes (Study III)

#### 5.3.2.1 Tet1-PMs administered by cochleostomy

Only the Tet1-PMs were detected in the tractus spiralis foraminosus (TSF) region (Fig. 12 and Fig. 13 A), which is multiple tiny osseous canals that allow axons to pass from the Rosenthal canal to the cochlea nerve in the modiolus. Tet1-PMs were colocalized with or adjacent to NF-200 immunostaining (Fig. 13 B and F). However, the ScrTet1-PMs and the unlabeled PMs were remote from NF-200 immunostaining (Fig. 13 C and D). All the three types of PMs were internalized by SGSCs which was identified by co-localization with S100 immunostaining (Fig. 14 C, F and I). None of the PMs were observed in the neuronal soma of SGCs.

In addition, all the tested PMs were observed in the RWM, the mesothelial cells in the ST and SV, the CN in the spiral lamina canal and in the modiolus, the spiral ganglion (SG) in Rosenthal's canal and the anterior and posterior spiral modiolar vein in modiolus. The scrambled and the unlabeled PMs were occasionally observed in Hensen and Claudius cells (Fig. 8 E). Tet1-PMs were observed in type II, III, IV and V SLFs. ScrTet1-PMs were detected in type I, II, III, IV and V SLFs. Unlabeled PMs were only detected in type III and IV SLFs.

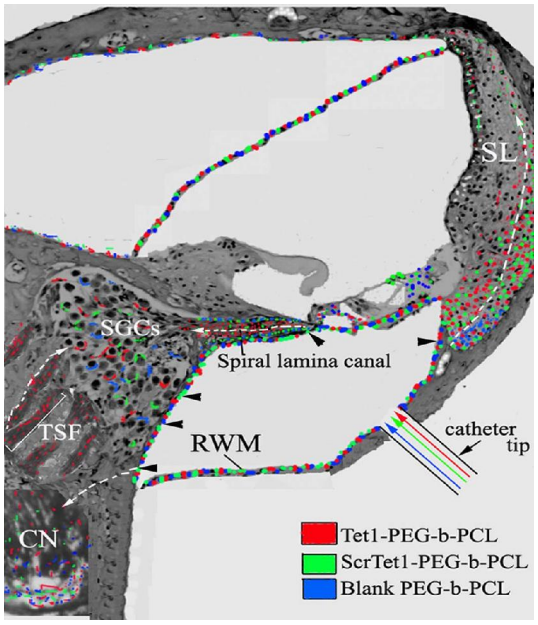


Fig. 12 Illustration of the distribution of Tet1-PMs, ScrTet1-PMs and unlabeled polymersomes after delivery using cochleostomy. In the CN within the spiral lamina canal, the CN in the tractus spiralis foraminosus (TSF) region and the SL, the distribution patterns of the Tet functionalized and control PMs were different. Arrowheads: the openings in ST that allowed the PMs to pass through (Rask-Andersen et al., 2006). White arrows with dashed line: the possible routes of PM distribution in the inner ear. CN: cochlear nerve; RWM: round window membrane; SL: spiral ligament; SGCs: spiral ganglion cells; TSF: tractus spiralis foraminosus. (Figure 4 in Study III)

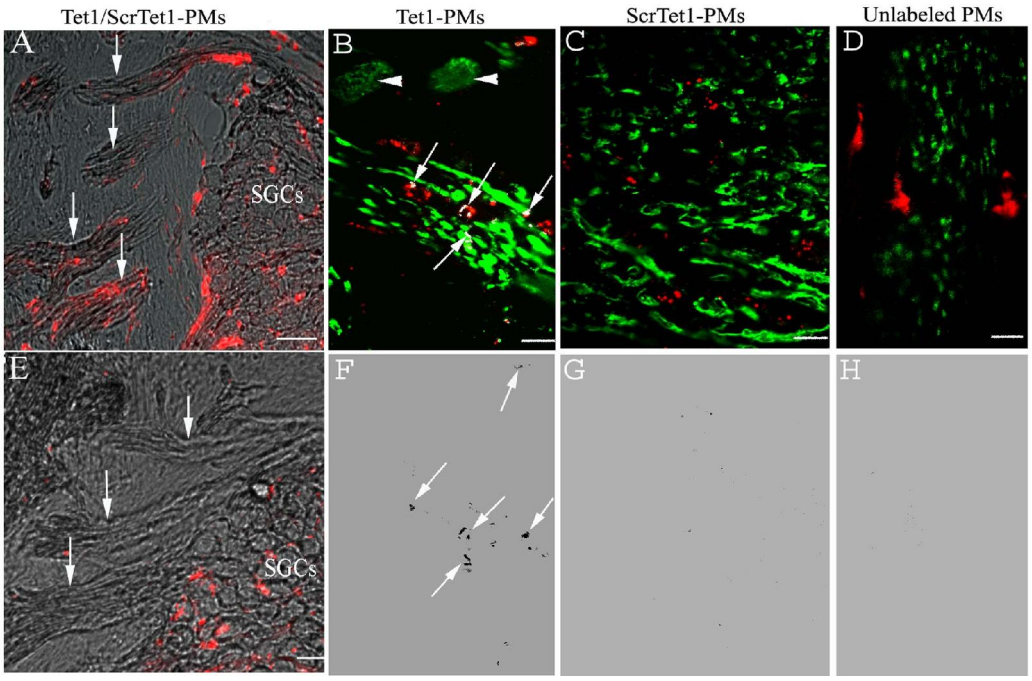


Fig. 13 Cryosections showing the distribution pattern of polymersomes with and without Tet1 functionalization in the rat cochlea following administration via cochleostomy. Tet1-PMs (A) and ScrTet1-PMs (E) were detected in the SGCs and in nerve fibers in the tractus spiralis foraminosus (TSF) region. Only Tet1-PMs were detected in the TSF region (arrows in A). Panels B-D show the co-localization of the PMs with NF-200 (arrows in panel B). The co-localized points are indicated by black dots in panels F (arrows), G

and H (analyzed by ImageJ software). Arrowheads in panel B point to SGCs. Red: PMs; Green: NF-200; Blue: DAPI. Gray: bright field. PMs: polymersomes; SGCs: spiral ganglion cells. Scale bar = 10 μm. (Figure 6 in Study III)

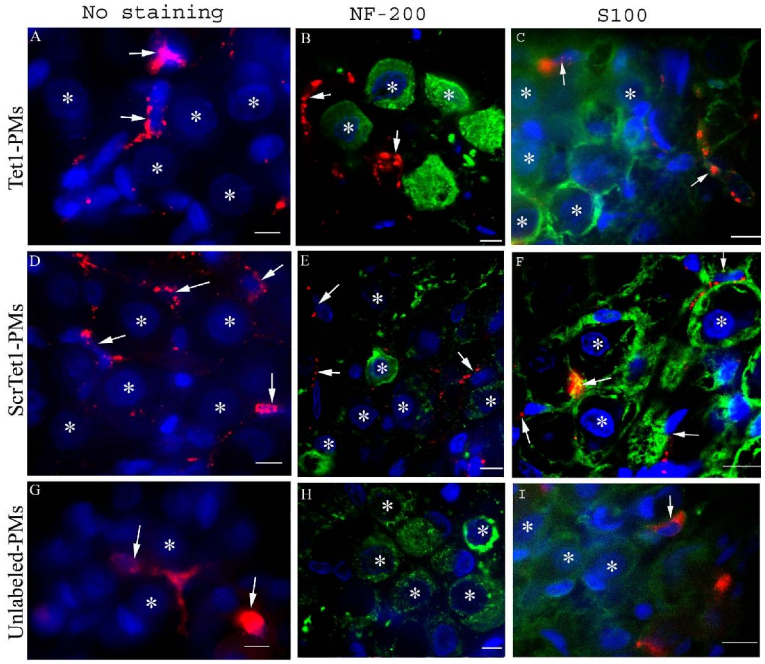


Fig. 14 Distribution of polymersomes in the spiral ganglion cells after administration via cochleostomy. All three types of the PMs administered by cochleostomy were located in SGSCs (arrows). PMs were not detected in the neuronal soma of the spiral ganglion clees (*: nucleus of type I spiral ganglion cells). Red: PMs; Green: NF-200 or S100 immunostaining. Blue: DAPI. PMs: polymersomes. Scale bar = 10 μm. (Figure 7 in Study III)

### 5.3.2.2 Tet1-PMs administered by transtympanic injection (Study III)

Tet1-PMs, ScrTet1-PMs and unlabeled PMs were detected in RWM, SLFs, mesothelial cells of the SV and ST, Reissner's membrane and the vestibular system. However, no PMs were observed in the SGCs or the CN (Fig. 15).

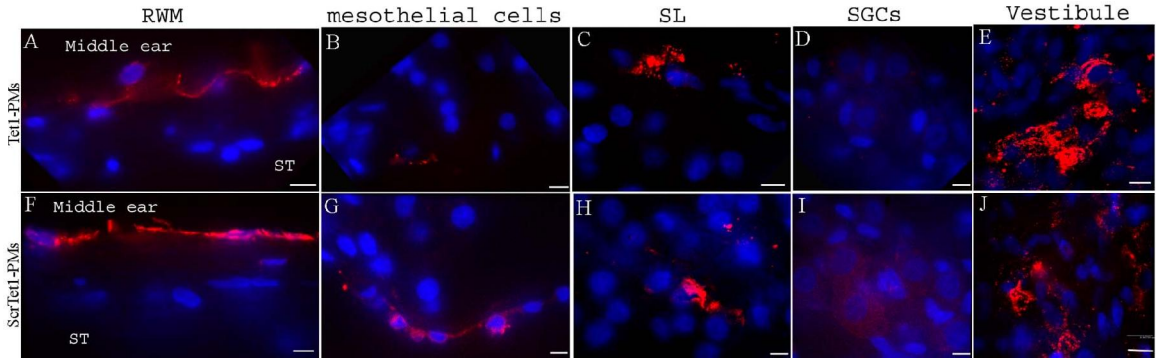


Fig. 15 Distribution pattern of Tet1- and ScrTet1-PMs in the inner ear. PMs: polymersomes; SGCs: spiral ganglion cells; SL: spiral ligament; ST: scala tympani. Red: PMs. Blue: DAPI. Scale bar = 10 μm.

## 5.4 Distribution and toxicity of lipid nanocapsules in the rat inner ear

### 5.4.1 Distribution of lipid nanocapsules in the rat inner ear (Study IV)

Following a topical RWM surface delivery of 30 min, LNCs were observed in the stapedial artery and in typeV SLFs (Fig. 16 A-E). Following an application of 1 hour, LNCs were also detected in the StrV and spiral prominence (Fig. 17 A and B). Following an application of 24 hours, intense accumulations of LNCs were observed in the RWM, the mesothelial cells beneath Corti's organ, the SL, the modiolus, and the stapedial artery (Fig. 16 F-J). Following 1-hour and 24-hour treatments, the LNC signal was stronger compared to the 30-min and 7-day applications (Fig. 17 C). In each of the groups, red fluorescence was frequently apart from green fluorescence.

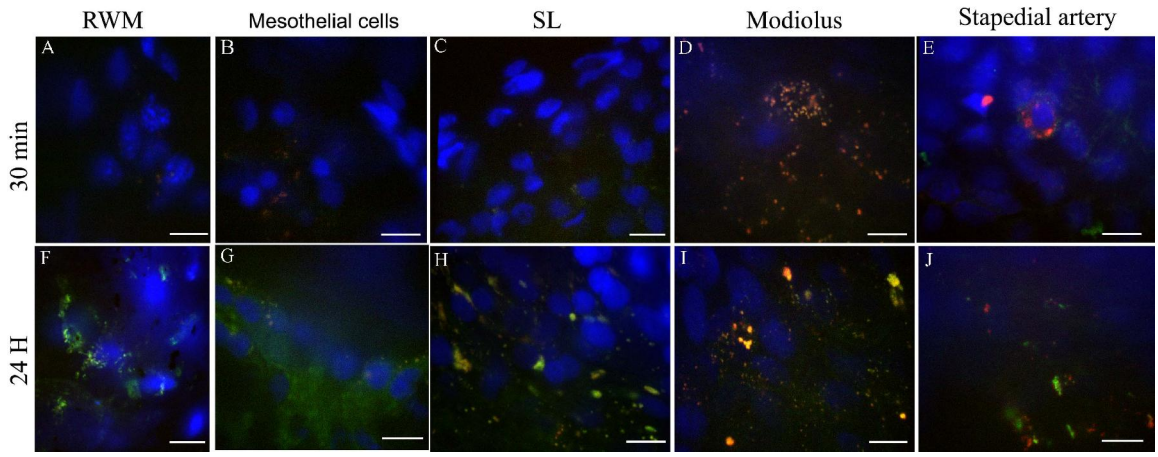


Fig. 16 Lipid nanocapsule distribution pattern in the cochlea. Panels A-C are pictures from cryosections. Panels E and J show that red and green fluorescence from the LNCs were separate in the stapedial artery (arrows: Nile Red; arrowheads: FITC). Red and Green: Nile Red and FITC from LNCs; Blue: DAPI. LNCs: lipid nanocapsules; RWM: round window membrane; SL: spiral ligament. Scale bar=10 μm. (Figure 2 C and M; Figure 4 A in Study IV)

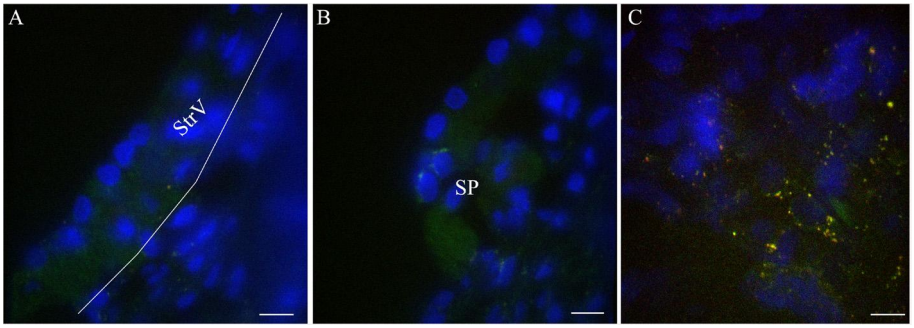


Fig. 17 Cryosections show the distribution of lipid nanocapsules. Panels A and B show LNCs in the StrV and the SP following a 1-hour application on the RWM. Panel C shows LNCs in the mesothelial cells beneath Corti's organ following a 7-day application. Green and Red: FITC and Nile Red from LNCs; Blue: DAPI. LNCs: lipid nanocapsules; StrV: strial vascularis; SP: spiral prominence. Scale bar=10 μm. (Figure 6 D in Study IV)

## 5.4.2 Toxicity study of lipid nanocapsules in the rat inner (Study V)

### 5.4.2.1 Hearing results

Immediately following LNC treatment (D0), ABR thresholds were increased in both the LNC-treated group and the NaCl control ($p < 0.05$; Table 5). After seven days of treatment (D7), ABR thresholds recovered to pre-treated level ($p > 0.05$). The ABR latency interval between peaks I and II ($Interval_{peakI-II}$) at 50dB was prolonged at D0 in both the NaCl control and LNC-treated groups when compared to pre-treatment, even though only the NaCl group was significantly different ($p < 0.01$; Table 6).

Table 5 Auditory brainstem response thresholds during test period (Mean±SEM)

| | Before | D0 | D7 | D14 | D21 | D28 |
|---|---|---|---|---|---|---|
| LNC-treated group | 24±3 | 33±3$^{\#}$ | 25±4$^{\#}$ | 23±1 | 20±2 | 24±2 |
| NaCl control | 22±4 | 33±3$^{\#}$ | 28±2$^{\#}$ | 22±2 | 23±3 | 20±8 |

#: $p < 0.05$ compared to the previous neighbouring time point (Bonferroni, ANOVA).
LNC: lipid nanocapsules

Table 6 Auditory brainstem response latency variance during test period (Mean±SEM)

| | Before | D0 | D7 | D14 | D21 | D28 |
|---|---|---|---|---|---|---|
| LNC-treated group | 0.74±0.03 | 0.88±0.02* | 0.82±0.06 | 0.73±0.03 | 0.78±0.03 | 0.81±0.03 |
| NaCl control | 0.73±0.03 | 0.94±0.01* $^{\#\#}$ | 0.77±0.01$^{\#}$ | 0.78±0.02 | 0.73±0.01 | 0.77±0.01 |

*: $p < 0.05$ comparison between the LNC-treated group and NaCl control (Bonferroni, ANOVA).
#: $p < 0.05$ and ##: $p < 0.01$ when compared to the previous neighbouring time point (Bonferroni, ANOVA).

### 5.4.2.2 Morphological results and cell viability detection

None of the animals exhibited middle ear infection during the treatment period. H&E staining indicated the morphology of the cochlea and the vestibule were well preserved following LNC treatment (Fig. 18). TUNEL-positive staining was consistently observed in the interdental cells and stria marginal cells, OHCs, IHCs, and endothelial cells of the semicircular canals in both the NaCl control and the LNC-treated rats (Fig. 18).

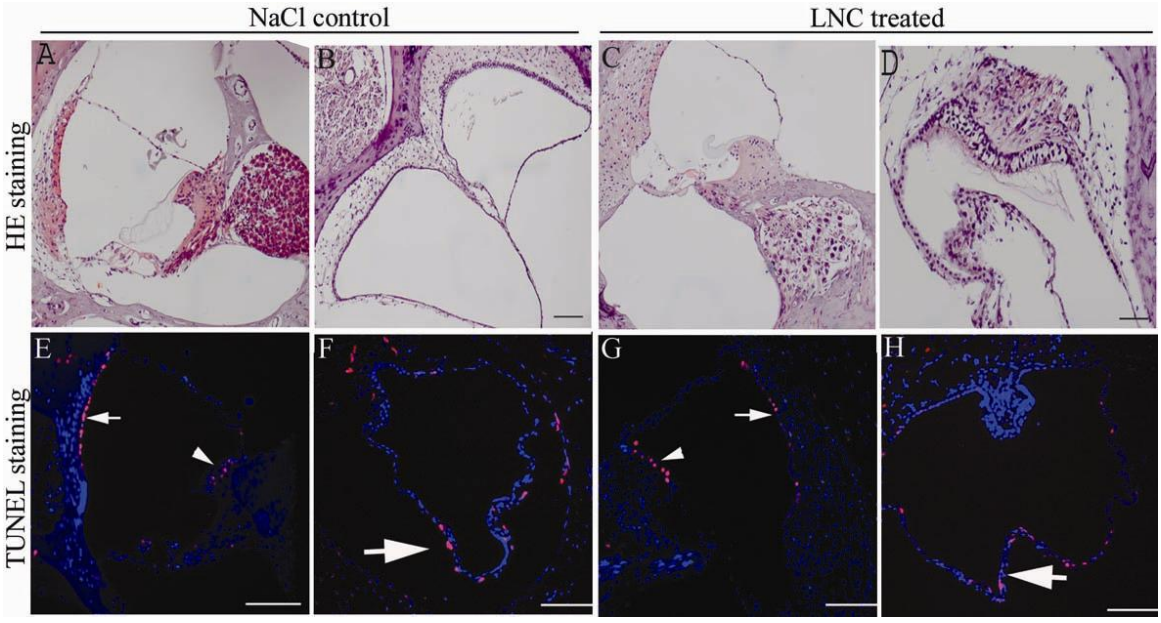


Fig. 18 The morphology of the inner ear was well preserved in control group and lipid nanocapsule treated group (A-D). TUNEL-positive staining was detected in stria marginal cells (arrows in E and G), interdental cells (arrowheads in E and G), OHCs (E), and endothelial cells of semicircular canals (arrows in F and H) both in the NaCl control and in the LNC treated rats (E-H). Red: TUNEL positive cells; Blue: DAPI. LNC: lipid nanocapsules; OHC: outer hair cells. Scale bar=100 μm. (Figure 4 and Figure 5 G-J in Study V)

### 5.4.2.3 The preservation of neural elements in the inner ear

At D28, NF-200 staining indicated that the nerve fibers innervating the IHCs and OHCs, the SGCs, and the CN in both the osseous spiral canal and the modiolus were well preserved in both the untreated and LNC-treated rats. The NF-200 fluorescence signals in SGCs ($P < 0.01$) and in the CN in osseous spiral canal ($P < 0.05$) of the LNC-treated group were significantly weaker than that of the untreated group (Table 7). The S-100 signal intensities in the LNC-treated group were decreased in Deiter's cells, SGCs and in the SL when compared to the untreated group. However, these differences were not statistically significant ($p>0.05$; Table 8).

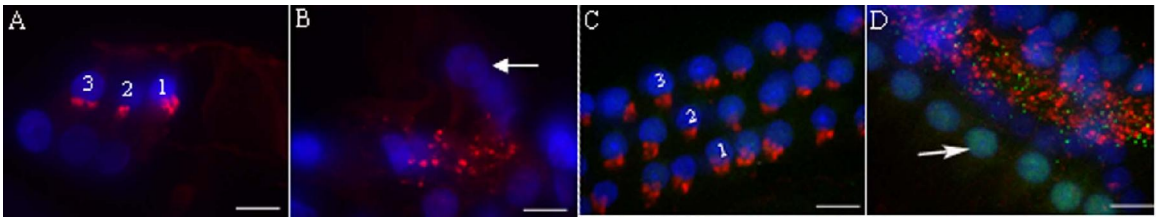


Fig. 19 Distribution of synaptophysin and ribbon synapses in paraffin slides (A and B) and whole mounted samples (C and D). Numbers in A and C mean the three rows of OHC (1 is close to modiolus; 3 is close to SL). Red: synaptophysin. Green: ribbon synapses. Blue: DAPI. Scale bar=100 μm. (Figure 7 in Study V)

Table 7 Comparison of NF-200 fluorescence intensity between LNC-treated and untreated rats

| | IHC (Mean±SEM) | SGCs (Mean±SEM) | CN in osseous spiral canal (Mean±SEM) | CN in modiolus (Mean±SEM) |
|---|---|---|---|---|
| LNC-treated | 5.71±0.51 | 1.69±0.07** | 2.64±0.46* | 2.41±0.32 |
| Untreated | 4.35±0.41 | 2.05±0.19** | 4.21±0.88* | 2.24±0.46 |

**: $p < 0.01$. *: $p < 0.05$ (Student's t-test)

CN: cochlear nerve; IHC: inner hair cells; LNC: lipid nanocapsules; SGC: spiral ganglion cells

Table 8 Comparison of S100 fluorescence intensity between LNC-treated and untreated rats

| | Deiter's cell (Mean±SEM) | SGCs (Mean±SEM) | SL (Mean±SEM) |
|---|---|---|---|
| LNC-treated | 3.53±0.89 | 2.00±0.10 | 2.96±0.31 |
| Untreated control | 5.89±1.33 | 2.38±0.17 | 6.03±0.52 |

Student's t-test

CN: cochlear nerve; IHC: inner hair cells; LNC: lipid nanocapsules; SGC: spiral ganglion cells

The synaptophysin was completely preserved in both the LNC-treated groups and the non-treated group. A typical distribution of synaptophysin was demonstrated within varicosities of efferent endings on the basal pole of the three OHC rows and small dot-like afferent endings at the bottoms of IHCs. Ribbon synapses were found at the bottoms of IHCs in the LNC-treated and untreated rats [11.83±0.62 (mean±SEM) and 13.31±1.77 (mean±SEM), respectively]. However, this difference was not significant ($p>0.05$, Student's t-test; Fig. 19).

# 6. DISCUSSION

## 6.1 Discussion of primary results

In general, observations of the distribution of nanocarriers in rat inner ear are difficult because their signal can be confused with autofluorescence. Autofluorescence impairs the detection of PM and LNC fluorescence signals in inner ear cells. In the whole-mounted samples, autofluorescence was observed in the subcuticular cytoplasm of IHCs, border cells, SGCs, strial marginal cells, SLFs, mesothelial cells of ST below the basilar membrane, and the epithelial cells of the Reissner's membrane; sparse autofluorescence was observed in OHCs. The red emission and the green emission were highly co-localized in the confocal image. In the LNC distribution study (Study IV), we did not quench the autofluorescence with $CuSO_4$. As a consequence, there was a certain degree of autofluorescence in combination with fluorescence from the LNCs. In this study, LNCs were recognized by a lower degree of colocalization between the red and green fluorescence (Fig. 16 and Fig. 17) when compared to autofluorescence signal. Decreased colocalization also indicated that the LNCs may have been degraded in the inner ear cells (Fig. 17). Because we noticed autofluorescence, we used $CuSO_4$ to quench the autofluorescence in the PM studies and it proved the $CuSO_4$ treatment does not decrease the fluorescence of DiI encapsulated PMs.

A comparison of topical RWM surface delivery, transtympanic injection and cochleostomy provided information regarding the optimization of inner ear drug delivery. Although transtympanic injection was not superior to topical RWM surface delivery of PMs into the cochlea, it was more efficient in delivering PMs into the vestibulum. However, none of these two methods was capable of introduce PMs into the spiral ganglion or into Corti's organ. Cochleostomy is the most efficient method to deliver PMs into the inner ear compare to topical RWM surface delivery and transtympanic injection. There are two pathways for PMs and LNCs to be transported from the middle ear cavity into the inner ear in rats: through RWM to the ST, and through the oval window annular ligament to the vestibular (Zou et al., 2010b; Zou et al., 2011b). Passage of PMs through the RWM can be achieved by functionalizing the PMs with TAT peptide. In the present study, the TAT-PMs delivered via topical RWM surface showed more uptakes in RWM and mesothelial cells of beneath Corti's organ than either the ScrTAT-PMs or the unlabeled PMs. TAT-PMs were also observed in outer sulcus cells and spiral ganglion, whereas ScrTAT-PMs and unlabeled PMs were not.

The Tet1-PMs and the control PMs delivered via transtympanic injection exhibited no targeting to either SGCs or CN, even though they were non-specifically internalized by SLFs because SLFs do not express GT1b receptors. This may be due to insufficient

number of PMs pass through the RWM. To support this idea we delivered PMs via cochleostomy and the PMs were present spiral ganglion Schwann cells (SGSCs). Tet1-PMs delivered via cochleostomy were observed in axons as determined by the localization of Tet1-PMs within or adjacent to neurofilaments. The Tet1 peptide is reported to bind to the GT1b receptor, which is abundantly expressed in neuronal membranes in the central nervous system and in peripheral nerve axolemmas (Ryu et al., 2002; Sheikh et al., 1999).

In the LNC distribution study (Study IV), red fluorescence was occasionally apart from green fluorescence (Fig. 16 and 17), indicating that the LNCs were degradated in the inner ear cells. But in which stage were the LNCs degradated needs further investigation. The hearing threshold evaluation, the neural element analysis and the cell viability detection showed no hint of toxicity of the LNCs in the rat inner ear. In another study, the LNCs administered via intracochlear injection did not cause hearing loss, nanocarrier application-related cell death, or morphological changes in the inner ear (Scheper et al., 2009). Our in vitro cell culture study using L929 cells and primary cochlear cells demonstrated that the LNC toxicity is dose-dependant (Zhang et al., 2011). LNC toxicity is primarily induced by the corona surfactant. However, higher surfactant concentrations in LNCs do not lead to higher cellular toxicity. An in vitro study demonstrated that the toxicity of the LNCs is surfactant type dependent but not concentration dependent (Maupas et al., 2011). In our study of the inner ear distribution and toxicity of LNCs, Solutol® HS 15 and Lipoïd® S75–3 were used as corona surfactants, and the cells survived with a relatively high concentration of LNCs. In L929 cells, an LC50 of 2.2 mg/mL was observed, and in primary cochlear cell culture the survival rate at 1.5 mg/mL was 37.94% (Zhang et al., 2011). The cell death is probably due to ‘overload phenomenon’, cell functions will be impaired when the nanoparticles occupy a certain volume of the cell (Moss, 2006). In macrophages, overload phenomenon occurs when ≥ 6% of the cell volume is taken up by nanoparticles.

## 6.2 Discussion of common results

### 6.2.1 Quenching autofluorescence in rat inner ear

The autofluorescence has a broad excitation/emission spectra, it can be detected with both the 607/45 nm (red) and 525/50 nm (green) emission filters using confocal microscopy (Kikugawa et al., 1997). The emission spectrum of autofluorescence ranges from 612 nm to 513 nm, overlaps many fluorophores (Haralampus-Grynaviski et al., 2003). A2E (2-[2,6-dimethyl-8-(2,6,6-trimethyl-1-cyclohexen-1-yl)-1E,3E,5E,7E-octatetraenyl]-1-(2-hydroxyethyl)-4-[4-methyl-6-(2,6,6-trimethyl-1-cyclohexen-1-yl)-1E,3E,5E-hexatrienyl]-pyridinium) is an isomer of a pyridinium bis-retinoid, which is thought to be the major autofluorescence substance (Haralampus-Grynaviski et al., 2003). The quenching mechanism of autofluorescence may be due to the cupric ion binding to amino acids close to A2E and inducing energy transfer which is that the cupric ion absorbs the energy at emission wavelength of the A2E without re-emitting the energy fluorescently (Gouanvé, 2007).

### 6.2.2 Comparison of the delivery methods to the rat inner ear (Study II)

The PMs and the LNCs delivered via topical RWM surface delivery were transported to the perilymph of the ST through the RWM. The PMs delivered via transtympanic injection can be transported to the perilymph via both the RWM and the oval window. The RWM is a semi-permeable membrane. The epithelial layer of the RWM has tight junctions (Goycoolea et al., 1997); the connective tissue layer and the endothelial layer are loosely arranged. Therefore, it is possible that PMs pass through the epithelial layer via a transcellular pathway; through the connective tissue and endothelial layers via an intercellular pathway (Goycoolea et al., 1997). PMs delivered via RWM surface and transtympanic injection were detected only in the epithelial layer of the RWM. However, PMs administered through cochleostomy were detected in all three RWM layers (Study II). This finding suggests that when PMs were delivered into the cochlear perilymph, they were 1) taken up by the endothelial cells, 2) diffused into the connective tissue core through loose intercellular gaps of the endothelium, and then 3) internalized by the epithelial cells of RWM. However, the PMs were unable to cross the tight junction of the epithelial layer of the RWM and certain amount of them failed to pass through the cellular membrane when they were administered via topical RWM surface delivery or transtympanic injection. Variable transport efficacies of different agents across the RWM have been reported in the literature. Topical RWM surface administration of gadolinium results in poor loading of the nanoparticles in rat inner ear as shown by in vivo magnetic resonance imaging (MRI) (Zou et al., 2010a). However, transtympanic injection of PEGylated liposome nanocarriers encapsulating Gd-DOTA passed through the RWM efficiently in vivo as determined by the Gd-DOTA MRI signal in the inner ear (Zou et al.,

2010b). The variable efficacies of different substances in crossing the middle-inner ear barriers may be dependent on the surface characteristics of the nanostructures.

As shown by a histological study in rats, the annular ligament across the stapedio-vestibular joint is a porous structure (Ohashi et al., 2008). This structure is more permeable to gadolinium than the RWM as determined by MRI studies (Zou et al., 2005; 2010a; 2011b). However, no difference was observed in the transport of liposome nanoparticles between the oval window and the RWM as shown by an in vivo MRI study using gadolinium as an imaging tag (Zou et al., 2010b).

Both transtympanic injection and topical RWM application failed to introduce the PMs into the spiral ganglion or Corti's organ. Transtympanic injection was more efficient in delivering PMs into the vestibulum than topical RWM surface administration, even though it was not superior to topical RWM application in terms of delivery into the cochlea. Cochleostomy is the most efficient method to deliver PMs into these locations. However cochleostomy is more traumatic than the other two methods. This method may contribute to the development of new strategies for the deliver therapeutics directly to the inner ear using modifications to existing cochlear implants.

### 6.2.3 Potential pathways of nanocarriers within the inner ear

Following entry into the perilymph through the RWM, the nanocarriers may enter the modiolus by way of openings on the modiolar wall of the SV and ST. The carriers are also penetrating to the SLFs through the mesothelial sheet of the SL facing the ST (Fig. 3) (Rask-Andersen et al., 2006; Zou et al., 2008). Nanocarriers may subsequently migrate within the modiolus and the lateral wall, reaching the higher turns of the cochlea (Salt et al., 2005; Zou et al., 2009). In the SL, the nanocarriers may initially be internalized by type III and IV SLFs through openings on the mesothelial cells that pave the SL in the ST (Fig. 9 B and C) and then be transported along the SL. In the study of PMs delivered via cochleostomy, the PMs were detected in the contralateral cochlea, suggesting that the PMs may pass through the cochlear aqueduct (Hofman et al., 2005); this was conclusively demonstrated in an in vivo MRI study (Zou et al., 2003a).

### 6.2.4 Peptide functionalization of the polymersomes

#### 6.2.4.1 TAT-functionalized polymersomes

Because the PMs diffuse in perilymph to target the cochlear cells, more intense PMs in cochlear cells indicates more PMs pass through the RWM and then presented in the perilymph. It has been reported that the TAT peptide allows nanocarriers to cross the epithelial monolayer via a transcellular pathway (Koch et al., 2005; Lindgren et al., 2004).

We suppose that the TAT-PMs also pass through the RWM by similar mechanism. Under traumatic circumstances, the penetration ability of TAT-conjugates was enhanced (Simon et al., 2010a; Simon et al., 2010c).

### 6.2.4.2 Targeting of the Tet1-PMs to axons

The Tet1-PMs and the control PMs were observed in SGSCs identified by S100 immunostaining. Tet1-PMs were detected in nerve fibers in the TSF region as determined by NF-200 immunostaining, but they were not observed in the neuronal soma. This may be because of 1) the SGCs are enclosed by SGSCs, and there is poor communication between these cells; 2) The Tet1-PMs were internalized by distal axon compartments of SGCs, which can not be transported to the cell body compartment (Cui et al., 2007; Vance et al., 1991).

Even though the free DiI can also be internalized by neurons (Sharma et al., 2000), the DiI was encapsulated in the PMs in the present study. In addition, the two control PMs, ScrTet1-PMs and unlabelled PMs, were not detected in the CN fibers. Furthermore based on our unpublished result, passing through the RWM did not destroy the liposome structure and the loaded Gd was not leaked out demonstrated by electronic microscopy. The structure of PMs is stronger than liposomes, so we suspect that passing through RWM do not destroy the structure of the PMs.

## 6.2.5 Toxicity study of lipid nanocapsules in rat inner ear

### 6.2.5.1 Hearing impairment

A threshold shift was observed at D0 in both LNC-treated and untreated groups. The $interval_{peakI\text{-}II}$ at 50 dB SPL was also prolonged at D0. Both the threshold shift and the $interval_{peakI\text{-}II}$ was recovered at D7 and remained stable during the four-week test period. The instant hearing impairment may be caused by trauma to the middle ear during operation.

Ribbon synapses consist of vesicles tethered by fine filaments in IHCs and vestibular hair cells of the inner ear and in photoreceptors and bipolar cells of the retina (Nouvian et al., 2006; Zenisek et al., 2004). The number of ribbon synapse is related to the sensitivity of the mammalian cochlea (Meyer, 2009). Synaptophysin is located at the efferent nerve endings that innervate OHCs and IHCs. It is an important synaptic protein for hair cell physiology and often disintegrates prior to hair cell death (Bartolome et al., 2009). Ribbon synapses and synaptophysin are two necessary parameters to verify any potential contribution of hair cell toxicity to the observed threshold shift. The ribbon synapses of IHCs were quantified and the synaptophysin morphology in both IHCs and OHCs was

evaluated at D0 (2 hours following LNC administration). In this study, LNC treatment did not alter the number of ribbon synapses or the expression pattern of synaptophysin. The threshold shift detected in animals following surgery may have been caused by trauma to the middle ear.

### 6.2.5.2 Inner ear neural elements

Neurofilament 200 (NF-200) is a marker for myelinated afferent neurons, and it is a structural protein of peripheral and central axons and plays a role in axonal transport (Hoffman, 1975; Miller, 2002). NF-200 absence or degradation occurred in many neurodegenerative diseases (Hwang, 2005; Posmantur, 1994; Posmantur, 2000). After LNC treatment, neurofilaments innervating IHCs and OHCs were well preserved. In SGCs and CN in osseous spiral canal, NF-200 levels were lower than the untreated control, whereas, hearing of the rats was not affected at D28. These changes need to be verified in future investigations.

S-100 is a marker of SGSCs. It was detected in inner sulcus cells, inner phalangeal cells, SL, spiral limbus, and intermediate cells of inner ear (Hurley et al., 2007). In this study S-100 was also observed in Deiters' cells, SGSCs, and the CN. S-100 is extensively expressed in the nucleus and moderately expressed in cytoplasm. Distribution of S-100 was not affected by LNC treatment, but the immunostaining intensities in Deiter's cells, SGSCs and SLFs of the LNC-treated rats were decreased compare to the untreated group. The mechanism needs further investigation. Pathologic level of S100 protein leads to sustained activation, cell death and disease (Heizmann, CW 2005). However, the decreased secretion of S100 proteins observed in the present study can rule out the potential pathological response which needs to be investigated in the future.

### 6.2.5.3 Morphological results and cell viability detection

TUNEL staining detects DNA breaks caused by apoptosis, late necrosis and autolysis (Gold, 1994). TUNEL-positive staining was observed in the normal inner ear in strial marginal cells, interdental cells, the epithelial cells of SSCs, IHCs and OHCs; this TUNEL-positive staining is due to autolysis that occurred during fixation (Nishizaki et al., 1999). In this study, the TUNEL-positive staining pattern in the untreated cochleae was similar to that observed in other reports. Furthermore, there was no difference in TUNEL staining between the LNC-treated and untreated samples, indicating that LNC treatment do not induce cell death in the inner ear.

## 6.3 Future perspectives

Future work should concentrate on the use of LNCs and PMs as carriers of drugs or genes to cure inner ear diseases. Furthermore, to reduce adverse effects, specific targeting of the drug- or gene-loaded LNCs and PMs using functional peptides should be investigated and comparison of general administration routes and the specific targeting routes of the drugs or genes needs to be performed.

# 7. SUMMARY AND CONCLUSIONS

The purposes of the present study were: 1) to evaluate the delivery efficacy of PMs into the inner ear by different methods; 2) facilitating the outcome of the cell-penetrating peptide-TAT; 3) determining the in vivo targetability of Tet1 peptide-functionalized PMs; and 4) examining the distribution and biocompatibility of LNCs in the rat inner ear.

The following primary conclusions can be drawn from the results of the present studies:

1. Autofluorescence can be observed using confocal microscopy in rat inner ear, and $CuSO_4$ can quench the autofluorescence without affecting the visualization of the PMs.

2. PMs can pass through the intact RWM and be internalized by the inner ear cells. Different PM delivery methods resulted in different distribution patterns in the inner ear cells. Cochleostomy was most efficient delivery method. Transtympanic injection induced more PM internalization in the vestibulum than did topical RWM delivery.

3. TAT-PMs exhibited more transportation through the RWM and internalization by inner ear cells than did the scrambled or unlabeled PMs, indicating that the TAT peptide increased penetration of the PMs through the RWM. In the second set of experiments, auditory nerve targeting of Tet1-PMs administered via cochleostomy was observed, conclusively demonstrating that the Tet1 peptide facilitated neuronal targeting of the PMs.

4. LNCs can pass through the RWM and can be internalized by the inner ear cells, and no evidence of toxicity was detected in the *in vivo* study.

# ACKNOWLEDGEMENTS

This study was performed at the Otolaryngology Department of Medical School of University of Tampere.

I wish to express my sincere and deepest appreciation to my principal supervisors Docent Jing Zou and Professor Ilmari Pyykkö, whose support, guidance, knowledgeable advice and gentle encouragement allowed me to efficiently and confidently complete my postgraduate study in Otolaryngology at the Medical School of University of Tampere. At the same time, my supervisors inspired me to think in a scientific manner. I have been studying with Docent Jing Zou for several years; he guided me on my transition from a layman into a student of the ENT field. Professor Ilmari Pyykkö guides me in a humorous, open minded and tolerant way, which gives me more confidence in achieving the goals of my study in otolaryngological science.

I wish to thank the official reviewers of the thesis, Professor Jyrki Heino from University of Turku and Docent Varpu Marjomäki from University of Jyväskylä, for their constructive expertise. I grateful to Professor Seppo Parkkila from Tampere University and Associate Professor Dennis Poe from Harvard University for participating in the supervisory committee of this thesis.

I have been very lucky to work with magnificent colleagues and co-workers from our EU partners. They helped me a great deal during these years, and we have had happy times during our collaboration. I want to send my warmest thanks to Dr. Tracey Newman and Dr. Alexander Johnston of the University of Southampton in the UK for their enthusiastic cooperation, their contribution of the PEG-b-PCL polymersomes and for providing helpful ideas for the original publications. I am also very grateful to Professor Patrick Saulnier and Dr. Thomas Perrier from Inserm U646 at the University of Angers in France for their passionate work in providing the lipid nanocapsules (LNCs). I am very grateful to Dr. Marian Löebler and Dr. Klaus-Peter Schmitz from the University of Rostock in Germany for their significant contribution to the original publication. I wish to thank my colleague Dr. Elena Surovtseva and my previous colleagues for the co-work in the ‘Nanoear’ project over these years. I also want to thank my husband Weikai Zhang, who is also my colleague, for his support and collaboration during these years.

The support of my family makes my professional and personal life more colorful and rewarding. I wish to express my gratitude to my family membranes.

This study was financially supported by the European Community 6th Framework Programme on Research, Technological Development and Demonstration

(Nanotechnology-based Targeted Drug Delivery. Contract number: NMP4-CT-2006-026556, Project acronym: NANOEAR).

*Tampere, August 2011*

*Ya Zhang*

# REFERENCES


Aarnisalo AA, Aarnisalo P, Pietola L, Wahlfors J, Jero J (2006) Efficacy of gene transfer through the round window membrane: an in vitro model. ORL J Otorhinolaryngol Relat Spec 68:220-227

Abdel-Mottaleb MM, Neumann D, Lamprecht A (2010) In vitro drug release mechanism from lipid nanocapsules (LNC). Int J Pharm 390:208-213

Adams ML, Lavasanifar A, Kwon GS (2003) Amphiphilic block copolymers for drug delivery. J Pharm Sci 92:1343-1355

Agterberg MJ, Versnel H, van Dijk LM, de Groot JC, Klis SF (2009) Enhanced survival of spiral ganglion cells after cessation of treatment with brain-derived neurotrophic factor in deafened guinea pigs. J Assoc Res Otolaryngol 10:355-367

Ahmed F, Discher DE (2004) Self-porating polymersomes of PEG-PLA and PEG-PCL: hydrolysis-triggered controlled release vesicles. J Control Release 96:37-53

Ballot S, Noiret N, Hindré F, Denizot B, Garin E, Rajerison H, Benoit JP (2006) 99mTc/188Re-labelled lipid nanocapsules as promising radiotracers for imaging and therapy: formulation and biodistribution. Eur J Nucl Med Mol Imaging 33:602-607

Baoum A, Xie SX, Fakhari A, Berkland C (2009) "Soft" calcium crosslinks enable highly efficient gene transfection using TAT peptide. Pharm Res 26:2619-2629

Béduneau A, Hindré F, Clavreul A, Leroux JC, Saulnier P, Benoit JP (2008) Brain targeting using novel lipid nanovectors. J Control Release 126:44-49

Béduneau A, Saulnier P, Anton N, Hindré F, Passirani C, Rajerison H, Noiret N, Benoit JP (2006) Pegylated nanocapsules produced by an organic solvent-free method: Evaluation of their stealth properties. Pharm Res 23:2190-2199

Béduneau A, Saulnier P, Hindré F, Clavreul A, Leroux JC, Benoit JP (2007) Design of targeted lipid nanocapsules by conjugation of whole antibodies and antibody Fab' fragments. Biomaterials 28:4978-4990

Bowe SN, Jacob A (2010) Round window perfusion dynamics: implications for intracochlear therapy. Curr Opin Otolaryngol Head Neck Surg 18:377-385

Carpenter AM, Muchow D, Goycoolea MV (1989) Ultrastructural studies of the human round window membrane. Arch Otolaryngol Head Neck Surg 115:585-590

Chiang A, Haller JA (2010) Vitreoretinal disease in the coming decade. Curr Opin Ophthalmol 21:197-202

Chiruvolu S, Walker S, Israelachvili J, Schmitt FJ, Leckband D, Zasadzinski JA (1994) Higher order self-assembly of vesicles by site-specific binding. Science 264:1753-1756

Christian NA, Milone MC, Ranka SS, Li G, Frail PR, Davis KP, Bates FS, Therien MJ, Ghoroghchian PP, June CH, Hammer DA (2007) Tat-functionalized near-infrared emissive polymersomes for dendritic cell labeling. Bioconjug Chem 18:31-40

Cornelissen J, Fischer M, Sommerdijk N, Nolte RJM (1998) Helical superstructures from charged Poly(styrene)-Poly(isocyanodipeptide) block copolymers. Science 280:1427-1430

Cui B, Wu C, Chen L, Ramirez A, Bearer EL, Li WP, Mobley WC, Chu S (2007) One at a time, live tracking of NGF axonal transport using quantum dots. Proc Natl Acad Sci U S A 104:13666-13671

Davidoff SN, Sevy JO, Brooks BD, Grainger DW, Brooks AE (2011) Evaluating antibiotic release profiles as a function of polymer coating formulation - biomed 2011. Biomed Sci Instrum 47:46-51

Del Pozo-Rodriguez A, Pujals, S., Delgado, D., Solinis, M.A., Gascon, A.R., Giralt, E., Pedraz, J.L (2009) A proline-rich peptide improves cell transfection of solid lipid nanoparticle-based non-viral vectors. J Control Release 133:52-59

Desai MP, Labhasetwar V, Amidon GL, Levy RJ (1996) Gastrointestinal uptake of biodegradable microparticles: effect of particle size. Pharm Res 13:1838-1845

Discher BM, Won YY, Ege DS, Lee JC, Bates FS, Discher DE, Hammer DA (1999) Polymersomes: tough vesicles made from diblock copolymers. Science 284:1143-1146

Dong X, Mumper RJ (2010) Nanomedicinal strategies to treat multidrug-resistant tumors: current progress. Nanomedicine (Lond) 5:597-615

Endo T, Nakagawa T, Kita T, Iguchi F, Kim TS, Tamura T, Iwai K, Tabata Y, Ito J (2005) Novel strategy for treatment of inner ears using a biodegradable gel. Laryngoscope 115:2016-2020

Engmer C, Laurell G, Bagger-Sjoback D, Rask-Andersen H (2008) Immunodefense of the round window. Laryngoscope 118:1057-1062

Ge X, Jackson RL, Liu J, Harper EA, Hoffer ME, Wassel RA, Dormer KJ, Kopke RD, Balough BJ (2007) Distribution of PLGA nanoparticles in chinchilla cochleae. Otolaryngol Head Neck Surg 137:619-623

Ghoroghchian PP, Lin JJ, Brannon AK, Frail PR, Bates FS (2006a) Quantitative Membrane Loading of Polymer Vesicles. Soft Matter 2:973-980

Ghoroghchian PP, Li G, Levine DH, Davis KP, Bates FS, Hammer DA, Therien MJ (2006b) Bioresorbable Vesicles Formed through Spontaneous Self-Assembly of Amphiphilic Poly(ethylene oxide)-block-polycaprolactone. Macromolecules 39:1673-1675

Gold R, Schmied M, Giegerich G, Breitschopf H, Hartung HP, Toyka KV, Lassmann H (1994) Differentiation between cellular apoptosis and necrosis by the combined use of in situ tailing and nick translation techniques. Lab Invest 71:219-225

Gouanvé F, Schuster T, Allard E, Méallet-Renault R, Larpent C (2007) Fluorescence Quenching upon Binding of Copper Ions in Dye-Doped and Ligand-Capped Polymer Nanoparticles: A Simple Way to Probe the Dye Accessibility in Nano-Sized Templates. Adv. Funct. Mater. 17:2746–2756

Goycoolea MV, Lundman L (1997) Round window membrane. Structure function and permeability: a review. Microsc Res Tech 36:201-211

Halperin A (1999) Polymer Brushes that Resist Adsorption of Model Proteins: Design Parameters. Langmuir 15:2525-2533

Haralampus-Grynaviski NM, Lamb LE, Clancy CM, Skumatz C, Burke JM, Sarna T, Simon JD (2003) Spectroscopic and morphological studies of human retinal lipofuscin granules. Proc Natl Acad Sci U S A 100:3179-3184

Harush-Frenkel O, Debotton N, Benita S, Altschuler Y (2007) Targeting of nanoparticles to the clathrin-mediated endocytic pathway. Biochem Biophys Res Commun 353:26-32

Heizmann CW (2005) The importance of calcium-binding proteins in childhood diseases. J Pediatr 147:731-738

Hellstrom S, Johansson U, Anniko M (1989) Structure of the round window membrane. Acta Otolaryngol Suppl 457:33-42

Herce HD, Garcia AE (2007) Molecular dynamics simulations suggest a mechanism for translocation of the HIV-1 TAT peptide across lipid membranes. Proc Natl Acad Sci U S A 104:20805-20810

Hoarau D, Delmas P, David S, Roux E, Leroux JC (2004) Novel long-circulating lipid nanocapsules. Pharm Res 21:1783-1789

Hoffman PN, Lasek RJ (1975) The slow component of axonal transport. Identification of major structural polypeptides of the axon and their generality among mammalian neurons. J Cell Biol 66:351-366

Horie RT, Sakamoto T, Nakagawa T, Ishihara T, Higaki M, Ito J (2011) Stealth-nanoparticle strategy for enhancing the efficacy of steroids in mice with noise-induced hearing loss. Nanomedicine (Lond) 5:1331-1340

Horie RT, Sakamoto T, Nakagawa T, Tabata Y, Okamura N, Tomiyama N, Tachibana M, Ito J (2010) Sustained delivery of lidocaine into the cochlea using poly lactic/glycolic acid microparticles. Laryngoscope 120:377-383

Hurley PA, Crook JM, and Shepherd RK (2007) Schwann cells revert to non-myelinating phenotypes in the deafened rat cochlea. Eur J Neurosci 26:1813-21.

Hureaux J, Lagarce F, Gagnadoux F, Clavreul A, Benoit JP, Urban T (2009) The adaptation of lipid nanocapsule formulations for blood administration in animals. Int J Pharm 379:266-269

Huynh NT, Passirani C, Saulnier P, Benoit JP (2009) Lipid nanocapsules: a new platform for nanomedicine. Int J Pharm 379:201-209

Hwang IK, Koh US, Lee JC, Yoo KY, Song JH, Jung JY, Nam YS, Lee IS, Kang TC, Won MH (2005) Transient ischemia-induced changes of neurofilament 200 kDa immunoreactivity and protein content in the main olfactory bulb in gerbils. J Neurol Sci 239:59-66

Jager E, Venturini CG, Poletto FS, Colome LM, Pohlmann JP, Bernardi A, Battastini AM, Guterres SS, Pohlmann AR (2009) Sustained release from lipid-core nanocapsules by varying the core viscosity and the particle surface area. J Biomed Nanotechnol 5:130-140

Jain JP, Kumar N (2010) Self assembly of amphiphilic (PEG)(3)-PLA copolymer as polymersomes: preparation, characterization, and their evaluation as drug carrier. Biomacromolecules 11:1027-1035

Jain S, Bates FS (2003) On the origins of morphological complexity in block copolymer surfactants. Science 300:460-464

Jero J, Mhatre AN, Tseng CJ, Stern RE, Coling DE, Goldstein JA, Hong K, Zheng WW, Hoque AT, Lalwani AK (2001) Cochlear gene delivery through an intact round window membrane in mouse. Hum Gene Ther 12:539-548

Jiang X, Musyanovych A, Rocker C, Landfester K, Mailander V, Nienhaus GU (2011) Specific effects of surface carboxyl groups on anionic polystyrene particles in their interactions with mesenchymal stem cells. Nanoscale 3:2028-2035

Kikugawa K, Beppu M, Sato A, Kasai H (1997) Separation of multiple yellow fluorescent lipofuscin components in rat kidney and their characterization. Mech Ageing Dev 97:93-107

Kim KD, Wright NM (2011) Polyethylene Glycol (PEG) Hydrogel Spinal Sealant (DuraSeal Spinal Sealant) as an Adjunct to Sutured Dural Repair in the Spine: Results of a Prospective, Multicenter, Randomized Controlled Study. Spine (Phila Pa 1976) 36:1906-1912

Kim SY, Lee YM, Baik DJ, Kang JS (2003) Toxic characteristics of methoxy poly(ethylene glycol)/poly(epsilon-caprolactone) nanospheres; in vitro and in vivo studies in the normal mice. Biomaterials 24:55-63

Kitamura Y, Teranishi M, Sone M, Nakashima T (2002) Round window membrane in young and aged C57BL/6 mice. Hear Res 174:142-148

Koch AM, Reynolds F, Merkle HP, Weissleder R, Josephson L (2005) Transport of surface-modified nanoparticles through cell monolayers. Chembiochem 6:337-345

Konishi M, Kawamoto K, Izumikawa M, Kuriyama H, Yamashita T (2008) Gene transfer into guinea pig cochlea using adeno-associated virus vectors. J Gene Med 10:610-618

Kopke RD, Wassel RA, Mondalek F, Grady B, Chen K, Liu J, Gibson D, Dormer KJ (2006) Magnetic nanoparticles: inner ear targeted molecule delivery and middle ear implant. Audiol Neurootol 11:123-133

Kreuter J, Alyautdin RN, Kharkevich DA, Ivanov AA (1995) Passage of peptides through the blood-brain barrier with colloidal polymer particles (nanoparticles). Brain Res 674:171-174

Kwon EJ, Lasiene J, Jacobson BE, Park IK, Horner PJ, Pun SH (2010) Targeted nonviral delivery vehicles to neural progenitor cells in the mouse subventricular zone. Biomaterials 31:2417-2424

Lalwani AK, Han JJ, Walsh BJ, Zolotukhin S, Muzyczka N, Mhatre AN (1997) Green fluorescent protein as a reporter for gene transfer studies in the cochlea. Hear Res 114:139-147

Lamprecht A, Bouligand Y, Benoit JP (2002) New lipid nanocapsules exhibit sustained release properties for amiodarone. J Control Release 84:59-68

Laurell G, Teixeira M, Sterkers O, Bagger-Sjoback D, Eksborg S, Lidman O, Ferrary E (2002) Local administration of antioxidants to the inner ear. Kinetics and distribution(1). Hear Res 173:198-209

Lee JC, Bermudez H, Discher BM, Sheehan MA, Won YY, Bates FS, Discher DE (2001) Preparation, stability, and in vitro performance of vesicles made with diblock copolymers. Biotechnol Bioeng 73:135-145

Li S, Byrne B, Welsh J, Palmer AF (2007) Self-assembled poly(butadiene)-b-poly(ethylene oxide) polymersomes as paclitaxel carriers. Biotechnol Prog 23:278-285

Lindgren ME, Hallbrink MM, Elmquist AM, Langel U (2004) Passage of cell-penetrating peptides across a human epithelial cell layer in vitro. Biochem J 377:69-76

Liu G, Ma S, Li S, Cheng R, Meng F, Liu H, Zhong Z (2010) The highly efficient delivery of exogenous proteins into cells mediated by biodegradable chimaeric polymersomes. Biomaterials 31:7575-7585

Liu JK, Teng Q, Garrity-Moses M, Federici T, Tanase D, Imperiale MJ, Boulis NM (2005) A novel peptide defined through phage display for therapeutic protein and vector neuronal targeting. Neurobiol Dis 19:407-418

Luebke AE, Foster PK, Muller CD, Peel AL (2001) Cochlear function and transgene expression in the guinea pig cochlea, using adenovirus- and adeno-associated virus-directed gene transfer. Hum Gene Ther 12:773-781

Lundman L, Juhn SK, Bagger-Sjoback D, Svanborg C (1992) Permeability of the normal round window membrane to Haemophilus influenzae type b endotoxin. Acta Otolaryngol 112:524-529

Maguchi S, Gasa S, Matsushima J, Saga Y, Kawano M, Makita A (1991) Glycolipids in rat cochlea. Auris Nasus Larynx 18:1-8

Mahmud A, Lavasanifar A (2005) The effect of block copolymer structure on the internalization of polymeric micelles by human breast cancer cells. Colloids Surf B Biointerfaces 45:82-89

Manil L, Roblot-Treupel L, Couvreur P (1986) Isobutyl cyanoacrylate nanoparticles as a solid phase for an efficient immunoradiometric assay. Biomaterials 7:212-216

Maria Visitación Bartolome PZ, Francisco Carricondo, Pablo Gil-Loyzaga (2009) Immunocytochemical detection of synaptophysin in C57BL/6 mice cochlea during aging process. Brain Res Rev 60:341-348

Maupas C, Moulari B, Béduneau A, Lamprecht A, Pellequer Y (2011) Surfactant dependent toxicity of lipid nanocapsules in HaCaT cells. Int J Pharm 411:136-141

Meyer AC, Frank T, Khimich D, Hoch G, Riedel D, Chapochnikov NM, Yarin YM, Harke B, Hell SW, Egner A, Moser T (2009) Tuning of synapse number, structure and function in the cochlea. Nat Neurosci 12:444-453

Miller CC, Ackerley S, Brownlees J, Grierson AJ, Jacobsen NJ, Thornhill P (2002) Axonal transport of neurofilaments in normal and disease states. Cell Mol Life Sci 59:323-330

Moss OR (2006) Insights into the health effects of nanoparticles: why numbers matter. CIIT Activaties 26:1-8

Mynatt R, Hale SA, Gill RM, Plontke SK, Salt AN (2006) Demonstration of a longitudinal concentration gradient along scala tympani by sequential sampling of perilymph from the cochlear apex. J Assoc Res Otolaryngol 7:182-193

Niu D, Ma Z, Li Y, Shi J (2010) Synthesis of core-shell structured dual-mesoporous silica spheres with tunable pore size and controllable shell thickness. J Am Chem Soc 132:15144-15147

Nouvian R, Beutner D, Parsons TD, Moser T (2006) Structure and function of the hair cell ribbon synapse. J Membr Biol 209:153-165

Oba M, Aoyagi K, Miyata K, Matsumoto Y, Itaka K, Nishiyama N, Yamasaki Y, Koyama H, Kataoka K (2008) Polyplex micelles with cyclic RGD peptide ligands and disulfide cross-links directing to the enhanced transfection via controlled intracellular trafficking. Mol Pharm 5:1080-1092

Ohashi M, Ide S, Kimitsuki T, Komune S, Suganuma T (2006) Three-dimensional regular arrangement of the annular ligament of the rat stapediovestibular joint. Hear Res 213:11-16

Ohashi M, Ide S, Sawaguchi A, Suganuma T, Kimitsuki T, Komune S (2008) Histochemical localization of the extracellular matrix components in the annular ligament of rat stapediovestibular joint with special reference to fibrillin, 36-kDa microfibril-associated glycoprotein (MAGP-36), and hyaluronic acid. Med Mol Morphol 41:28-33

Paasche G, Bögel L, Leinung M, Lenarz T, Stöver T (2006) Substance distribution in a cochlea model using different pump rates for cochlear implant drug delivery electrode prototypes. Hear Res 212:74-82

Panyam J, Zhou WZ, Prabha S, Sahoo SK, Labhasetwar V (2002) Rapid endo-lysosomal escape of poly(DL-lactide-co-glycolide) nanoparticles: implications for drug and gene delivery. Faseb J 16:1217-1226

Park IK, Lasiene J, Chou SH, Horner PJ, Pun SH (2007) Neuron-specific delivery of nucleic acids mediated by Tet1-modified poly(ethylenimine). J Gene Med 9:691-702

Petros RA, DeSimone JM (2010) Strategies in the design of nanoparticles for therapeutic applications. Nat Rev Drug Discov 9:615-627

Plontke SK, Biegner T, Kammerer B, Delabar U, Salt AN (2008) Dexamethasone concentration gradients along scala tympani after application to the round window membrane. Otol Neurotol 29:401-406

Posmantur R, Hayes RL, Dixon CE, Taft WC (1994) Neurofilament 68 and neurofilament 200 protein levels decrease after traumatic brain injury. J Neurotrauma 11:533-545

Posmantur RM, Newcomb JK, Kampfl A, Hayes RL (2000) Light and confocal microscopic studies of evolutionary changes in neurofilament proteins following cortical

impact injury in the rat. Exp Neurol 161:15-26

Praetorius M, Brunner C, Lehnert B, Klingmann C, Schmidt H, Staecker H, Schick B (2007) Transsynaptic delivery of nanoparticles to the central auditory nervous system. Acta Otolaryngol 127:486-490

Pyykkö I, Zou J, Poe D, Nakashima T, Naganawa S (2010) Magnetic resonance imaging of the inner ear in Meniere's disease. Otolaryngol Clin North Am 43:1059-1080

Rafat M, Cleroux CA, Fong WG, Baker AN, Leonard BC, O'Connor MD, Tsilfidis C (2010) PEG-PLA microparticles for encapsulation and delivery of Tat-EGFP to retinal cells. Biomaterials 31:3414-3421

Rask-Andersen H, Schrott-Fischer A, Pfaller K, Glueckert R (2006) Perilymph/modiolar communication routes in the human cochlea. Ear Hear 27:457-465

Robey AB, Morrow T, Moore GF (2010) Systemic side effects of transtympanic steroids. Laryngoscope 120 Suppl 4:S217

Roy S, Johnston AH, Newman TA, Glueckert R, Dudas J, Bitsche M, Corbacella E, Rieger G, Martini A, Schrott-Fischer A (2010) Cell-specific targeting in the mouse inner ear using nanoparticles conjugated with a neurotrophin-derived peptide ligand: potential tool for drug delivery. Int J Pharm 390:214-224

Ruben S, Perkins A, Purcell R, Joung K, Sia R, Burghoff R, Haseltine WA, Rosen CA (1989) Structural and functional characterization of human immunodeficiency virus tat protein. J Virol 63:1-8

Ryu JK, Shin WH, Kim J, Joe EH, Lee YB, Cho KG, Oh YJ, Kim SU, Jin BK (2002) Trisialoganglioside GT1b induces in vivo degeneration of nigral dopaminergic neurons: role of microglia. Glia 38:15-23

Saber A, Laurell G, Bramer T, Edsman K, Engmer C, Ulfendahl M (2009) Middle ear application of a sodium hyaluronate gel loaded with neomycin in a Guinea pig model. Ear Hear 30:81-89

Sahay G, Batrakova EV, Kabanov AV (2008) Different internalization pathways of polymeric micelles and unimers and their effects on vesicular transport. Bioconjug Chem 19:2023-2029

Salt AN, Ma Y (2001) Quantification of solute entry into cochlear perilymph through the round window membrane. Hear Res 154:88-97

Salt AN, Ohyama K, Thalmann R (1991) Radial communication between the perilymphatic scalae of the cochlea. II: Estimation by bolus injection of tracer into the sealed cochlea. Hear Res 56:37-43

Salt AN, Plontke SK (2005) Local inner-ear drug delivery and pharmacokinetics. Drug Discov Today 10:1299-1306

Santi PA, Mancini P, Barnes C (1994) Identification and localization of the GM1 ganglioside in the cochlea using thin-layer chromatography and cholera toxin. J Histochem Cytochem 42:705-716

Scheper V, Wolf M, Scholl M, Kadlecova Z, Perrier T, Klok HA, Saulnier P, Lenarz T, Stöver T (2009) Potential novel drug carriers for inner ear treatment: hyperbranched polylysine and lipid nanocapsules. Nanomedicine (Lond) 4:623-635

Sharma K, Leonard AE, Lettieri K, Pfaff SL (2000) Genetic and epigenetic mechanisms contribute to motor neuron pathfinding. Nature 406:515-519

Sheikh KA, Deerinck TJ, Ellisman MH, Griffin JW (1999) The distribution of ganglioside-like moieties in peripheral nerves. Brain 122:449-460

Shepherd RK, Xu J (2002) A multichannel scala tympani electrode array incorporating a drug delivery system for chronic intracochlear infusion. Hear Res 172:92-98

Silhol M, Tyagi M, Giacca M, Lebleu B, Vives E (2002) Different mechanisms for cellular internalization of the HIV-1 Tat-derived cell penetrating peptide and recombinant proteins fused to Tat. Eur J Biochem 269:494-501

Simon MJ, Kang WH, Gao S, Banta S, Iii BM (2010) TAT Is Not Capable of Transcellular Delivery Across an Intact Endothelial Monolayer In Vitro. Ann Biomed Eng 39:394-401

Simon MJ, Kang WH, Gao S, Banta S, Morrison B (2010) Increased delivery of TAT across an endothelial monolayer following ischemic injury. Neurosci Lett 486:1-4

Song WJ, Du JZ, Sun TM, Zhang PZ, Wang J (2009) Gold Nanoparticles Capped with Polyethyleneimine for Enhanced siRNA Delivery. Small 6:239-246

Staecker H, Praetorius M, Brough DE (2011) Development of gene therapy for inner ear disease: Using bilateral vestibular hypofunction as a vehicle for translational research. Hear Res 276:44-51

Stöver T, Yagi M, Raphael Y (2000). Transduction of the contralateral ear after adenovirus-mediated cochlear gene transfer. Gene Ther 7:377-83

Stöver T, Kawamoto K, Kanzaki S, Raphael Y (2001) Feasibility of inner ear gene transfer after middle ear administration of an adenovirus vector. Laryngorhinootologie 80:431-435

Suzuki M, Yamasoba T, Suzukawa K, Kaga K (2003) Adenoviral vector gene delivery via the round window membrane in guinea pigs. Neuroreport 14:1951-1955

Swan EE, Mescher MJ, Sewell WF, Tao SL, Borenstein JT (2008) Inner ear drug delivery for auditory applications. Adv Drug Deliv Rev 60:1583-1599

Takahashi H, Sando I (1992) Three-dimensional surgical anatomy for stapes surgery computer-aided reconstruction and measurement. Laryngoscope 102:1159-1164

Tamaki Y (2009) Prospects for nanomedicine in treating age-related macular degeneration. Nanomedicine (Lond) 4:341-352

Tamura T, Kita T, Nakagawa T, Endo T, Kim TS, Ishihara T, Mizushima Y, Higaki M, Ito J (2005) Drug delivery to the cochlea using PLGA nanoparticles. Laryngoscope 115:2000-2005

Tan BT, Foong KH, Lee MM, Ruan R (2008) Polyethylenimine-mediated cochlear gene transfer in guinea pigs. Arch Otolaryngol Head Neck Surg 134:884-891

Thaler M, Roy S, Fornara A, Bitsche M, Qin J, Muhammed M, Salvenmoser W, Rieger G, Fischer AS, Glueckert R (2011) Visualization and analysis of superparamagnetic iron oxide nanoparticles in the inner ear by light microscopy and energy filtered TEM. Nanomedicine 7:360-369

Torchilin VP (2007) Tatp-mediated intracellular delivery of pharmaceutical nanocarriers. Biochem Soc Trans 35:816-820

Ulfendahl M, Scarfone E, Flock A, Le Calvez S, Conradi P (2000) Perilymphatic fluid compartments and intercellular spaces of the inner ear and the organ of Corti. Neuroimage

12:307-313

Vance JE, Pan D, Vance DE, Campenot RB (1991) Biosynthesis of membrane lipids in rat axons. J Cell Biol 115:1061-1068

Vives E, Brodin P, Lebleu B (1997) A truncated HIV-1 Tat protein basic domain rapidly translocates through the plasma membrane and accumulates in the cell nucleus. J Biol Chem 272:16010-16017

Vonarbourg A, Passirani C, Desigaux L, Allard E, Saulnier P, Lambert O, Benoit JP, Pitard B (2009) The encapsulation of DNA molecules within biomimetic lipid nanocapsules. Biomaterials 30:3197-3204

Wadia JS, Stan RV, Dowdy SF (2004) Transducible TAT-HA fusogenic peptide enhances escape of TAT-fusion proteins after lipid raft macropinocytosis. Nat Med 10:310-315

Wang H, Murphy R, Taaffe D, Yin S, Xia L, Hauswirth WW, Bance M, Robertson GS, Wang J (2011) Efficient cochlear gene transfection in guinea-pigs with adeno-associated viral vectors by partial digestion of round window membrane. Gene Ther (doi:10.1038/gt.2011.91)

Yan X, Lei Z (2011) Silicon dioxide hollow microspheres with porous composite structure: Synthesis and characterization. J Colloid Interface Sci. 362(2):253-260

Zenisek D, Horst, N. K., Merrifield, C., Sterling, P., and Matthews, G. (2004) Visualizing synaptic ribbons in the living cell. J Neurosci 24:9752-9759

Zhang W, Zhang Y, Löbler M, Schmitz KP, Ahmad A, Pyykkö I, Zou J (2011) Nuclear entry of hyperbranched polylysine nanoparticles into cochlear cells. Int J Nanomedicine 6:535-546

Zhang Y, Schlachetzki F, Zhang YF, Boado RJ, Pardridge WM (2004) Normalization of striatal tyrosine hydroxylase and reversal of motor impairment in experimental parkinsonism with intravenous nonviral gene therapy and a brain-specific promoter. Hum Gene Ther 15:339-350

Zhang Y, Zhang W, Löbler M, Schmitz KP, Saulnier P, Perrier T, Pyykkö I, Zou J (2011) Inner ear biocompatibility of lipid nanocapsules after round window membrane application. Int J Pharm 404:211-219

Zheng C, Qiu L, Zhu K (2009) Novel polymersomes based on amphiphilic graft polyphosphazenes and their encapsulation of water-soluble anti-cancer drug. Polymer 50:1173-1177

Zou J, Pyykkö I, Bjelke B, Dastidar P, Toppila E (2005) Communication between the perilymphatic scalae and spiral ligament visualized by in vivo MRI. Audiol Neurootol 10:145-152

Zou J, Sood R, Ranjan S, Poe D, Ramadan UA, Kinnunen PK, Pyykkö I (2010a) Manufacturing and in vivo inner ear visualization of MRI traceable liposome nanoparticles encapsulating gadolinium. J Nanobiotechnology 8:32

Zou J, Poe D, Bjelke B, Pyykkö I (2009) Visualization of inner ear disorders with MRI in vivo: from animal models to human application. Acta Otolaryngol Suppl:22-31

Zou J, Pyykkö I, Counter SA, Klason T, Bretlau P, Bjelke B (2003a). In vivo observation of dynamic perilymph formation using 4.7 T MRI with gadolinium as a tracer. Acta Otolaryngol 123, 910-5.

Zou J, Pyykkö I, Counter S, Klason T, Bretlau P, Bjelke B (2003b) In vivo observation of dynamic perilymph formation using 4.7 T MRI with gadolinium as a tracer. Acta Otolaryngol 123:910-915

Zou J, Saulnier P, Perrier T, Zhang Y, Manninen T, Toppila E, Pyykkö I (2008) Distribution of lipid nanocapsules in different cochlear cell populations after round window membrane permeation. J Biomed Mater Res B Appl Biomater 87:10-18

Zou J, Sood R, Ranjan S, Poe D, Ramadan UA, Kinnunen PK, Pyykkö I (2010b) Manufacturing and in vivo inner ear visualization of MRI traceable liposome nanoparticles encapsulating gadolinium. J Nanobiotechnology 8:32

Zou J, Zhang W, Poe D, Qin J, Fornara A, Zhang Y, Ramadan UA, Muhammed M, Pyykkö I (2010c). MRI manifestation of novel superparamagnetic iron oxide nanoparticles in the rat inner ear. Nanomedicine (Lond) 5:739-54

# ROLE IN PUBLICATIONS

I. **Ya Zhang**, Weikai Zhang, Alexander. H. Johnston, Tracey. A. Newman, Ilmari Pyykkö, Jing Zou (2010). *Improving the visualization of fluorescently tagged nanoparticles and fluorophore-labeled molecular probes by treatment with $CuSO_4$ to quench autofluorescence in the rat inner ear*. Hearing Res. 105(4): 120-126.

Contribution: Main designer of this study. Executed experiments, analyzed results and wrote paper.

II. **Ya Zhang**, Weikai Zhang, Alexander. H. Johnston, Tracey. A. Newman, Ilmari Pyykkö, Jing Zou (2011). *Comparison of the distribution pattern of PEG-b-PCL polymersomes delivered into the rat inner ear via different methods*. Acta Oto-laryngol. doi:10.3109/00016489.2011.615066.

Contribution: Performed experiments, analyzed results and wrote paper. Also involved in designing of this study.

III. **Ya Zhang**, Weikai Zhang, Alexander. H. Johnston, Tracey. A. Newman, Ilmari Pyykkö, Jing Zou. *Modified distribution of PEG-b-PCL PMs in the rat cochlea through surface functionalization with TAT and Tet1 peptides*. Manuscript submitted.

Contribution: Performed experiments, analyzed results and wrote the manuscript.

IV**.** Jing Zou, Patrick Saulnier, Thomas Perrier, **Ya Zhang**, Tommi Manninen, Esko Toppila, Ilmari Pyykkö (2008). *Distribution of lipid nanocapsules in different cochlear cell populations after round window membrane permeation*. J Biomed Mater Res B Appl Biomater. 87(1):10-8.

Contribution: Performed experiments and analyzed results. Also involved in writing this paper.

V. **Ya Zhang**, Weikai Zhang, Marian Löbler, Klaus-Peter Schmitz, Patrick Saulnier, Thomas Perrier, Ilmari Pyykkö, Jing Zou (2011). *Inner ear biocompatibility of lipid nanocapsules after round window membrane application*. Int J Phar. 404(1-2): 211-9.

Contribution: Performed experiments, analyzed results and wrote paper. Also involved in designing of this experiment.

- Did not involve in designing and manufacturing of the nanocarriers. All the nanocarriers tested were provided by partners.

# ORIGINAL PUBLICATIONS

Hearing Research 269 (2010) 1–11

Contents lists available at ScienceDirect

Hearing Research

journal homepage: www.elsevier.com/locate/heares

Methodological paper

# Improving the visualization of fluorescently tagged nanoparticles and fluorophore-labeled molecular probes by treatment with $CuSO_4$ to quench autofluorescence in the rat inner ear

Ya Zhang [a], Weikai Zhang [a], Alexander H. Johnston [b], Tracey. A. Newman [b], Ilmari Pyykkö [a], Jing Zou [a,*]

[a] Department of Otolaryngology, University of Tampere, Medical School, FM1, 3rd Floor, Biokatu 6, 33520 Tampere, Finland
[b] School of Biological Sciences, University of Southampton, Southampton SO16 7PX, UK

ARTICLE INFO

*Article history:*
Received 27 January 2010
Received in revised form
9 July 2010
Accepted 14 July 2010
Available online 24 July 2010

ABSTRACT

Fluorescent tags and fluorophore-conjugated molecular probes have been extensively employed in histological studies to demonstrate nanoparticle distribution in inner ear cell populations. However, autofluorescence that exists in the rodent cochleae disturbs visualization of the fluorescent tags and fluorophore labeling. In the present work, we aimed to improve the visualization of fluorescently tagged nanoparticles and fluorophore-labeled molecular probes by treatment with $CuSO_4$ to quench autofluorescence in the rat inner ear. The *in vivo* study was performed on eight- to nine-month-old rats using confocal laser scanning microscopy, and the *in vitro* study was carried out with DiI-tagged poly(ethylene glycol) and poly(capro-lactone) polymersomes and different fluorescent-labeling agents using a spectrofluorometer. The nanoparticles were intratympanically administered using either an osmotic pump or transtympanic injection. Abundant autofluorescence was detected in spiral ganglion cells (SGCs), stria marginal cells, spiral ligament fibrocytes (SL) and the subcuticular cytoplasm of inner hair cells (IHCs). Sparsely distributed faint autofluorescence was also visualized in outer hair cells (OHCs). The autofluorescence was eliminated by treatment with 1 mM $CuSO_4$ (in 0.01 M ammonium acetate buffer) for 70 −90 min, while the fluorescent tag in the nanoparticle was absolutely preserved and the labeling fluorescence signals of the molecular probes were mostly retained.



## 1. Introduction

Hearing loss is a major public health problem that ranks eighth among the most common diseases in the EU. Traditional treatment strategies for sensorineural hearing loss (SNHL) have not been very successful. Bypassing the membranous borders and providing direct contact with cochlear partitions, cochlear implantation is a well-established method to restore the auditory pathway in severe or profound hearing loss. However, hearing performance after implantation is variable due to several factors (El-Hakim et al., 2002; Gantz et al., 1993; Geers et al., 2002; Osberger et al., 2002). Therefore, an ideal treatment for SNHL will depend on novel techniques, such as gene or drug delivery using multifunctional nanoparticles (MFNPs), in addition to cochlear implantation (Pyykko, 2009).

In the Nanoear project, MFNPs were conjugated to several types of fluorescent tags, including Nile red, tetramethylrhodamine isothiocyanate (TRITC), fluorescein isothiocyanate (FITC), and 1,1′-Dioctadecyl-3,3,3′,3′-tetramethyl-indocarbocyanine perchlorate (DiI), for their visualization in the cochlea (Scheper et al., 2009; Zou et al., 2008; Zou et al., 2009a; Zou et al., 2009b). However, the appearance of autofluorescence from lipofuscin granules, which result from the aging process, impairs the detection of the fluorescence signals of the MFNP targets (Feeney, 1978; Haralampus-Grynaviski et al., 2003; Igarashi and Ishii, 1990; Rajawat et al., 2009; Xu et al., 2008). Lipofuscin is widely found in human cochlea (Ishii, 1977; Walther and Westhofen, 2007), chinchilla cochlea (Bohne et al., 1990), guinea pig cochlea (Horner and Guilhaume, 1995) and rat spiral ganglion (Igarashi and Ishii, 1990), which has complicated fluorescent-labeling studies in the inner ear.

*Abbreviations:* DAPI, 4′,6-diamidino-2-phenylindole; DiI, 1,1'-Dioctadecyl-3,3,3′,3′-tetramethyl-indocarbocyanine perchlorate; FITC, fluorescein isothiocyanate; IHC, inner hair cells; NIH3T3, mouse embryonic fibroblast cell line; OHC, outer hair cells; PBS, phosphate buffered saline; SGCs, spiral ganglion cells; SL, spiral ligament; SNHL, sensorineural hearing loss; StrMC, strial marginal cells; StrV, stria vascularis; TRITC, tetramethylrhodamine isothiocyanate.

* Corresponding author. Tel.: +358 3 31164129; fax: +358 3 35517700.
*E-mail address:* jing.zou@uta.fi (J. Zou).

0378-5955/$ – see front matter © 2010 Elsevier B.V. All rights reserved.
doi:10.1016/j.heares.2010.07.006

Lipofuscin is a yellow fluorescent aging pigment that is commonly thought to be an end product of membrane lipid autoxidation, which usually occurs in enteric neurons. In some reports, it has been shown that the bluish fluorescence of the lipofuscin-like granules is generated in tissues during lipid peroxidation, and the yellow fluorescent pigments have been determined to be proteinaceous (Kikugawa et al., 1997). Atomic force microscopy (AFM) of retinal pigment epithelium (RPE) from the human eye has revealed that the surface of the lipofuscin granules is smooth and comprised of substructures that are about 50 nm in diameter and separated by thin boundary layers (Haralampus-Grynaviski et al., 2003).

The emission spectrum of lipofuscin granules involves multiple fluorophores, and its emission maxima range from 612 nm to 513 nm (Haralampus-Grynaviski et al., 2003). Due to its broad excitation/emission spectrum, it overlaps with commonly used fluorophores. Four kinds of distinct fluorescence have been reported in a sodium dodecyl sulfate extract of male Wistar rat kidneys fed normal diets: blue fluorescence with excitation/emission maxima at 360/440 nm, greenish fluorescence at 460/530 nm, yellow fluorescence at 400/620 nm and 580/620 nm. The yellow fluorescence at 400/620 nm accumulates with aging, and its excitation and emission maxima are close to those observed histochemically under a fluorescence microscope (Kikugawa et al., 1997).

The fluorescence of yellow fluorescent lipofuscin can be quenched by ferrous chloride and cupric sulfate ($CuSO_4$) but remains stable upon borohydride treatment (Kikugawa et al., 1997). In previous studies, $CuSO_4$ and Sudan Black B have been used to eliminate autofluorescence from the lipofuscin granules in sections of human, monkey and rat neural tissue as well as in neurofilament-reactive neuron types in human small intestines (Brehmer et al., 2004; Schnell et al., 1999).

In the current study, we investigated the distribution of greenish and yellow autofluorescence in the inner ear cellular populations of adult Sprague–Dawley (SD) rats using confocal laser scanning microscopy. The interference of $CuSO_4$ on the autofluorescence and DiI-tagged poly(ethylene glycol) and poly(capro-lactone) (PEG-PCL) polymersomes and the commonly used labeling fluorophores FITC and TRITC was analyzed using a spectrofluorometer. The visibility of fluorescently tagged nanoparticles and fluorophore-labeled molecular probes was evaluated in the rat inner ear.

## 2. Materials and methods

### 2.1. Manufacturing and characterization of PEG-PCL polymersomes

Anhydrous *N*, *N*-dimethylformamide, poly(ethylene glycol)-*block*-poly(ϵ-capro-lactone) methyl ether, PEG average *M*n ~5000, and PCL average *M*n ~5000 (PEG5K-*b*-PCL5K) was purchased from Sigma–Aldrich (USA). 1,1′-Dioctadecyl-3,3,3′,3′-tetramethylindocarbocyanine perchlorate (DiI) was obtained from Invitrogen. Phosphate buffered saline (PBS) was made using phosphate buffered saline tablets (Oxoid, UK) and $H_2O$ (purified using a Milli-Q Ultrapure Water Purification System [resistance of 18.2 M Ω cm at 25 °C]). Dialysis tubing with a 12–14 kDa cutoff and 6.3 mm diameter was supplied from Medicell International Ltd. (UK). Dynamic light scattering was performed on a Coulter N4 Plus particle sizer using N4 Plus version 1.10 software for data analysis.

A 0.1 mg/mL solution of DiI in anhydrous *N*, *N*-dimethylformamide was prepared. $PEG_{5000}$-*b*-$PCL_{5000}$ (6.0 mg) was dissolved in the DiI-DMF solution (0.4 mL), and the solution was sonicated until complete dissolution. The polymer solution was then added dropwise (~1 drop every 8 s) to PBS (1.60 mL) while stirring. The sample was dialyzed against PBS (400 mL), and the buffer solution was replaced four times over the course of 48 h. Analysis by dynamic light scattering revealed that the typical size of the NPs was 83.5 ± 17.6 nm and that they were stable in solution for at least two weeks.

### 2.2. Impact of fixation on polymersome internalization

In order to evaluate the potential disturbance of free extracellular polymersomes on the observation of internalization during specimen dissection, PEG-PCL polymersome internalization was compared between live and pre-fixed NIH3T3 cells (mouse embryonic fibroblast cell line). NIH3T3 cells were plated into a 4-well Lab-Tek®II Chamber Slide™ System (Nalge Nunc International, Naperville, USA) containing 1.0 ml defined medium/well (Dulbecco's modified eagle's medium supplemented with 10% fetal bovine serum and 1% antibiotic-penicillin/streptomycin solution). The cells were cultured at 37 °C in a $CO_2$ incubator until 85% confluence reached. PCL-PEG polymersomes with 100 fold dilution were added to the medium of either live cells or pre-fixed cells (4% paraformaldehyde, PFA) and incubated for 12 h. After washing with 0.01 M PBS, fixation with 4% PFA (live cells), and staining with 4′,6-diamidino-2-phenylindole (DAPI, 10 μg/ml) for 10 min, the cells were mounted with Fluoromount (Sigma–Aldrich, USA) for confocal microscopy. Each test (live cells and pre-fixed cells) was repeated in 6 wells.

### 2.3. Animals

Sixteen eight- to nine-month-old male SD rats with normal Pryer's reflexes and weighing 600–700 g (supplied by the experimental animal unit, University of Tampere) were used in this study. All were treated in accordance with the directives of the local ethics committee of the University of Tampere (permission: LSLH-2006-4143/Ym23). The left or right bulla of each animal was randomly selected for analysis. Five cochleae were used in the autofluorescence study, five were stained with FITC-conjugated phalloidin, four were stained with TRITC-conjugated phalloidin, and two were stained with an antibody against Neurofilament-200 (the secondary antibody was conjugated with FITC) using whole mounting method. Two cochleae were employed in paraffin embedding, sectioning, and immunostaining with an antibody against Neurofilament-200 (the secondary antibody was conjugated with Alexa Fluor-568). In all of the fluorescence tissue-staining processes, half of each cochlea was treated with $CuSO_4$ and the other half was not treated. Twelve bullae from six rats were used in the *in vivo* investigation of the distribution of PEG-PCL polymersomes in the inner ear and the impact of $CuSO_4$ treatment on the visualization of PEG-PCL polymersomes. The PEG-PCL polymersomes were either applied to the inner ear by osmotic pumps (1003D, Alzet, Canada) for 3 days (6 cochleae) or by transtympanic injection (40 μl) for 3 days (4 cochleae) or 5 days (2 cochleae). The injection volume was defined according to the literature report that an average volume of SD rat middle ear cavity is 42 μl (Kania et al., 2006). All experimental procedures were performed under general anesthesia, induced and maintained by intraperitoneal injections of a mixture of Domitor (1 mg/ml, Domitor, Orion, Finland) and Ketalar (50 mg/ml, Pfizer, UK) (0.6 ml for induction and 0.3 ml for maintenance) (Domitor:Ketalar = 1:2).

### 2.4. Administration of PEG-PCL polymersomes to the inner ear

All of the PEG-PCL polymersome administrations were performed under an operating microscope. In the osmotic pump delivery approach, surgical towels were autoclaved and operating instruments were sterilized by a bead sterilizer (STERI 250,

Switzerland). Post-auricular hairs were shaved and the skin was sterilized by 70% ethanol. The animals were placed on a thermo-regulated heated pad covered with surgical towel in a rightward lateral position. A retro-auricular incision was used to expose the left bulla after local analgesia with 1% lidocaine. A hole was drilled on the bulla with a 2-mm diameter burr. After visualizing the stapedial artery, the round window membrane was identified above the artery. A small piece of gelatin sponge (Gelfoam®) pledget soaked in PEG-PCL polymersomes (around 8 $mm^3$ after soaking with an NP solution) was placed near the round window niche. The micro-osmotic pump was filled with 100 μl of PEG-PCL polymersomes and connected to a catheter (PE60, Becton Dickinson and Company) prefilled with the same solution. The catheter tip was placed onto the gelatin sponge, the catheter was fixed on the bulla with Phosphate Cement (Heraeus Kulzer GmbH, Germany), and the osmotic pump was implanted subcutaneously in the neck. In the transtympanic injection, an approximately 1-mm incision was made on the first quadrant (anterior upper quadrant) of the tympanic membrane by a 27 gauge needle to remove any potential air bubbles. Next, 0.04 ml of PEG-PCL polymersomes was injected into the middle ear cavity via the second quadrant of the tympanic membrane. During the procedure, the animal eyes were protected by Terra-Cortril-P (Pfizer, UK). Atipamezole hydrochloride (2 mg/kg) was injected i.p. immediately after the operation to accelerate the animals' recoveries from anesthesia. Saline (2 mL) was administered through subcutaneous injection on the neck. RIMADYL (1.0 mg/kg, Pfizer, UK) was injected to relieve pain. Baytril (10 mg/kg, Orion, Germany) was injected i.p. once a day to prevent potential middle ear infection.

### 2.5. Autofluorescence and specific fluorescence observation

The rats were anaesthetized using 0.8 mg/kg of medetomidine hydrochloride (Domitor, Orion, Finland) and 80 mg/kg of ketamine hydrochloride (Ketalar, Pfizer, UK). The bullae were fixed by cardiac perfusion with 4% paraformaldehyde (Merck, Germany) [0.01 M PBS containing 0.6% (v/v) heparin, pH 7.4 to remove the blood before fixation]. No inflammation was found in the middle ear cavity of any animals. The isolated cochleae were rinsed with tap water for 1 min to remove potential free PEG-PCL polymersomes remained on the outer surface and further stored in the fixation solution for 2 h. After washing with PBS, the basal turn, middle turn, and apex (include Corti's organ, spiral ligament, and modiolus) of the cochlea and the round window membrane and ampullae of the vestibule were isolated. The tectorial membrane was removed under a stereomicroscope. The specimens were stained with 4′,6-diamidino-2-phenylindole (DAPI) (10 μg/ml, Sigma–Aldrich, USA) for 10 min at room temperature in the dark. After washing with PBS, the specimens were placed on 8-well slides (Cel-Line/Thermo scientific, USA) and mounted with Fluoromount (Sigma–Aldrich, USA) for confocal microscopy.

### 2.6. Effect of $CuSO_4$ treatment on the autofluorescence, fluorescencently tagged nanoparticles, and fluorophore-labeled molecular probes

#### 2.6.1. Time response of the labeling fluorescence and nanoparticle tag to $CuSO_4$ treatment using a spectrofluorometer

DiI-tagged PEG-PCL polymersome nanoparticles and FITC/TRITC-conjugated phalloidin solutions were prepared with 1 mM $CuSO_4$ in 0.01 M ammonium acetate buffer (pH 5.0). The final concentration of FITC/TRITC-conjugated phalloidin was 0.25 μg/ml and the fluorescence intensity was measured at different time points (0, 30, 60, 90, and 120 min) by a spectrofluorometer (Photon Technology International, UK, serial number: 2406) equipped with FeliX32 operating software. For the PEG-PCL polymersome nanoparticles, the fluorescence intensity was measured at 0 and 90 min. The reference solution was made with 1 mM $CuSO_4$ in 0.01 M ammonium acetate buffer (pH 5.0). For the untreated control, FITC/TRITC-conjugated phalloidin solutions were prepared with 0.1 M PBS to a final concentration of 0.25 μg/ml and were measured at the same time points as the $CuSO_4$-treated samples. The reference solution was made with PBS. The excitation/emission wavelengths were 494 nm/517 nm for FITC-conjugated phalloidin, 540 nm/572 nm for TRITC-conjugated phalloidin, and 543 nm/568 nm for PEG-PCL polymersome nanoparticles. The areas of the emission spectra within the wavelength range of 509–529 nm for FITC-conjugated phalloidin, 562–582 nm for TRITC-conjugated phalloidin, and 562–572 nm for PEG-PCL polymersome nanoparticles were selected as defined signal intensities. The fluorescence signal intensities of the $CuSO_4$-treated and untreated samples were corrected with the $CuSO_4$ and PBS references, respectively. Considering a signal intensity of 1 at 0 min treatment, the rates of the signal intensities of FITC/TRITC-conjugated phalloidin solutions were acquired at 30, 60, 90 and 120 min and compared with that at 0 min. Five trials were repeated for each study.

#### 2.6.2. Histology study

First, the interaction of the $CuSO_4$ treatment on fluorescent tags of nanoparticles (NPs) was investigated using the DiI-tagged PEG-PCL polymersomes as a model system. After washing with PBS, the lateral wall of the cochlea was dissected in PBS and the tectorial membrane was removed from the Corti's organ under a stereomicroscope. The specimens of the lateral wall, modiolus and basilar membrane were cut into pieces corresponding to the basal turn, middle turn, and apex. In addition, the ampullae of the semicircular canals were isolated. After treatment with $CuSO_4$ for 90 min, the specimens were washed with PBS, nuclei counterstained with 10 μg/ml of DAPI, washed again with PBS, and mounted with Fluoromount for confocal microscopy.

Since identifying spiral ganglion cells using immunofluorescence techniques has been applied in the Nanoear study, the interaction of $CuSO_4$ treatment during the antibody staining procedure was analyzed using a primary antibody against Neurofilament-200 and a secondary antibody conjugated with FITC (Zou et al., 2008). The inner ear specimens were treated with 0.5% Triton X-100 for 15 min, washed with pure water (Millipore, USA), incubated with goat serum (1:20 in 0.1% BSA), incubated with rabbit anti-Neurofilament-200 (NF-200) (Sigma–Aldrich, USA, 1:200 in 0.1% BSA) overnight at 4 °C, washed with PBS-T (PBS containing 0.1% Tween 20), incubated with FITC-labeled goat anti-rabbit IgG (1:400, Sigma–Aldrich, USA) for 1 h at room temperature, washed with PBS-T and then stained with 10 μg/ml DAPI for 10 min. After washing with PBS, the lateral wall, basilar membrane, and osseous spiral lamina of each turn were cut into two parts. One piece of each turn was treated with 1 mM $CuSO_4$ in 0.01 M ammonium acetate buffer (pH 5.0) for 90 min, washed with pure water, and mounted with Fluoromount for confocal microscopy; the other part was set as an untreated control and directly mounted with Fluoromount for confocal microscopy. Immunofluorescence staining for NF-200 was also performed on paraffin sections of two EDTA-decalcified bullae using the standard procedure.

The cellular skeleton including the hair cells was visualized by probing for F-actin with FITC/TRITC-conjugated phalloidin, as in the Nanoear project (Zou et al., 2008). The effects of $CuSO_4$ treatment on FITC/TRITC-conjugated phalloidin were further evaluated. After washing with pure water, the basal turn, middle turn and apex (including the lateral wall, basilar membrane, and osseous spiral lamina) of the cochlea and the ampullae of the semicircular canals were isolated, and the tectorial membrane was removed. The

specimens were incubated with 50 μg/ml of FITC/TRITC-conjugated phalloidin (Sigma–Aldrich, USA) at room temperature for 45 min and then stained with DAPI (10 μg/ml) for 10 min. Each turn of the cochlear tissues was cut into two parts. One part was treated with $CuSO_4$ for 70 or 90 min and mounted with Fluoromount for confocal microscopy after washing with PBS-T, and the other part was directly mounted for confocal microscopy as the untreated control.

### 2.7. Confocal microscopy

The whole mount samples were observed under an Olympus microscope IX70 installed with ANDOR IQ. The excitation filters were 488 nm (blue excitation) and 568 nm (green excitation) with an Ar–Kr laser as the excitation source. The corresponding emission filters were 525/50 nm (FITC) and 607/45 nm (TRITC and DiI). DAPI was excited with a 340–380 nm filter and detected using a 500 LP filter. For 3D scanning, the interslice thickness was 0.5 μm. For semi-quantification, the mean fluorescence signal intensities of the irregular IHC hair bundles, the 'V-shaped' OHC hair bundles (single row) and the strial marginal cells of each confocal graph were measured by Image J software (1.41). A background area was chosen as the reference in each confocal micrograph. The final signal/noise ratio was acquired by dividing the mean signal intensity value of the target region by the mean noise intensity value of the reference area.

The colocalization of autofluorescent plots triggered with different wavelengths under confocal microscopy was analyzed using Image J software (1.41).

### 2.8. Statistics

Statistical analyses were performed using the SPSS 11.5 software package. For confocal microscopy studies, the signal/noise values of IHC hair bundles, OHC hair bundles and stria marginal cells between the $CuSO_4$-treated and untreated specimens were analyzed using Student's *t*-tests. For the spectrofluorometer study, the fluorescence signal intensities and the remaining rates of the fluorescence signal intensities between $CuSO_4$-treated and untreated samples were compared using Student's *t*-tests at different time points. Changes in the fluorescence signal intensities and the remaining rates of the fluorescence intensities between two adjacent time points in each group were analyzed with a Bonferroni correction of the analysis of variance (ANOVA). Differences were considered to be statistically significant at $p < 0.05$.

## 3. Results

### 3.1. Impact of fixation on polymersome internalization in NIH3T3 cells

In live NIH3T3 cells, PEG-PCL polymersome internalization was repeatedly observed in cytoplasm with the typical appearance of vesicles (Fig. 1A). However, the internalization was completely abolished by the fixation of the cells with 4% PFA (Fig. 1B).

### 3.2. Autofluorescence in the rat inner ear

Abundant autofluorescence dots were observed in the subcuticular cytoplasm of inner hair cells (IHCs) and Border cells. Obvious autofluorescence dots were also detected in SGCs, strial marginal cells, spiral ligament fibrocytes, mesothelial cells of the scala tympani below the basilar membrane, and epithelial cells of the Reissner's membrane. A sparse distribution of autofluorescence was found in outer hair cells (OHCs). However, no autofluorescence was discovered in the supporting cells, including Deiters' cells and Hensen cells. A variable phenotype of autofluorescence was observed, which was larger in size and less dense in the Reissner's membrane and larger and denser in type I SGCs in comparison to other cell populations showing smaller dots homogeneously distributed in the cytoplasm (Fig. 2D, H, and L).

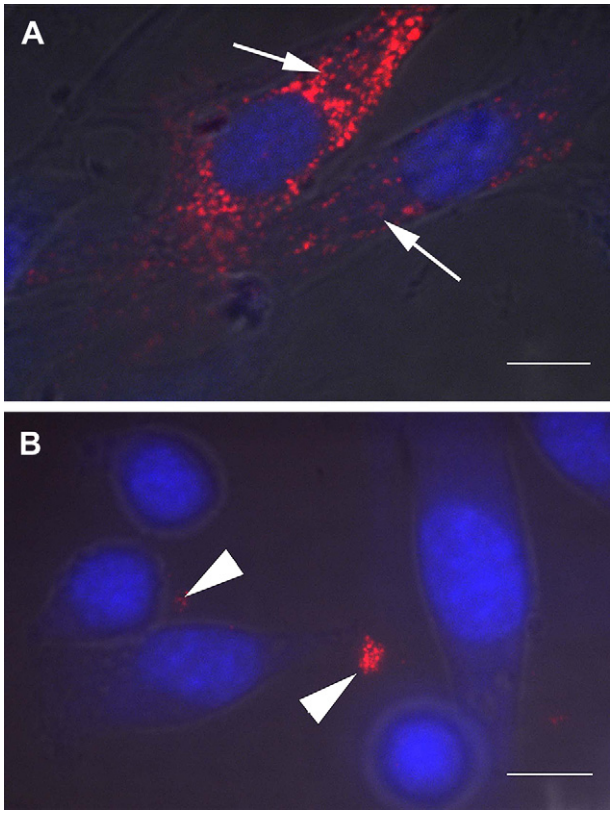


**Fig. 1.** Internalization of PCL-PEG polymersomes in NIH3T3 cells. Panel A, PEG-PCL polymersomes appeared in cytoplasm in abundant quantity (arrow). Panel B, No PEG-PCL polymersome was internalized by pre-fixed NIH3T3 cells, but sparsely aggregated in the extracellular region of the slide (arrowhead). Scale bar = 10 μm.

Brilliant red autofluorescence was observed with the 607/45 nm emission filter, while obscure yellowish-green autofluorescence was visualized with the 525/50 nm emission filter. Quantification was performed on the confocal microscopy images by measuring the colocalization of the autofluorescent dots with the above-mentioned filters. The overlap rates of autofluorescence triggered by both wavelengths were 97.16% in spiral ligament fibrocytes, 96.55% in SGCs, 93.77% in stria marginal cells, and 95.40% in IHCs (Fig. 2).

### 3.3. The effect of $CuSO_4$ treatment on the labeling fluorescence using a spectrofluorometer

The fluorescent signal intensity of PEG-PCL polymersomes was not changed after treated with $CuSO_4$ for 90 min when compared with the untreated control (Fig. 3A and B; $p > 0.05$).

The fluorescence signal intensities between the $CuSO_4$-treated TRITC-conjugated phalloidin and the untreated control were compared at time points of 0, 30, 60, 90, and 120 min. The fluorescent signal was not significantly influenced by treatment with $CuSO_4$ ($p > 0.05$; Fig. 3C). In addition, the signal intensities between the corresponding neighboring time points of either the $CuSO_4$-treated samples or the control were not significantly different

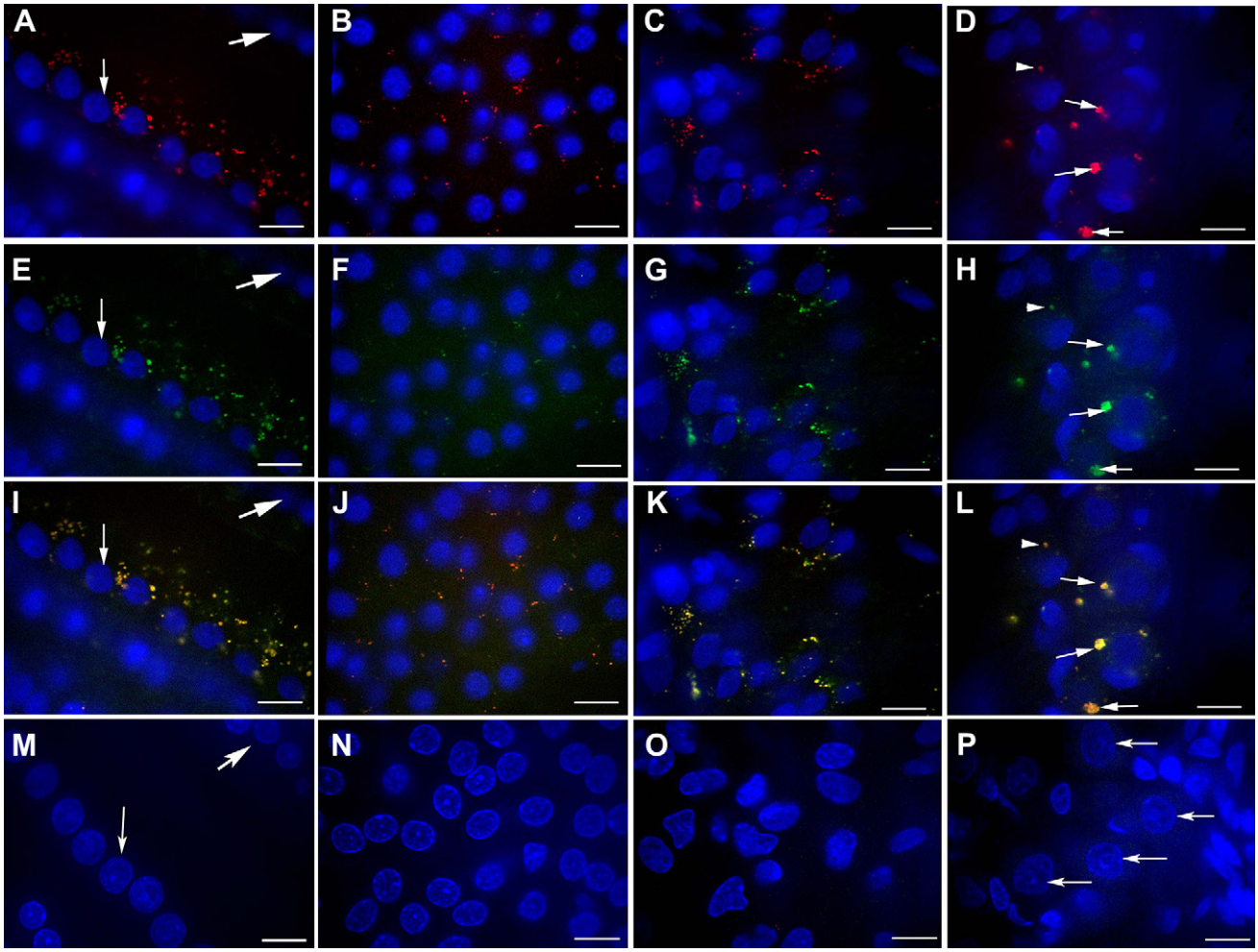


**Fig. 2.** Appearance of autofluorescence in the rat cochleae and the effect of treatment with $CuSO_4$ demonstrated by confocal microscopy. Panels A–D show the red autofluorescence using the 607/45 nm emission filter. Panels E–H show the greenish autofluorescence using the 525/50 nm emission filter. Panels I–L demonstrate the colocalization of the red autofluorescence and the greenish autofluorescence (the overlap rate analyzed by Image J 1.41). Panels A, E, and I depict the abundant autofluorescent dots in IHCs with a red and the greenish fluorescent overlap rate of 95.40% (*z*-series pictures; down pointing arrow: IHC; right pointing arrow: OHC). Panels B, F, and J show the autofluorescence in the stria marginal cells with a red and green overlap rate of 93.77%. Panels C, G, and K demonstrate the autofluorescence in the spiral ligament fibrocytes with a red and green overlap rate of 97.16%. Panels D, H, and L show the large and irregular lipofuscin granules in SGCs (arrows) and small lipofuscin in the spiral ganglion satellite cells (arrow heads) with a red and greenish overlap rate of 96.55%. Panels M (*z*-series picture), N, O and P show the disappearance of autofluorescence in IHC (M), stria marginal cells (N), spiral ligament fibrocytes (O), and SGCs (P) after treatment with $CuSO_4$ for 90 min (Blue: nucleus stained with DAPI; Panels I–P: RGB pictures). Scale bar = 10 μm.

($p > 0.05$) (Fig. 3C). The remaining rates of the $CuSO_4$-treated samples at 30 min ($p < 0.01$, Bonferroni of ANOVA) and 60 min ($p < 0.05$) and the untreated control at 30 min ($p < 0.01$) were significantly decreased in comparison with earlier time points (Fig. 3D). There was no statistically significant decay in the rates of the remaining fluorescent signals between the $CuSO_4$-treatment samples and the untreated control at 0, 30, 60, 90 and 120 min ($p > 0.05$; Fig. 3D). At 120 min post-treatment, 43.40 and 43.52% of the fluorescence signal intensity remained in the $CuSO_4$-treatment samples and the untreated control, respectively, compared to the signal intensity of the untreated control at 0 min.

The fluorescence signal of the FITC-conjugated phalloidin was significantly decreased immediately after treatment with $CuSO_4$ at 0 min ($p < 0.01$, Student's *t*-test), and this decrease was maintained until 30 min after treatment ($p < 0.05$, Student's *t*-test) (Fig. 3E). Analysis of the fluorescence signal between neighboring time points revealed no significant decay in the untreated control, which ruled out fluorescence blanching ($p > 0.05$, Student's *t*-test). In the $CuSO_4$-treated samples, a significant decay in the remaining rate was observed at 30 min post-treatment (Fig. 3F; $p < 0.01$, Bonferroni of ANOVA). No further significant decay was detected at later time points. At 120 min post-treatment, 1.27 and 51.74% of the fluorescence signal intensity remained in the $CuSO_4$-treated samples and the untreated control, respectively, compared to the signal intensity of the untreated control at 0 min.

### 3.4. $CuSO_4$ treatment quenches autofluorescence while preserving the nanoparticle tag and labeling fluorescence in the rat inner ear

At 90 min post-treatment, no autofluorescence was visible in the tissue (Fig. 4a–e). However, in the specimens treated with $CuSO_4$ for 70 min, autofluorescence disappeared in IHCs, mesothelial cells of the scala tympani below the basilar membrane, and stria marginal cells. In the cochlear spiral ligament fibrocytes and vestibule, autofluorescence disappeared in most of the cells. However, less condensed dots were still detected in a few of the cells, which were mainly located in the central zone of the spiral ligament. In SGCs, autofluorescence remained, but with greatly reduced intensity (Fig. 4D, d).

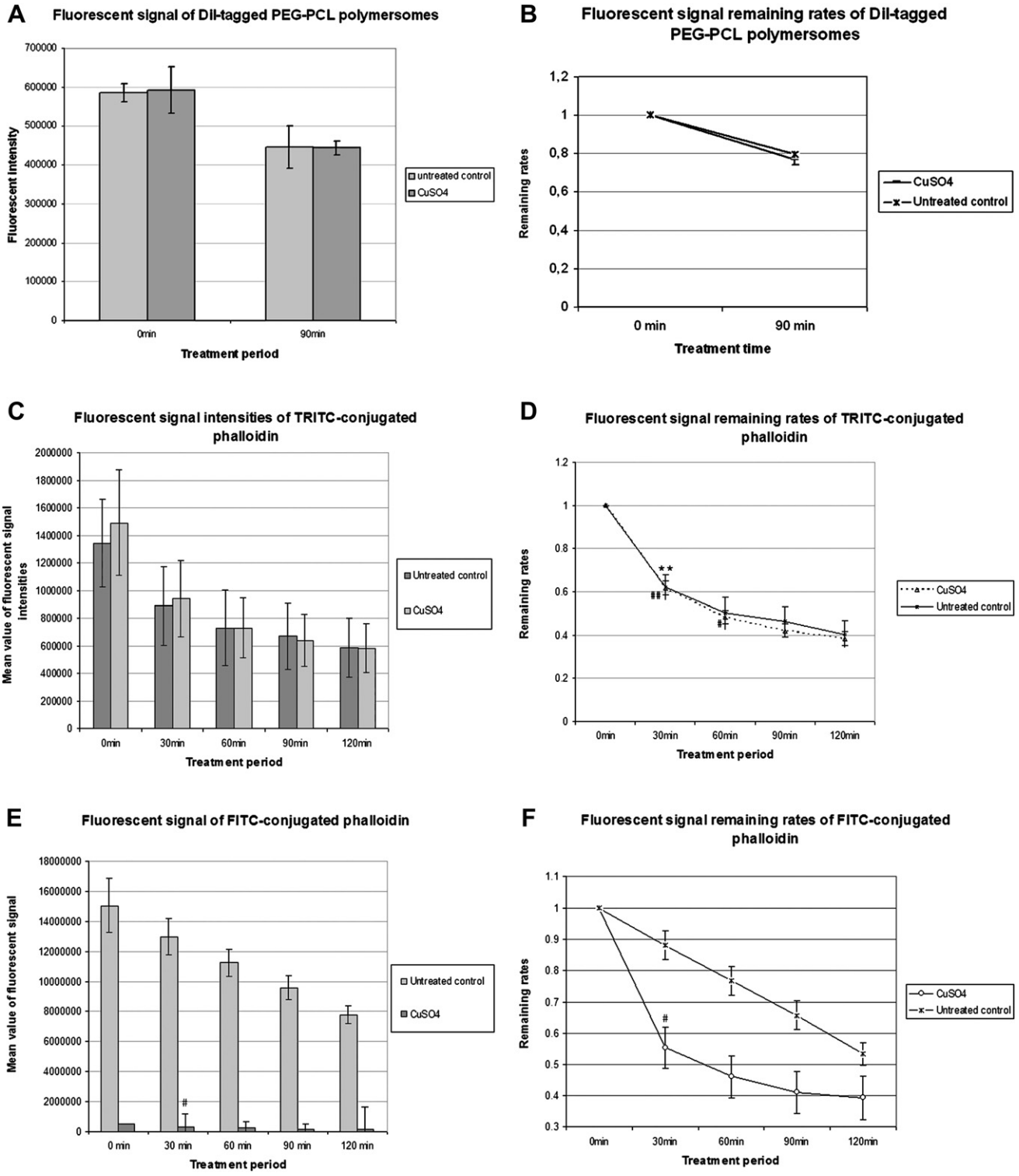


**Fig. 3.** Impact of $CuSO_4$ treatment on the fluorescent signal intensities of FITC/TRITC-conjugated phalloidin. Panels A and B show that there was no statistically significant differences in the fluorescent signal intensities and remaining rates of DiI-tagged PEG-PCL polymersomes between the $CuSO_4$ treatment and untreated control at time points of 0 min and 90 min treatment ($p > 0.05$, Student's *t*-test). Panels C and D shows that there was no significant difference in the fluorescent signal intensities and remaining rates of TRITC-conjugated phalloidin between the $CuSO_4$ treatment and untreated controls at each time point ($p > 0.05$, Student's *t*-test). Panel E shows that there were statistically significant differences in the fluorescence signal intensities of FITC-conjugated phalloidin between the $CuSO_4$-treated and untreated samples at each time point ($p < 0.01$, Student's *t*-test). Panel F shows that there were significant differences in the FITC fluorescent signal remaining rates between the $CuSO_4$-treated and untreated samples at 30 min ($p < 0.01$, Student's *t*-test) and 60 min ($p < 0.01$, Student's *t*-test). Comparison of the fluorescent signal between each defined time point and its earlier neighboring time point within the group showed the following results: $^{*}p < 0.05$ in untreated control; $^{\#}p < 0.05$ in $CuSO_4$-treated group; $^{**}p < 0.01$ in untreated control; $^{\#\#}p < 0.01$ in $CuSO_4$-treated group (Bonferroni of ANOVA).

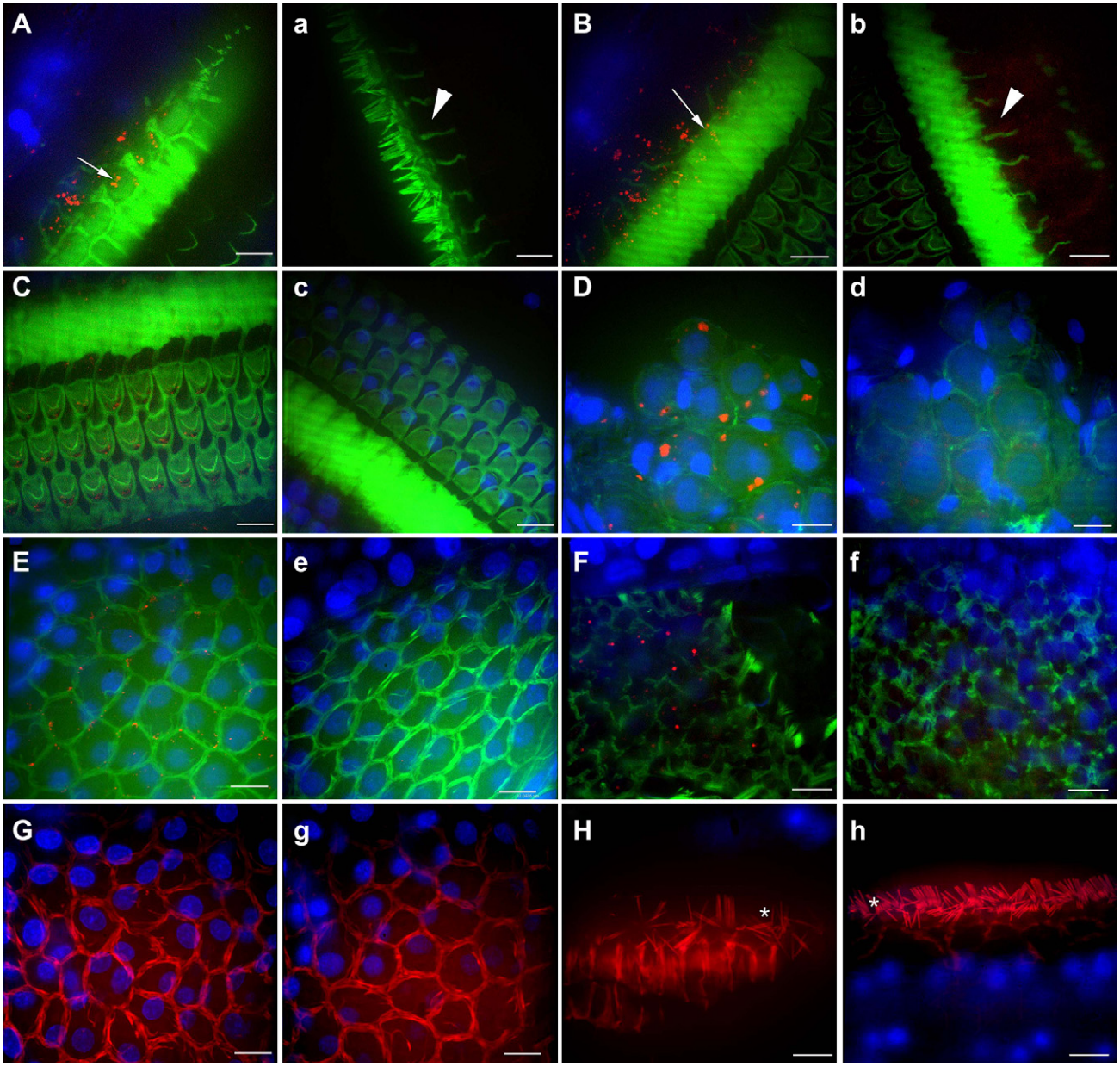


**Fig. 4.** Visualization of F-actin labeled by FITC (green)/TRITC (red)-conjugated phalloidin, and the autofluorescence that was eliminated by $CuSO_4$ treatment in the inner ear cell populations. Panels A–H show the untreated controls. Panels a–h show the specimens treated with 1 mM $CuSO_4$ for 70 min (f) or 90 min (a, b, c, d, e, g, h) after staining with FITC/TRITC-conjugated phalloidin. The F-actin labeling remained while the autofluorescence was eliminated. Panels A and B show the autofluorescence in the subcuticular cytoplasm of IHCs and the Border cells. Panel C shows that the autofluorescence in OHCs. Panel D shows the large autofluorescent dots in SGCs. Panel E shows the autofluorescence in the stria marginal cells. Panel F shows the autofluorescence in the hair cells of the ampullae. Panels G, g, H and h show visualization of F-actin labeling by TRITC-conjugated phalloidin on strial marginal cells (G) and Inner hair bundles (H) are not affected after $CuSO_4$ treatment (g and h) (Asterisks: hair bundles of IHCs; arrows: autofluorescent dots in IHCs; arrow heads: autofluorescence disappeared after $CuSO_4$ treatment; Blue: nucleus stained with DAPI; B, b, C, c: *z*-series image). Scale bar = 10 μm.

DiI-tagged PEG-PCL polymersome nanoparticles appeared as vesicles when internalized. They were detected on the outer epithelial layer of the round window membrane as being dispersed in the cytoplasm at 3 days post-administration via osmotic pump and were homogeneous in the peri-nuclear region at 3 days and 5 days post-intratympanic injection (Figs. 5A, F and 6). There were sparse nanoparticles in the connective tissue core of the round window membrane in all animals (Fig. 5C). Nanoparticles were also found in mesothelial cells of scala tympani and suprastrial area of scala vestibuli, Capillaries of the stria vascularis of the first turn at 3 days post-administration via osmotic pump (Fig. 5B). The PEG-PCL polymersome nanoparticles were visualized in the mesothelial cells of the scala tympani beneath the Corti's organ (Fig. 5I), cells within the suprastrial area (Fig. 5H), and capillary of the stria vascularis (Fig. 5G) of whole coil on 3 day and 5 day post-transtympanic injection. PEG-PCL polymersomes were also detected in utricle, saccule, and ampulla of the vestibule (Fig. 5J). Polymersomes were also observed in auditory nerve region and spiral ganglion region (Figs. 5D, E and 6) on 5 day post-transtympanic injection. No PEG-PCL polymersomes were detected in IHCs, OHCs, supporting cells of Corti's organ, and marginal cells of stria vascularis.

Neurofilament-200 was immunofluorescently observed in the bodies of SGCs, cochlear nerve fibres, tunnel fibres, and nerve endings on IHCs and OHCs (Fig. 7). The immunofluorescence

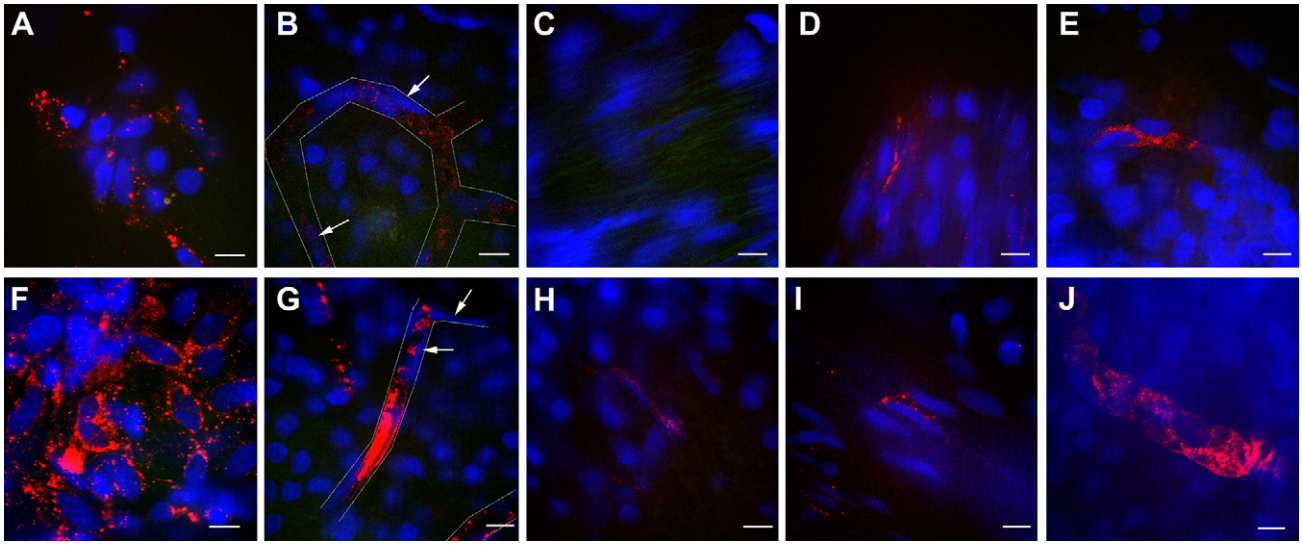


**Fig. 5.** The distribution of the PEG-PCL polymersomes in the inner ear cell populations after $CuSO_4$ treatment. Panels A–C, showed the distribution of polymersomes at 3 days post-administration via osmotic pump. Panels D–J, showed the distribution of polymersomes at 5 days post-transtympanic injection. Panels A and F showed the distribution of the nanoparticles in the outer epithelial layer of the round window membrane at 3 days (panel A) and 5 days (panel F). Panels B and G showed the distribution of nanoparticles in the capillary endothelial cells of the stria vascularis at 3 days (panel B) and 5 days (panel G). The nuclei of the endothelial cells are indicated by arrows. Panel C showed the connective tissue core of the round window membrane without nanoparticle at 3 days. Panels D, E, H, I, and J demonstrated the nanoparticle appearance in the auditory nerve region (D), the spiral ganglion region (E), fibrocytes within the suprastrial area (H), mesothelial cells beneath the Corti's organ (I) and cells in the vestibule (J), respectively. The vessel walls in Panels B and G were outlined with dashed white lines by Photoshop. (Red: PEG-PCL polymersome targeted with DiI; Blue: nucleus stained with DAPI). Scale bar = 10 μm.

staining was not visibly reduced by treatment of $CuSO_4$ for 90 min (Fig. 7). Because of the irregular distribution of Neurofilament-200 in the tissue, quantification was not performed.

Both FITC-conjugated phalloidin and TRITC-conjugated phalloidin were used to label the hair bundles of the IHCs and OHCs, the bodies of the inner and outer pillar cells, the intercellular junctions of stria marginal cells, and the cytoplasm of SGCs. The $CuSO_4$ treatment did not affect the visualization of the labeled F-actin by either FITC-conjugated phalloidin or TRITC-conjugated phalloidin. After treatment with $CuSO_4$ for 90 min, the fluorescence intensity (signal/noise) of FITC labeling showed a statistically significant difference in IHCs and stria marginal cells ($p < 0.01$, Student's *t*-test), but not in OHCs ($p > 0.05$, Student's *t*-test) (Fig. 3; Table 1). The TRITC labeling fluorescence intensity (signal/noise) was significantly decreased in the stria marginal cells ($p < 0.01$, Student's *t*-test) but was not affected in the IHCs or OHCs ($p > 0.05$, Student's *t*-test; Table 2).

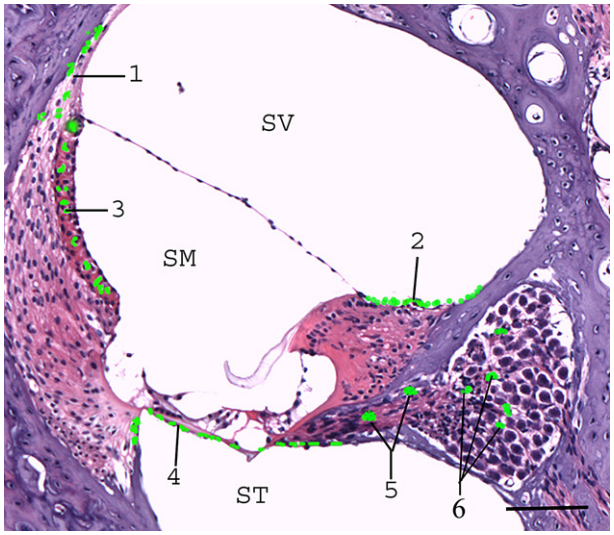


**Fig. 6.** PEG-PCL polymersome distribution in inner ear cell populations was drawn in green using Photoshop. 1: suprastrial area. 2: mesothelial cells lining bony labyrinth of SV. 3: stria vascularis. 4: mesothelial cells beneath Corti's organ. 5: cells of auditory nerve. 6: cells in spiral ganglion region. Scale bar = 100 μm.

## 4. Discussion

In this study, abundant autofluorescence was observed in the subcuticular cytoplasm of IHCs and border cells. Obvious autofluorescence was detected in SGCs, strial marginal cells, spiral ligament fibrocytes, mesothelial cells of scala tympani below the basilar membrane, and epithelial cells of the Reissner's membrane. Additionally, a sparse distribution of autofluorescence was found in OHCs. In contrast, no autofluorescence was found in Deiters' cells or Hensen cells. Our observation of autofluorescence in rat cochlea was different from a report using chinchilla, which demonstrated more autofluorescence distribution in OHCs and much less in IHCs (Bohne et al., 1990). These results suggest differential metabolism and aging processes in the hair cells of different species (Feeney, 1978; Haralampus-Grynaviski et al., 2003; Igarashi and Ishii, 1990; Kikugawa et al., 1997; Rajawat et al., 2009; Xu et al., 2008). Our observation of autofluorescence in SGCs was in accordance with previous reports regarding their morphology and subcellular distribution (Igarashi and Ishii, 1990).

The high overlap of the red and greenish autofluorescence (97.16% in the SL, 96.55% in the SGCs, 93.77% in the StrV, 95.40% in the IHCs), which was detected with both the 607/45 nm (red) and 525/50 nm (green) emission filters using confocal microscopy, supports a previous study, which found that lipofuscin (autofluorescence) has a broad excitation/emission spectra (Fig. 1) (Kikugawa et al., 1997), whereas the fluorophores (TRITC/FITC) have narrow excitation/emission spectra. Under the green emission filter, it was visually easier to distinguish the autofluorescence from the specific green fluorophores, because the autofluorescence appeared yellow and the specific fluorescence was pure green.

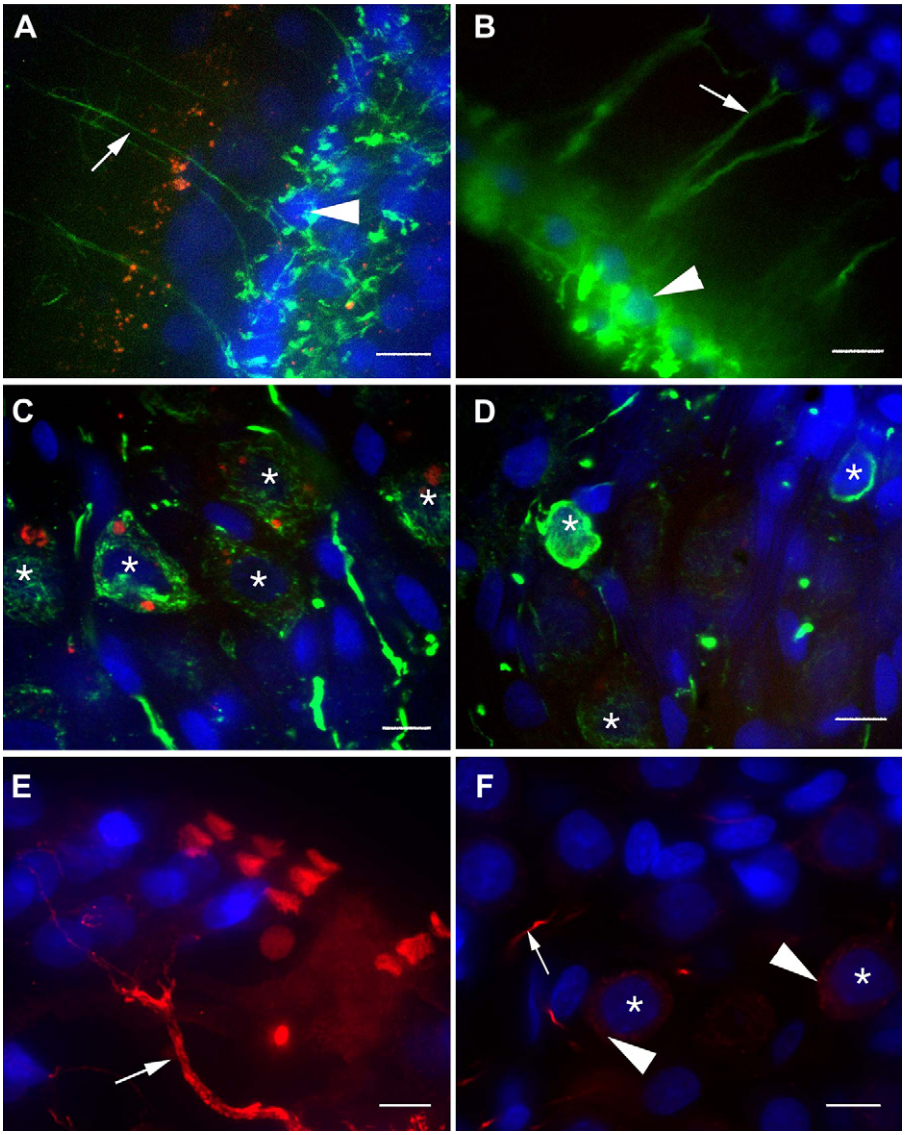


**Fig. 7.** Visualization of the immunofluorescent staining of neurofilament-200 (NF-200) in the inner ear when the autofluorescence was eliminated by $CuSO_4$ treatment. Panel A shows a *z*-series image of the appearance of autofluorescence in IHCs (arrowhead) and NF-200 staining on nerve fibres (arrow) in the Corti's tunnel innervating OHCs in the no treatment control. Panel B shows a *z*-series image of NF-200 staining of nerve fibres (arrow). The fluorescence of NF-200 staining remained while the autofluorescence disappeared in IHCs (arrowhead) after treatment with $CuSO_4$ for 90 min. Panel C demonstrates the appearance of autofluorescence (red dots) and NF-200 staining (green) in SGCs (nuclei of SGCs are indicated by asterisks) of no treatment controls. Panel D shows the NF-200 staining remains in SGCs while the autofluorescent dots disappear after treatment with $CuSO_4$. Panel E shows NF-200 staining on nerve fibres (arrow) in the Corti's tunnel innervating OHCs in paraffin embedded slices (*z*-series image of 20-μm thickness paraffin section). Panel F shows NF-200 staining of the cytoplasm (arrow head) and processes (arrow) of SGCs (nuclei are indicated by asterisks) and the nerve fibres (arrow) in paraffin embedded slices. (Blue: nucleus stained with DAPI). Scale bar = 10 μm.

Under the red emission filter, the autofluorescence was characterized by a bright signal and disturbed weak specific fluorescence signals, such as from TRITC conjugation.

Amphiphilic block copolymers have been shown to self-assemble into polymersomes in an aqueous environment (Letchford and Burt, 2007). Polymersomes are a class of vesicles, nano-sized spheres that encapsulate an aqueous solution. They have potential to act as drug delivery vehicles as they can carry therapeutic agents and their surfaces can also be modified with tissue-specific targeting moieties. In addition, small molecular weight hydrophobic molecules can be incorporated into the membrane (Ghoroghchian et al., 2007) and hydrophilic molecules can be encapsulated in the aqueous core (Lomas et al., 2007). The polymersome surface can be functionalized with groups that promote cellular uptake (Christian et al., 2007) or target specific cell types. These properties result in prolonged circulation times of the polymersome within the body. Furthermore, $CuSO_4$ treatment eliminated the autofluorescence in the inner ear, whereas the signal from DiI was absolutely preserved. The fluorescence signal of

**Table 1**
Fluorescent signal changes of FITC-phalloidin binding in the cochlear cell populations induced by $CuSO_4$.

| Groups | IHC | | OHC | | StrMC | |
|---|---|---|---|---|---|---|
| | *n* | Means ± SEM | *n* | Means ± SEM | *n* | Means ± SEM |
| No treatment | 35 | 2.8 ± 0.1 | 58 | 1.8 ± 0.1 | 26 | 1.8 ± 0.1 |
| $CuSO_4$ treatment | 35 | 3.6 ± 0.2** | 99 | 1.9 ± 0.0 | 37 | 2.1 ± 0.1** |

** $p < 0.01$.
IHC: hair bundles of the inner hair cells; OHC: hair bundles of the outer hair cells, StrMC: strial marginal cells.

**Table 2**
Fluorescent signal changes of TRITC-phalloidin binding in the cochlear cell populations induced by $CuSO_4$.

| Groups | IHC | | OHC | | StrMC | |
|---|---|---|---|---|---|---|
| | *n* | Means ± SEM | *n* | Means ± SEM | *n* | Means ± SEM |
| No treatment | 22 | 4.9 ± 0.4 | 51 | 3.0 ± 0.1 | 32 | 3.4 ± 0.1 |
| $CuSO_4$ treatment | 39 | 5.5 ± 0.3 | 79 | 3.0 ± 0.1 | 43 | 3.0 ± 0.1** |

** $p < 0.01$.
IHC: hair bundles of the inner hair cells; OHC: hair bundles of the outer hair cells, StrMC: strial marginal cells.

DiI may not have been affected by $CuSO_4$. Alternatively, DiI was encapsulated in the PEG-PCL polymersome nanoparticles and the hydrophobic membrane of the nanoparticle prevented the passage of $CuSO_4$ into the core to react with the DiI tag. Similar mechanisms may operate in other types of nanoparticles, such as the lipidic core nanocapsules that encapsulate Nile red in the hydrophobic core (Scheper et al., 2009; Zou et al., 2008). The method presented herein greatly increased the specificity of nanoparticle detection in the inner ear without compromising sensitivity.

Internalization of PEG-PCL polymersomes in live NIH3T3 cells but not pre-fixed cells proved that potential contamination of free nanoparticles did not disturb the observation of internalization in the inner ear cell populations since the dissection was performed after fixation with 4% PFA. PEG-PCL polymersomes were observed in mesothelial cells of the scala tympani and vestibuli, capillaries of the stria vascularis, spiral ligament fibrocytes and spiral ganglion region after 5 days transtympanic injection (Fig. 5). The potential routes for PEG-PCL to access the spiral ganglion cell region after intratympanic delivery is that the nanoparticles diffuse from the scala perilymph to the "perimodiolar lymph" via the porous modiolar wall of the scala tympani and scala vestibuli (Rask-Andersen et al., 2006; Zou et al., 2008, 2009a,b, 2010). Distribution of PEG-PCL in the stria vasculature may take the passage of trans-spiral ligament diffusion (Zou et al., 2005, 2010). The details will be investigated in the near future. However, PEG-PCL polymersomes were not detected in the cells facing endolymph, such as IHCs, OHCs, supporting cells of Corti's organ, and stria marginal cells. These results indicate poor transport of PEG-PCL polymersomes into endolymph.

In the TRITC/FITC-labeled inner ear specimens, $CuSO_4$ treatment resulted in diverse signal intensity changes in the hair bundles of IHC and OHC, and stria marginal cells according to quantification. The deviation in the fluorescence signal intensity might have been artificially generated during sampling, potentially due to different focus planes under the confocal microscope or the region selection for quantification. However, the treatment greatly preserved the labeling abilities of the fluorescence signals, including the binding of F-actin and the antibody, which have both been employed to identify the cellular populations of the inner ear during the Nanoear study with whole mounting techniques (Scheper et al., 2009; Zou et al., 2008). Although the fluorescence of FITC-conjugated phalloidin was greatly reduced by $CuSO_4$ treatment, the visualization of inner ear cells labeled by FITC-conjugated phalloidin was not compromised.

Heavy-metal ion treatment, including $CuSO_4$, significantly decreases the fluorescence intensity of extracted lipofuscin components (Kikugawa et al., 1997). Metals in close proximity to chromophores are known to quench fluorescence in a distance dependent fashion (Richmond et al., 2000). Cupric ion was reported to quench fluorescence of DsRed (a bright red fluorescent protein), eGFP, and fluorescent dyes entrapped in nanoparticles by binding to amino acids close to the chromophores (Eli and Chakrabartty, 2006; Richmond et al., 2000; Gouanvé et al., 2007). When the emission spectra of chromophores (donor) are overlapped with the absorption spectrum of cupric ion (accepter), energy transfer from the donor to the accepter would happen. Cupric ion absorbs the energy at emission wavelength of the donor without re-emitting the energy fluorescently resulting in fluorescent quenching (Gouanvé et al., 2007). Yellow fluorescent components in lipofuscin are composed of proteinaceous material (Kikugawa et al., 1997). A2E (2-[2,6-dimethyl-8-(2,6,6-trimethyl-1-cyclohexen-1-yl)-1E,3E,5E,-7E-octatetraenyl]-1-(2-hydroxyethyl)-4-[4-methyl-6-(2,6,6-trimethyl-1-cyclohexen-1-yl)-1E,3E,5E-hexatrienyl]-pyridinium), an isomer of a pyridinium bis-retinoid, dominates the red edge of the emission spectrum of lipofuscin (Haralampus-Grynaviski et al., 2003). We suspect that the mechanism of $CuSO_4$ treatment to quench autofluorescence in the rat inner ear is through binding to amino acids close to A2E and induce energy transfer. The fluorescence of TRITC-conjugated phalloidin and DiI-tagged PEG-PCL polymersomes preserved by $CuSO_4$ treatment might be caused by the absence of binding site or an inefficient remote binding site in the agents. Therefore, the specific fluorescent signal was distinguished from the autofluorescence after $CuSO_4$ treatment.

In conclusion, visualization of fluorescently tagged nanoparticles in the inner ear was greatly improved by $CuSO_4$ treatment, which eliminated autofluorescence in the inner ear cell populations while absolutely preserving the specific tag. The ability to identify the inner ear cell populations using fluorophore-conjugated molecular probes was not comprised by $CuSO_4$ treatment. This method can be applied in studies of inner ear histology involving fluorescence techniques, such as the Nanoear project.

## Acknowledgements

This study was supported by the European Community 6th Framework Programme on Research, Technological Development and Demonstration (Nanotechnology-based Targeted Drug Delivery. Contract number: NMP4-CT-2006-026556, Project acronym: NANOEAR).

## References

Bohne, B.A., Gruner, M.M., Harding, G.W., 1990. Morphological correlates of aging in the chinchilla cochlea. Hearing Research 48, 79–91.
Brehmer, A., Blaser, B., Seitz, G., Schrodl, F., Neuhuber, W., 2004. Pattern of lipofuscin pigmentation in nitrergic and non-nitrergic, neurofilament immunoreactive myenteric neuron types of human small intestine. Histochemistry and Cell Biology 121, 13–20.
Christian, N.A., Milone, M.C., Ranka, S.S., Li, G., Frail, P.R., Davis, K.P., Bates, F.S., Therien, M.J., Ghoroghchian, P.P., June, C.H., Hammer, D.A., 2007. Tat-functionalized near-infrared emissive polymersomes for dendritic cell labeling. Bioconjugate Chemistry 18, 31–40.
El-Hakim, H., Abdolell, M., Mount, R.J., Papsin, B.C., Harrison, R.V., 2002. Influence of age at implantation and of residual hearing on speech outcome measures after cochlear implantation: binary partitioning analysis. The Annals of Otology, Rhinology & Laryngology 189, 102–108.
Eli, P., Chakrabartty, A., 2006. Variants of DsRed fluorescent protein: development of a copper sensor. Protein Science 15, 2442–2447.
Feeney, L., 1978. Lipofuscin and melanin of human retinal pigment epithelium. Fluorescence, enzyme cytochemical, and ultrastructural studies. Investigative Ophthalmology & Visual Science 17, 583–600.
Gantz, B.J., Woodworth, G.G., Knutson, J.F., Abbas, P.J., Tyler, R.S., 1993. Multivariate predictors of audiological success with multichannel cochlear implants. The Annals of Otology, Rhinology & Laryngology 102, 909–916.
Geers, A., Brenner, C., Nicholas, J., Uchanski, R., Tye-Murray, N., Tobey, E., 2002. Rehabilitation factors contributing to implant benefit in children. The Annals of Otology, Rhinology & Laryngology 189, 127–130.
Ghoroghchian, P.P., Frail, P.R., Li, G., Zupancich, J.A., Bates, F.S., Hammer, D.A., Therien, M.J., 2007. Controlling bulk optical properties of emissive polymersomes through intramembranous polymer-fluorophore interactions. Chemistry of Materials 19, 1309–1318.
Gouanvé, F., Schuster, T., Allard, E., Méallet-Renault, R., Larpent, C., 2007. Fluorescence quenching upon binding of copper ions in dye-doped and ligand-capped polymer nanoparticles: a simple way to probe the dye accessibility in nanosized templates. Advanced Functional Materials 17, 2746–2756.

Haralampus-Grynaviski, N.M., Lamb, L.E., Clancy, C.M., Skumatz, C., Burke, J.M., Sarna, T., Simon, J.D., 2003. Spectroscopic and morphological studies of human retinal lipofuscin granules. Proceedings of the National Academy of Sciences of the United States of America 100, 3179–3184.

Horner, K.C., Guilhaume, A., 1995. Ultrastructural changes in the hydropic cochlea of the guinea-pig. The European Journal of Neuroscience 7, 1305–1312.

Igarashi, Y., Ishii, T., 1990. Lipofuscin pigments in the spiral ganglion of the rat. European Archives of Oto-Rhino-Laryngology 247, 189–193.

Ishii, T., 1977. The fine structure of lipofuscin in the human inner ear. Archives of Oto-rhino-laryngology 215, 213–221.

Kania, R.E., Herma, P., Tran, B.H.P., Ar, A., 2006. Role of nitrogen in transmucosal gas exchange rate in the rat middle ear. Journal of Applied Physiology 101, 1281–1287.

Kikugawa, K., Beppu, M., Sato, A., Kasai, H., 1997. Separation of multiple yellow fluorescent lipofuscin components in rat kidney and their characterization. Mechanisms of Ageing and Development 97, 93–107.

Lomas, H., Canton, I., MacNeil, S., Du, J., Armes, S.P., Ryan, A.J., Lewis, A.L., Battagila, G., 2007. Biomimetic pH sensitive polymersomes for efficient DNA encapsulation and delivery. Advanced Materials 19, 4238–4243.

Letchford, K., Burt, H., 2007. A review of the formation and classification of amphiphilic block copolymer nanoparticulate structures: micelles, nanospheres, nanocapsules and polymersomes. European Journal of Pharmaceutics and Biopharmaceutics 65, 259–269.

Osberger, M.J., Zimmerman-Phillips, S., Koch, D.B., 2002. Cochlear implant candidacy and performance trends in children. The Annals of Otology, Rhinology & Laryngology 189, 62–65.

Pyykko, I., 2009. NANOEAR: 3g-Nanotechnology based targeted drug delivery using the inner ear as a model target organ [Online]. http://www.nanoear.org/.

Rajawat, Y.S., Hilioti, Z., Bossis, I., 2009. Aging: central role for autophagy and the lysosomal degradative system. Ageing Research Reviews 8, 199–213.

Rask-Andersen, H., Schrott-Fischer, A., Pfaller, K., Glueckert, R., 2006. Perilymph/modiolar communication routes in the human cochlea. Ear and Hearing 27, 457–465.

Richmond, T.A., Takahashi, T.T., Shimkhada, R., Bernsdorf, J., 2000. Engineered metal binding sites on green fluorescence protein. Biochemical and Biophysical Research Communications 268, 462–465.

Scheper, V., Wolf, M., Scholl, M., Kadlecova, Z., Perrier, T., Klok, H.A., Saulnier, P., Lenarz, T., Stover, T., 2009. Potential novel drug carriers for inner ear treatment: hyperbranched polylysine and lipid nanocapsules. Nanomedicine (London, England) 4, 623–635.

Schnell, S.A., Staines, W.A., Wessendorf, M.W., 1999. Reduction of lipofuscin-like autofluorescence in fluorescently labeled tissue. The Journal of Histochemistry and Cytochemistry 47, 719–730.

Walther, L.E., Westhofen, M., 2007. Presbyvertigo-aging of otoconia and vestibular sensory cells. Journal of Vestibular Research: Equilibrium & Orientation 17, 89–92.

Xu, H., Chen, M., Manivannan, A., Lois, N., Forrester, J.V., 2008. Age-dependent accumulation of lipofuscin in perivascular and subretinal microglia in experimental mice. Aging Cell 7, 58–68.

Zou, J., Poe, D., Bjelke, B., Pyykko, I., 2009a. Visualization of inner ear disorders with MRI in vivo: from animal models to human application. Acta Oto-Laryngologica: Supplementum, 22–31.

Zou, J., Pyykko, I., Bjelke, B., Dastidar, P., Toppila, E., 2005. Communication between the perilymphatic scalae and spiral ligament visualized by in vivo MRI. Audiology & Neuro-Otology 10, 145–152.

Zou, J., Zhang, W., Poe, D., Zhang, Y., Ramadan, U.A., Pyykko, I., 2010. Differential passage of gadolinium through the mouse inner ear barriers evaluated with 4.7 T MRI. Hearing Research 259, 36–43.

Zou, J., Saulnier, P., Perrier, T., Zhang, Y., Manninen, T., Toppila, E., Pyykko, I., 2008. Distribution of lipid nanocapsules in different cochlear cell populations after round window membrane permeation. Journal of Biomedical Materials Research 87, 10–18.

Zou, J., Zhang, Y., Zhang, W., Ranjan, S., Sood, R., Mikhailov, A., Kinnunen, P., Pyykkö, I., 2009b. Internalization of liposome nanoparticles functionalized with TrkB ligand in rat cochlear cell populations. European Journal of Nanomedicine 3, 8–14.

*Acta Oto-Laryngologica*, 2011; Early Online, 1–8

informa
healthcare

**ORIGINAL ARTICLE**

# Comparison of the distribution pattern of PEG-*b*-PCL polymersomes delivered into the rat inner ear via different methods

YA ZHANG[1], WEIKAI ZHANG[1], ALEXANDER H. JOHNSTON[2], TRACEY A. NEWMAN[3], ILMARI PYYKKÖ[1] & JING ZOU[1]

[1]*Department of Otolaryngology, University of Tampere, Medical school and University Hospital of Tampere, Tampere, Finland,* [2]*School of Biological Sciences and* [3]*School of Medicine, University of Southampton, Southampton, UK*



**Abstract**

*Conclusion:* Cochleostomy is the most efficient approach in delivering PEG-*b*-PCL polymersomes (PMs) to the inner ear. PMs can be delivered to the vestibule by transtympanic injection or cochleostomy. *Objective:* To evaluate the efficiency of delivering PEG-*b*-PCL PMs into the inner ear using different approaches. *Methods:* The PEG-*b*-PCL PMs were administered either by sustained topical round window membrane (RWM) delivery using gelatin sponge pledgets in combination with an osmotic pump, transtympanic injection, or cochleostomy. The distribution of the PMs in the inner ear was observed by confocal microscopy using either whole mount specimens or cryosections. *Results:* Cochleostomy resulted in distribution of the PMs in the spiral ligament (SL), mesothelial cells beneath the organ of Corti, supporting cells in the organ of Corti, and spiral ganglion cells (SGCs). Transtympanic injection induced uptake of the PMs in the SL and mesothelial cells beneath the organ of Corti. Topical administration showed distribution of the PMs only in the SL. In the vestibulum, transtympanic injection and cochleostomy induced more distribution of the PMs than did topical RWM delivery ($p < 0.05$, Kruskal-Wallis test).

**Keywords:** *Drug delivery, nanocarrier, imaging, animal*

## Introduction

Due to their targetability towards specific cell types, biocompatibility, and versatility in carrying payloads of different therapeutic agents, polymersomes (PMs) have potential as drug delivery vectors for the treatment of sensorineural hearing loss. PMs are vesicle-like nanoparticles formed from synthetic amphiphilic block copolymers such as poly(ϵ-caprolactone)-*block*-poly(ethylene glycol) (PEG-*b*-PCL) [1]. PMs have been previously investigated as delivery vehicles of therapeutic agents to the inner ear [2–4]. In in vitro cultures, the uptake of PMs into spiral ganglion neurons and glial cells was observed after periods of 24 h with no indication of toxicity [3]. In cochlea explants they displayed increased affinity for spiral ganglion cells (SGCs) when labelled with a short peptide sequence that specifically binds to the tyrosine kinase B (TrkB) receptor [4].

In the clinic, several techniques including transtympanic injection, topical round window membrane (RWM) permeation, and a catheter installed through the eustachian tube [5–7] are used for the transtympanic administration of therapeutic agents. We have previously reported that PEG-*b*-PCL PMs delivered by transtympanic injection passed the middle-inner ear barriers and were distributed within the cochlea and vestibulum [2]. As investigations have begun to elucidate the mechanisms and pharmacokinetics of the topical application of medication destined for the inner ear, newer strategies of delivery of therapeutics directly to the inner ear are beginning to emerge. These include modifications to existing cochlear implant technologies, osmotic pumps, and trans-RWM injection [8].

Correspondence: Jing Zou, Department of Otolaryngology, University of Tampere, Medical School, FM1, 3rd Floor, Biokatu 6, 33520 Tampere, Finland. E-mail: Jing.Zou@uta.fi

*(Received 31 May 2011; accepted 26 July 2011)*

ISSN 0001-6489 print/ISSN 1651-2251 online © 2011 Informa Healthcare
DOI: 10.3109/00016489.2011.615066

More recently, the micro-cannula portion of the drug delivery device has been modified to permit longer drug infusion times, as well as bolus dosing (such as for viral vector delivery) [9]. In this study, the distribution patterns of PEG-*b*-PCL PMs within the inner ear after intracochlear delivery using an osmotic pump were compared to those observed after transtympanic administration by transtympanic injection and topical RWM permeation.

## Material and methods

*Manufacturing and characterization of PMs*

$NH_2$-PEG5.8K-*b*-PCL19K (60 mg) was dissolved in 2 ml anhydrous *N*, *N*-dimethylformamide (DMF, Sigma-Aldrich, UK). 4-Nitrophenyl-iodoacetate (10 mg, Sigma-Aldrich) was added and the reaction mixture was stirred for 4 h. Diethyl ether (50 ml, Polymer Source Inc., Canada) was added and the solution was left overnight; the resulting precipitate was filtered and washed with diethyl ether to give iodoacetate-PEG5.8K-*b*-PCL19K (Polymer Source Inc.) functionalized polymer (45 mg, 75% yield). Then 15 mg of the solid was dissolved into DMF (1 ml) to give a pale yellow solution that turned clear when cystine terminated peptide (1 mg) was added. The reaction mixture was stirred overnight, concentrated in vacuo, and used crude in nanoparticle preparation.

The preparation of PEG-*b*-PCL PMs has been reported previously [4]. Briefly, 1,1′-dioctadecyl-3,3,3'3′-tetramethylindocarbocyanine perchlorate (DiI, Invitrogen, UK) was dissolved in DMF at a concentration of 0.1 mg/ml. PEG5.8K-*b*-PCL19K (6.0 mg) was dissolved in 0.4 ml of the DiI/DMF solution (0.4 ml). The polymer solution was then added dropwise (~1 drop every 8 s) to rapidly stirring phosphate-buffered saline (PBS; 1.60 ml). The sample was dialyzed against PBS for 48 h with regular changes of buffer solution. Dynamic light scattering (DLS) was performed on a Coulter N4 Plus particle sizer using N4 Plus version 1.10 software for data analysis. The typical PM hydrodynamic diameter was 62.6 ± 9.2 nm. Before use in in vivo experiments the PMs were sterile filtered through a 0.2 μm cellulose acetate syringe filter.

## Animals

Five-month-old male Sprague Dawley rats with normal Preyer's reflexes and weighing 350–450 g (supplied by the experimental animal unit, University of Tampere) were used in this study. Experiments were performed in accordance with the directives of the local ethics committee of the University of Tampere (permission: LSLH-2006-4143/Ym23).

Three methods were used for delivery of PEG-*b*-PCL PMs: transtympanic injection was applied to four rats bilaterally, topical RWM delivery was used in three rats bilaterally, and cochleostomy via osmotic pump was performed in five rats unilaterally. Two untreated rats were used as the control group.

All experimental procedures were performed under general anesthesia by intraperitoneal injection of a mixture of of medetomidine hydrochloride (0.8 mg/kg) (Domitor, Orion, Finland) and ketamine hydrochloride (80 mg/kg) (Ketalar, Pfizer, UK). Three days after treatment was started the animals were sacrificed and the cochleae were harvested. They were either whole mounted for confocal microscopy, or decalcified with 10% EDTA and prepared for cryosectioning.

## Administration of PMs to the inner ear

PM administration was performed under an operating microscope. For transtympanic membrane injection, 40 μl of PMs were injected into the middle ear cavity using 28-gauge needles. The injection volume was defined according to the literature report that the average volume of an adult rat middle ear cavity is 42 μl [10]. During the procedure the animal eyes were protected by Terra-Cortril-P (Pfizer).

For topical RWM delivery, the post-auricular procedure was performed with an operating microscope under aseptic conditions. The bulla was opened with a 2 mm diameter burr. The stapedial artery was exposed and the RWM was identified above the artery. An 8 $mm^3$ gelatin sponge pledget saturated with PMs was placed on the RWM. An osmotic pump filled with 100 μl of PMs was installed using a catheter (PE60, Becton Dickinson Co.), in conjunction with a gelatin sponge pledget that had been primed with the same solution. For cochleostomy, the bony wall of the scala tympani (ST) was opened by drilling with a 0.5 mm burr. The micro-osmotic pump was filled with 100 μl of PMs and connected to a catheter (PE60 tube and PE10 tube were linked by a PE30 tube; Becton Dickinson Co.), which was primed with the same solution. The catheter tip (PE10) was inserted into the ST and sealed with Histoacryl® (B|BRAUN, Germany). The catheter tube was fixed on the bulla with phosphate cement (Heraeus Kulzer GmbH, Germany) and the osmotic pump was implanted subcutaneously in the neck.

Atipamezole hydrochloride (2 mg/kg) was injected intraperitoneally immediately after the operation to accelerate the animals' awakening from anesthesia. Saline (2 ml) was administered through a subcutaneous injection in the neck. Rimadyl (1.0 mg/kg, Pfizer) was

injected to relieve pain. Baytril (10 mg/kg; Orion, Germany) was injected intraperitoneally once a day to prevent potential infection.

### *Histological studies*

*Whole mount sample preparation.* The bullae were fixed by cardiac perfusion with 4% paraformaldehyde (Merck, Germany) (0.01 M PBS containing 0.6% v/v heparin, pH 7.4, to remove the blood before fixation). The isolated cochleae were rinsed with water for 1 min to remove PMs remaining on the outer surface, then stored in the fixation solution for 2 h (whole mount samples) or overnight (cryosection).

After washing with PBS, the basal turn, middle turn, and apex (including the organ of Corti, spiral ligament (SL) and modiolus) of the cochlea, the RWM, and the utricle, the saccule and the ampullae of the vestibular were isolated. The tectorial membrane was removed under a stereo-microscope. The specimens were stained with 4′,6-diamidino-2-phenylindole (DAPI) (10 μg/ml, Sigma-Aldrich) for 10 min at room temperature in the dark. To diminish autofluorescence, the specimens were treated with 1 mM copper sulfate ($CuSO_4$) in 0.01 M ammonium acetate buffer (pH 5.0) [2]. After washing with PBS, the specimens were placed on eight-well slides (Cel-Line/Thermoscientific, USA) and mounted with Fluoromount (Sigma-Aldrich) for confocal microscopy.

*Cryosection preparation.* After 3 weeks of decalcification, the cochleae were washed with PBS, transferred to 30% sucrose for 24 h, and embedded with OCT™ component (Sakura Finetek). Tissue was cut at 30 μm sections using a cryostat (Leica CM3050S, Germany).

The cryoslides were washed with PBS for 5 min to remove the OCT™ component, stained with DAPI (10 μg/ml) for 10 min, washed with PBS, and mounted with Fluoromount for confocal microscopy.

*Confocal microscopy.* Both the whole mount specimens and the cryoslides were observed under a Nikon inverted microscope Eclipse Ti installed with ANDOR IQ. The excitation lasers were 568 nm and 405 nm from an Andor Laser Combiner system. The corresponding emission filters were 607/45 nm (TRITC and DiI) and 450–465 nm (DAPI). For 3D scanning, the interslice thickness was 0.5 μm.

### *Statistics*

The fluorescence of PMs on confocal microscopic images of the RWM, SL, and vestibulum (utricle and saccule) was measured using ImageJ 1.42q software (Table I). The fluorescence intensity was counted as pixels with gray value ≥1 after subtracting the noise signals. The fluorescence intensities of the PMs delivered by the three methods were compared by Kruskal-Wallis test using SPSS 11.5 software. A $p$ value $< 0.05$ was considered to be a significant difference.

Table I. Number of confocal microscopic images counted in the fluorescence intensity analysis.

| Method | RWM | SL | Vestibulum |
|---|---|---|---|
| TRWM | 21 | 25 | 4 |
| TTI | 27 | 32 | 18 |
| Cochleostomy | 5 | 25 | 5 |

RWM, round window membrane; SL, spiral ligament; TRWM, topical round window membrane; TTI, transtympanic injection.

## Results

### *Cochlear distribution of the PMs*

The RWM distribution of the PMs was detected in all animals, with significantly lower fluorescence signal in the topical RWM group than in the other two groups ($p < 0.01$, Kruskal-Wallis test; Figure 1). However, the distribution pattern varied among different groups; PMs were detected only in the outer epithelial layer in the topical RWM and transtympanic injection groups, but in all three layers in the cochleostomy group (Figure 2A1 and A2, Figure 3A and E).

In the SL, PMs were detected in all animals, as shown by whole mount specimens (Figure 2). When the

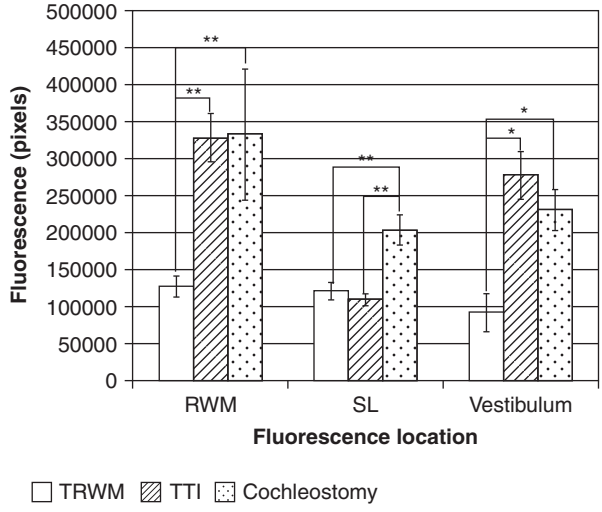


Figure 1. Comparison of the PEG-*b*-PCL polymersome fluorescence signal intensities in the rat inner ear 3 days after administration using different approaches. RWM, round window membrane; SL, spiral ligament; TRWM, topical RWM delivery; TTI, transtympanic injection. $^{**}p < 0.01$, $^{*}p < 0.05$ (Kruskal-Wallis test).

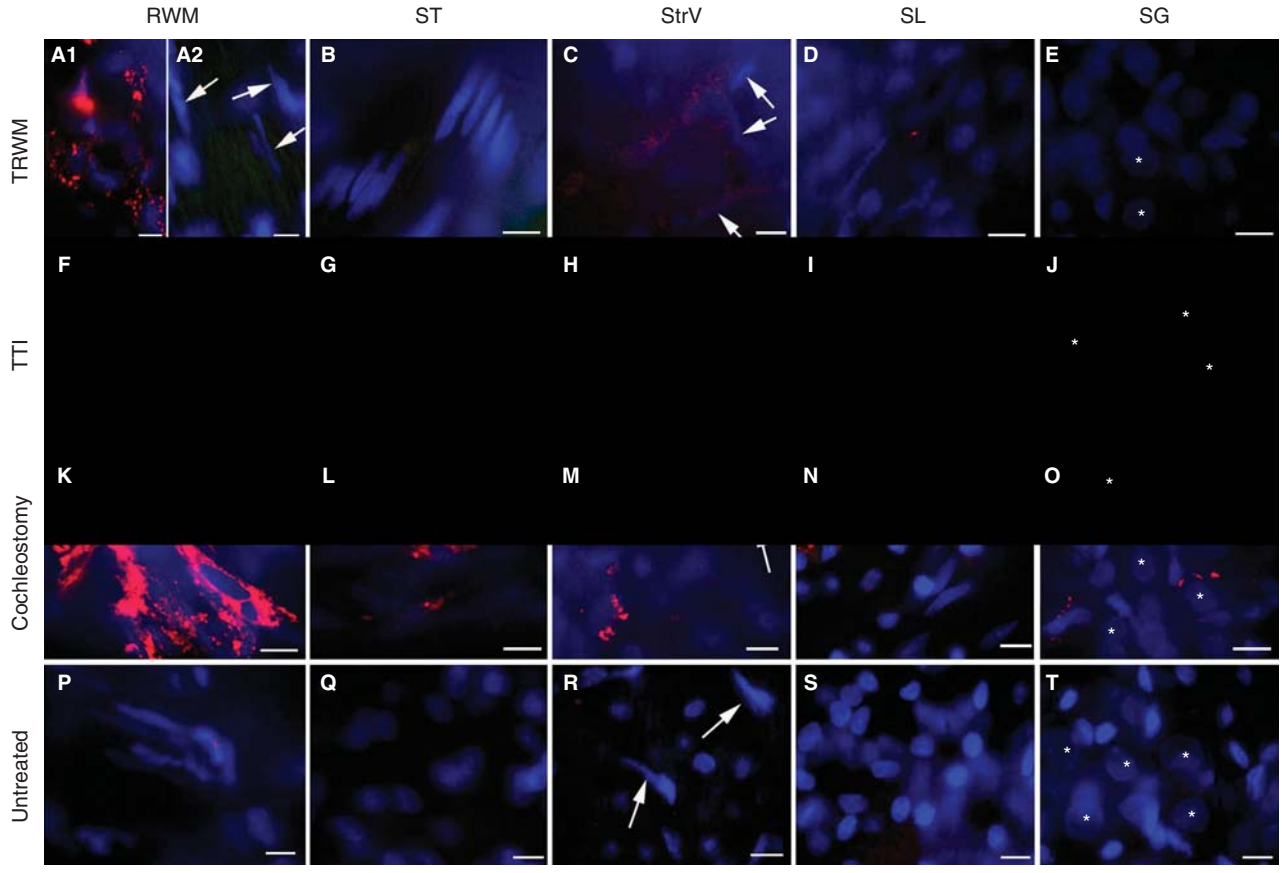


Figure 2. Panels A–O show the distribution of the PEG-*b*-PCL polymersomes in the rat inner ear 3 days after administration by different methods demonstrated by whole mount specimen confocal microscopy. Panels P–T show the untreated specimens. A1 shows the epithelial layer of the RWM. Arrows in A2 show the connective tissue layer of the RWM. Arrows in C, H, M, and R show the nuclei of the endothelial cells of the capillaries in StrV. Red: polymersomes. *Spiral ganglion cells. B, G, L, and Q, cells lining ST beneath the organ of Corti. RWM, round window membrane; SG, spiral ganglion; SL, spiral ligament; ST, scala tympani; StrV, stria vascularis; TRWM, topical RWM delivery; TTI, transtympanic injection. Blue: DAPI. Scale bar = 10 μm.

specimens were cryosectioned, PMs became visible only in the type III SL fibrocytes of animals receiving cochleostomy administration (Figure 3C and G; Figure 4). In the stria vascularis, PMs were found in the lumens of the capillaries in the topical RWM group and in the pericytes of the capillaries in the cochleostomy group (Figure 2C and M). In the organ of Corti, PMs were observed in Hensen cells and Claudius cells in the cochleostomy group (Figure 3F). Distribution of PMs in the spiral ganglion was also shown in the cochleostomy group (Figure 2N and O, Figure 3H). In the ST, PMs were detected in the mesothelial cells beneath the organ of Corti in the transtympanic injection group and the cochleostomy group (Figure 2G and L, Figure 3B and F).

*Vestibular distribution of the PMs*

Vestibular distribution of the PMs was detected in all animals. Cochleostomy and transtympanic injection induced a greater relative amount of PMs in the utricle and semicircular canal (SCC) compared with topical RWM administration. Relative distributions were obtained by measuring the fluorescence signal on confocal microscopic images of whole mount specimens ($p < 0.05$, Kruskal-Wallis test, Figures 1 and 4). Different PM distribution patterns between the transtympanic injection and cochleostomy groups were observed on the cryoslides; these differences were not seen using the whole mount specimens. Post transtympanic injection, PMs were detected in the endolymphatic and perilymphatic space of the vestibulum, while post cochleostomy they were detected in the utricular branch of the vestibular nerve and mesothelial cells of the SCC, facing the perilymph (Figure 5G–J).

*Migration of the PMs to the contralateral cochlea*

Post cochleostomy, PMs were detected in the contralateral cochleae but this was not observed after topical RWM or transtympanic injection. In the

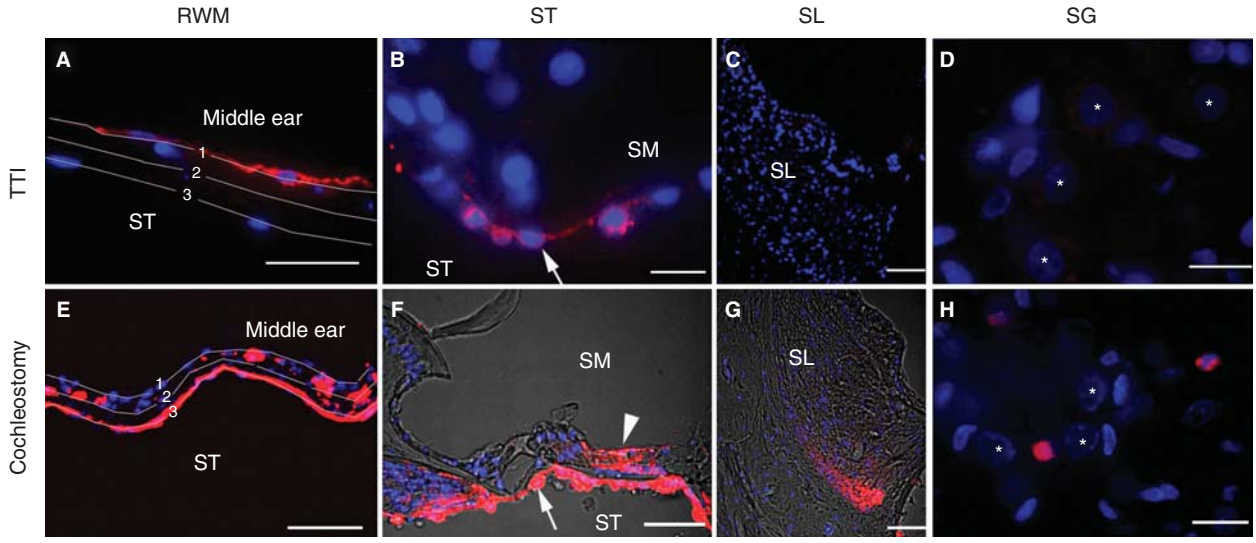


Figure 3. Distribution of the PEG-*b*-PCL polymersomes (PMs) in the rat inner ear 3 days after administration by different delivery methods, as demonstrated by cryosection confocal microscopy. TTI induced the distribution of the PMs in the outer epithelium of the RWM, while cochleostomy resulted in the distribution of the PMs in all three layers of the membrane. Arrows in (B) and (F) highlight the distribution of the PMs in the mesothelial cells of the ST beneath the organ of Corti. The arrowhead in (F) shows PMs in the Claudius cells and the Hensen cells. (G) Distribution of the PMs in the type III spiral ligament fibrocytes. (H) PMs in spiral ganglion glial cells. RWM, round window membrane; SG, spiral ganglion; SL, spiral ligament; SM, scala media; ST, scala tympani; TTI, transtympanic injection; 1, outer epithelial layer of the RWM; 2, connective tissue layer of the RWM; 3, inner endothelial layer of the RWM. Red: PMs. Blue: DAPI. Gray in (F) and (G): bright field. *Nuclei of type I SGCs. Scale bar in A, C, and E–G = 50 μm. Scale bar in B, D, and H = 20 μm.

contralateral cochleae, the PMs were observed in the mesothelial cells of ST in the first turn, the epineurium of the cochlear nerve in the modiolus, and in the cochlear nerve in the internal meatus (Figure 6).

## Discussion

There are two pathways for drugs to be transported from the middle ear cavity into the inner ear in rats: through the RWM to the perilymph in the ST or through the annular ligament of the oval window to the vestibular perilymph [11]. The RWM is a semi-permeable membrane that prevents hazardous substances from entering the inner ear, but it also prevents the effective passage of therapeutics. The epithelial layer has tight junctions [12], whereas the connective tissue layer and the endothelial layer are loosely arranged. It is likely that the PMs pass through the epithelial layer via a transcellular pathway, then through the connective tissue layer and the endothelial layer via an intercellular pathway [12]. The PMs were detected in only the epithelial layer of the RWM when

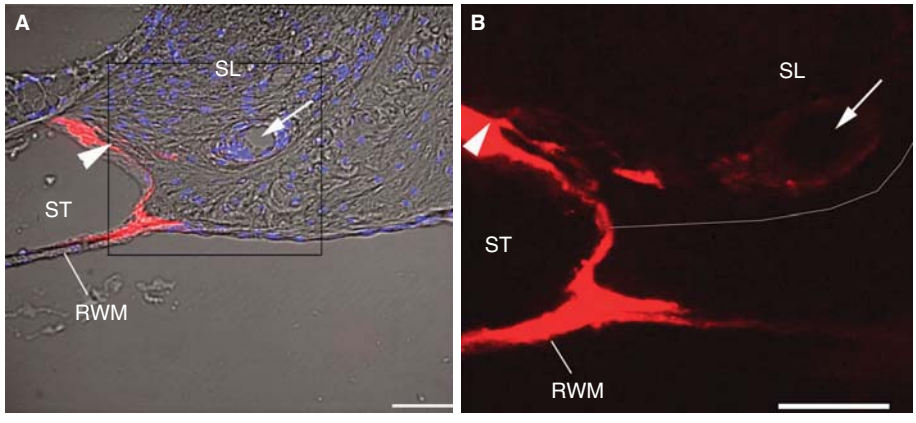


Figure 4. Migration of the polymersomes (PMs) from the scala tympani (ST) to the round window membrane (RWM) and spiral ligament (SL) after cochleostomy administration as shown by cryosection confocal microscopy. Arrowheads show the mesothelium of the ST; arrows show a blood vessel in the type III spiral ligament fibrocytes region. (A) Merged images from the red channel, blue channel, and bright field. (B) Enlarged window of the red channel in (A) allows visualization of the PMs. Red: PMs. Blue: DAPI. Scale bar = 100 μm.

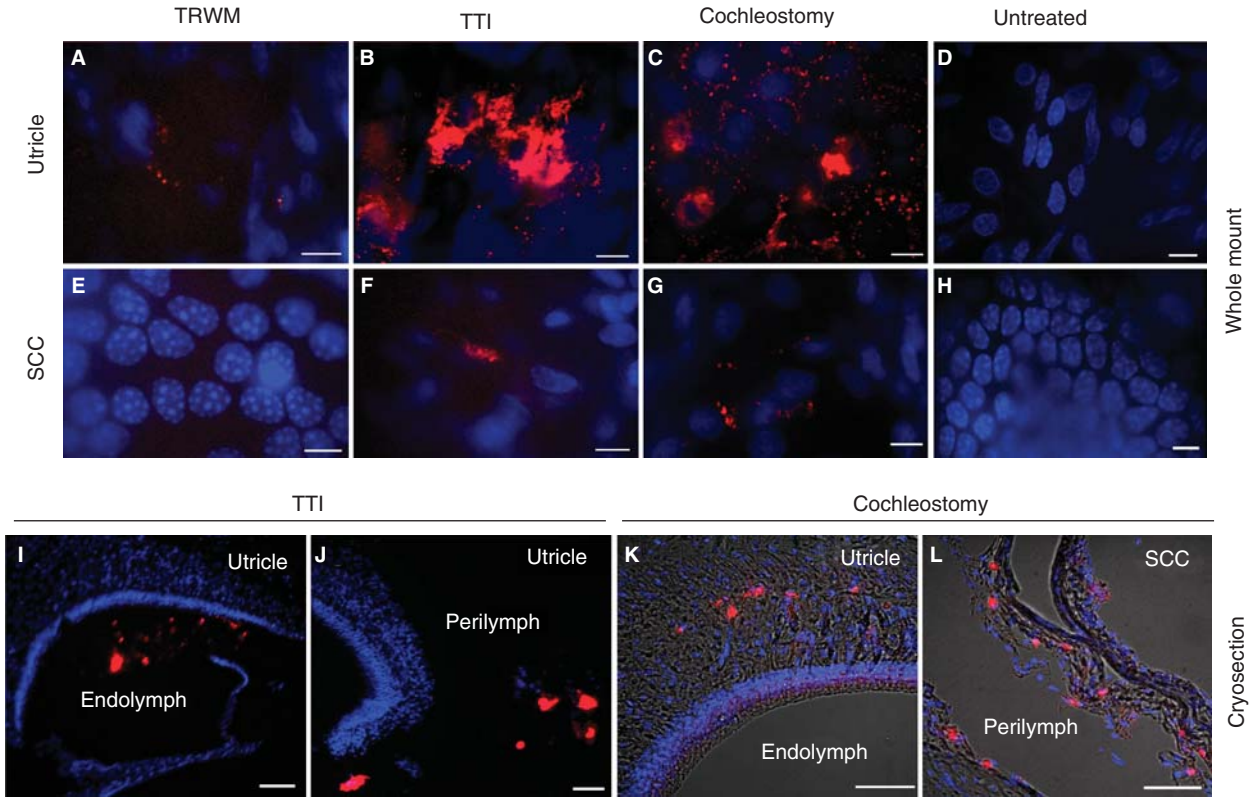


Figure 5. Vestibular distribution of the PEG-b-PCL polymersomes (PMs). Whole mount samples show the appearance of the PMs in the utricle (A–C) as well as in the semicircular canal (SCC) (E–G) when delivered via TRWM (topical round window membrane), TTI (transtympanic injection), and cochleostomy and the untreated specimens (D and H). Cryosections show the endolymphatic (I) and perilymphatic (J) distributions of the PMs in the utricle after TTI delivery; the PMs were found in the utricular branch of the vestibular nerve (K) and in the epithelial cells of SCC (L) after cochleostomy administration. Red: PMs. Blue: DAPI. Scale bar in A–F = 10 μm. Scale bar in G–J = 100 μm.

delivered by topical RWM delivery and transtympanic injection; however, they were detected in all three layers of the RWM when administered via cochleostomy. This finding suggests that PMs were taken up by the endothelial cells while diffusing through loose intercellular gaps of the endothelium to the connective tissue core. The PMs were then internalized by the epithelial cells after entering into the cochlear perilymph. However, after topical RWM delivery and transtympanic injection most of the PMs were internalized by the epithelial layer of the RWM and most of them failed to be transported to the connective tissue layer and the endothelial layer of the RWM. Variable transport efficacy of different agents across the RWM has been reported in the literature. Trimethylphenylammonium (TMPA) passed the

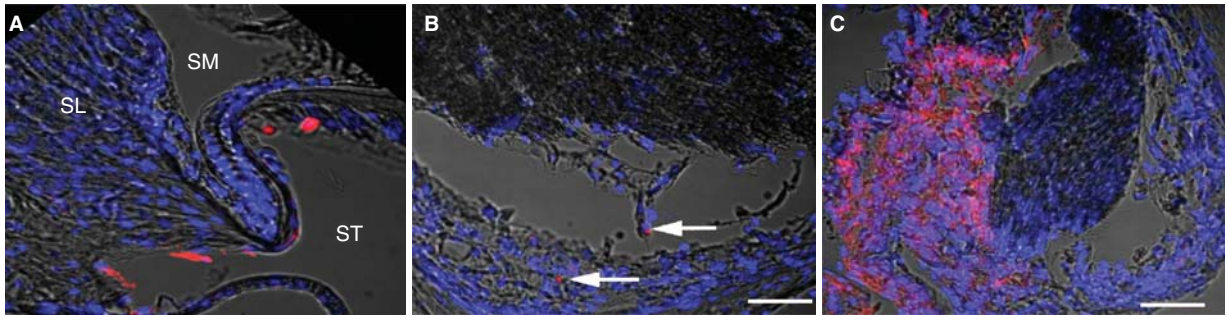


Figure 6. Appearance of the PEG-*b*-PCL polymersomes (PMs) in the contralateral cochlea after administration via cochleostomy. The PMs were detected in the mesothelial cells of ST in the basal turn (A), perineurium of the cochlear nerve in the modiolus (arrows in B), and in the internal meatus (C). SL, spiral ligament; SM, scala media; ST, scala tympani. Red: PMs. Blue: DAPI. Scale bar = 50 μm.

RWM and was detected at 16.5% of the original concentration in the ST of the basal turn 90 min after RWM administration [13]. Proteins such as bacterial endotoxins have shown poor passage through the RWM; the concentration detected in the perilymph was 0.01% of the original concentration when applied by topical RWM delivery [14]. Topical RWM administration of nanocarriers carrying a payload of gadolinium resulted in poor loading of the nanoparticles in the rat inner ear as shown by in vivo magnetic resonance imaging (MRI) [6]. However, transtympanic injection of PEGylated liposome nanocarriers encapsulating gadolinium-tetra-azacyclododecane-tetra-acetic acid (Gd-DOTA) passed the RWM efficiently, as detected by the Gd-DOTA signal in the inner ear using in vivo MRI [11]. The variable efficacy in crossing the middle-inner ear barriers is likely dependent on the different surface characteristics of the nanocarriers.

After transtympanic injection, more PMs were detected in the vestibulum than in the cochlea, indicating that the PMs entered the vestibulum through the oval window [11]. A histological study in rats demonstrated that the annular ligament across the stapedio-vestibular joint is a porous structure composed of fibrillin, 36 kDa microfibril-associated glycoprotein (MAGP-36), and hyaluronic acid, which supports our MRI results [15]. Our serial human and animal MRI studies constantly demonstrated greater uptake of gadolinium in the vestibulum than in the ST when administered to the middle ear cavity by different means [6]. Recently, we showed that the oval window is an effective pathway for transport of Gd-DOTA from the middle ear to the vestibulum and is more efficient than the RWM [16].

Administration via cochleostomy displayed the broadest distribution of PMs in the inner ear. The organ of Corti has a loose structure and dextran applied to the perilymph of the ST gained access the majority of cell types within the cochlea, as well as the nerve fibers in the peripheral processes of the spiral ganglion cells [17]. Zou et al. have also hypothesized that lipid nanocapsules may reach the spiral ganglion cells through a 'nerve pathway' from the Corti's fluid (inside the Corti's tunnel) [18]. A short-cut between the perilymph and modiolus was also indicated by both electron microscopy studies on human cochlea and in vivo MRI investigations in guinea pigs [19–21]. This short-cut may also be utilized as the PMs migrate to the spiral ganglion cells from the ST. Transportation of the PMs from the ST to the scala vestibuli may be mediated by either the SL or the modiolus [20]. Consequently, the PMs are further distributed from the vestibule to the scala vestibuli. Cochlear distribution of PMs was mostly preserved using the whole mount histological method, but significantly decreased by cryosectioning. It is likely that loosely deposited PMs in the intercellular space were washed away during the cryosectioning procedure. This indicates that whole mount method is a preferable method to demonstrate tissue location of PMs in the cochlea. However, preparation of samples using cryosectioning may provide additional information on the spatial location of PMs restrained in the inner ear.

Our study contributes to the optimization of PM-mediated inner ear drug delivery. Although transtympanic injection of the PMs was not superior to topical RWM application in terms of their delivery into the cochlea, it was more efficient in delivering the PMs into the vestibulum than topical RWM administration. However, both methods failed to distribute the PMs into the spiral ganglion or the organ of Corti. Among the evaluated delivery approaches, cochleostomy is the most promising method with which to deliver the PMs into these locations. This supports the development of new strategies for the delivery of therapeutics directly to the inner ear using either modifications to existing cochlear implant technologies or osmotic pumps. This information is also relevant to exploring trans-RWM injection of PMs.

The appearance of the PMs in the contralateral cochlea and internal auditory canal may be mediated by the cochlear aqueduct, which is located in the hook region of the basal turn of the ST. This passage was identified in an in vivo MRI study by Zou et al. in the guinea pig, which showed that blockage of the cochlea aqueduct prevented backflow of gadolinium from the perilymph in the ST to the cerebrospinal fluid (CSF) [19]. Communication between the perilymph and CSF may cause adverse effects in the brain and contralateral cochlea during inner ear drug delivery. We expect that the advanced nanocarriers (including PMs) equipped with targeting moieties will fine-tune the use of these agents.

## Conclusions

Cochleostomy is the most efficient approach to delivery of PEG-*b*-PCL PMs to the cochlear cells and vestibular cells. Transtympanic injection induced a broader vestibular distribution of the PMs than the topical RWM approach. Different inner ear drug delivery approaches should be considered according to the purpose of treatment.

## Acknowledgments

This study was supported by the European Community 6th Framework Programme on Research, Technological Development and Demonstration (Nanotechnology-based Targeted Drug Delivery.

Contract number: NMP4-CT-2006-026556, Project acronym: NANOEAR).

***Declaration of interest:*** The authors report no conflicts of interest. The authors are responsible for the content and writing of the paper.

## References

[1] Johnston AH, Dalton PD, Newman TA. Polymersomes, smaller than you think: ferrocene as a TEM probe to determine core structure. J Nanopart Res 2010;12:1997–2001.

[2] Zhang Y, Zhang W, Johnston AH, Newman TA, Pyykko I, Zou J. Improving the visualization of fluorescently tagged nanoparticles and fluorophore-labeled molecular probes by treatment with $CuSO_4$ to quench autofluorescence in the rat inner ear. Hear Res 2010;269:1–11.

[3] Anderson M, Johnston AH, Newman TA, Dalton PD, Rask-Andersen H. Internalization of nanoparticles into spiral ganglion cells. Journal of Nanoneuroscience 2008;1:1–10.

[4] Roy S, Johnston AH, Newman TA, Glueckert R, Dudas J, Bitsche M, et al. Cell-specific targeting in the mouse inner ear using nanoparticles conjugated with a neurotrophin-derived peptide ligand: potential tool for drug delivery. Int J Pharm 2010;390:214–24.

[5] Thomsen J, Charabi S, Tos M. Preliminary results of a new delivery system for gentamicin to the inner ear in patients with Meniere's disease. Eur Arch Otorhinolaryngol 2000; 257:362–5.

[6] Zou J, Ramadan UA, Pyykko I. Gadolinium uptake in the rat inner ear perilymph evaluated with 4.7 T MRI: a comparison between transtympanic injection and gelatin sponge-based diffusion through the round window membrane. Otol Neurotol 2010;31:637–41.

[7] Kaasinen S, Pyykko I, Ishizaki H, Aalto H. Intratympanic gentamicin in Meniere's disease. Acta Otolaryngol 1998;118: 294–8.

[8] McCall AA, Swan EE, Borenstein JT, Sewell WF, Kujawa SG, McKenna MJ. Drug delivery for treatment of inner ear disease: current state of knowledge. Ear Hear 2010; 31:156–65.

[9] Prieskorn DM, Miller JM. Technical report: chronic and acute intracochlear infusion in rodents. Hear Res 2000;140:212–15.

[10] Kania RE, Herman P, Tran Ba Huy P, Ar A. Role of nitrogen in transmucosal gas exchange rate in the rat middle ear. J Appl Physiol 2006;101:1281–7.

[11] Zou J, Sood R, Ranjan S, Poe D, Ramadan UA, Kinnunen PK, et al. Manufacturing and in vivo inner ear visualization of MRI traceable liposome nanoparticles encapsulating gadolinium. J Nanobiotechnology 2010;8:32.

[12] Goycoolea MV, Lundman L. Round window membrane. Structure function and permeability: a review. Microsc Res Tech 1997;36:201–11.

[13] Salt AN, Ma Y. Quantification of solute entry into cochlear perilymph through the round window membrane. Hear Res 2001;154:88–97.

[14] Lundman L, Juhn SK, Bagger-Sjoback D, Svanborg C. Permeability of the normal round window membrane to Haemophilus influenzae type b endotoxin. Acta Otolaryngol 1992;112:524–9.

[15] Ohashi M, Ide S, Sawaguchi A, Suganuma T, Kimitsuki T, Komune S. Histochemical localization of the extracellular matrix components in the annular ligament of rat stapediovestibular joint with special reference to fibrillin, 36-kDa microfibril-associated glycoprotein (MAGP-36), and hyaluronic acid. Med Mol Morphol 2008;41:28–33.

[16] Zou J, Yoshida T, Ramadan UA, Pyykkö I. Dynamic enhancement of the rat inner ear after ultra-small volume administration of Gd-DOTA to the medial wall of the middle ear cavity. ORL J Otorhinolaryngol Relat Spec 2011 (in press).

[17] Ulfendahl M, Scarfone E, Flock A, Le Calvez S, Conradi P. Perilymphatic fluid compartments and intercellular spaces of the inner ear and the organ of Corti. Neuroimage 2000;12: 307–13.

[18] Zou J, Saulnier P, Perrier T, Zhang Y, Manninen T, Toppila E, et al. Distribution of lipid nanocapsules in different cochlear cell populations after round window membrane permeation. J Biomed Mater Res B Appl Biomater 2008;87:10–18.

[19] Zou J, Pyykko I, Counter S, Klason T, Bretlau P, Bjelke B. In vivo observation of dynamic perilymph formation using 4.7 T MRI with gadolinium as a tracer. Acta Otolaryngol 2003; 123:910–15.

[20] Rask-Andersen H, Schrott-Fischer A, Pfaller K, Glueckert R. Perilymph/modiolar communication routes in the human cochlea. Ear Hear 2006;27:457–65.

[21] Zou J, Poe D, Bjelke B, Pyykko I. Visualization of inner ear disorders with MRI in vivo: from animal models to human application. Acta Otolaryngol Suppl 2009:22–31.

# Distribution of Lipid Nanocapsules in Different Cochlear Cell Populations After Round Window Membrane Permeation

**Jing Zou,[1] Patrick Saulnier,[2] Thomas Perrier,[2] Ya Zhang,[1] Tommi Manninen,[1] Esko Toppila,[1] Ilmari Pyykkö[1]**

[1] Department of Otolaryngology, University of Tampere, School of Medicine, 33520 Tampere, Finland

[2] Université d'Angers-INSERM U646 Ingénierie de la Vectorisation Particulaire, 49100 Angers, France

*Received 25 October 2007; revised 10 December 2007; accepted 18 December 2007*
*Published online 24 April 2008 in Wiley InterScience (www.interscience.wiley.com). DOI: 10.1002/jbm.b.31058*

**Abstract: Hearing loss is a major public health problem, and its treatment with traditional therapy strategies is often unsuccessful due to limited drug access deep in the temporal bone. Multifunctional nanoparticles that are targeted to specified cell populations, biodegradable, traceable *in vivo*, and equipped with controlled drug/gene release may resolve this problem. We developed lipid core nanocapsules (LNCs) with sizes below 50 nm. The aim of the present study is to evaluate the ability of the LNCs to pass through the round window membrane and reach inner ear targets. FITC was incorporated as a tag for the LNCs and Nile Red was encapsulated inside the oily core to assess the integrity of the LNCs. The capability of LNCs to pass through the round window membrane and the distribution of the LNCs inside the inner ear were evaluated in rats via confocal microscopy in combination with image analysis using ImageJ. After round window membrane administration, LNCs reached the spiral ganglion cells, nerve fibers, and spiral ligament fibrocytes within 30 min. The paracellular pathway was the main approach for LNC penetration of the round window membrane. LNCs can also reach the vestibule, middle ear mucosa, and the adjacent artery. Nuclear localization was detected in the spiral ganglion, though infrequently. These results suggest that LNCs are potential vectors for drug delivery into the spiral ganglion cells, nerve fibers, hair cells, and spiral ligament.** © 2008 Wiley Periodicals, Inc. J Biomed Mater Res Part B: Appl Biomater 87B: 10–18, 2008

**Keywords: nanoparticles; inner ear; drug delivery; neuron; biological barrier**

## INTRODUCTION

Hearing loss is a major public health problem that ranks 8th among common diseases in the EU. The traditional treatment strategy for sensorineural hearing loss (SNHL) has not been very successful. The human cochlea is deeply buried in the temporal bone, and its access is limited by membranous partitions. The blood supply derived from the intracerebral vessels hampers any efforts for intravascular treatment. Cochlear implantation (CI) bypasses the membranous borders and provides direct contact with cochlear partitions. Thus far, only electrical stimulation has been used in hearing rehabilitation, and CI is a well-established method for restoring severe or profound hearing loss. However, hearing performance after implantation is variable due to several causes.[1–4] A cure for SNHL would thus depend on novel concepts such as successful gene or drug delivery alone or in combination with CI.[5]

To achieve an ideal outcome with a minimum amount of adverse effects, novel multifunctional nanoparticles (MNPs) could be used. These must possess special characteristics such as the ability to be targeted to specified cell populations, as well as being biodegradable, traceable *in vivo*, and equipped with controlled drug/gene release. In clinical practice, a minimally invasive delivery approach is desired. One such method is round window membrane permeation, which is an efficient and minimally invasive method of administering substances into the inner ear, as has been proved in both animal and human studies.[6,7] The method is also feasible, as suggested by reports on gene delivery through intact round window membranes and expression in the cochlea.[8,9] Reports from clinical observation of transtympanic steroid treatments for SNHL indicate that the presence of a controlled sustained release of drug into the inner ear can determine the outcome of patients.[10–12] According to Praetorius et al., silica nanoparticles can reach all cell populations of the inner ear upon delivery onto the round window membrane.[13] Hitherto, silica nano-

*Correspondence to:* J. Zou (e-mail: Jing.Zou@uta.fi)
Contract grant sponsor: EU project Nanoear; Grant numbers: NMP4-CT-2006-026556

particles face problems in loading and releasing drugs in a controlled fashion.

Lipid core nanocapsule (LNC) possesses sustained release property for amiodarone.[14] For this study, the LNC was further modified to be made visible in tissues by incorporating FITC into the LNC to serve as a tag. Nile Red was encapsulated inside the oily core to assess the integrity of the LNC *in vivo*. If FITC and Nile Red co-localize inside the tissues, the LNC must be intact; otherwise it is considered degraded. The aim of the present work is to demonstrate that the LNC can permeate the round window membrane, pass the cochlear partitions, and address inner ear cell populations.

**TABLE 1. Grouping of the Ear for Round Window Membrane Delivery of LNC**

| Groups[a] | Side of the Ear | Number of Animals | Number of the Ear |
|---|---|---|---|
| 30 min | Left side | 5 | 5 |
| 60 min | Right side | | 4 |
| 180 min | Right side | | 1 |
| 1 day[b] | Both side | 2 | 4 |
| 7 day[b] | Both side | 2 | 4 |

[a] The time between sampling and the administration of LNC.

[b] Left ear with transient administration of LCN (30 min), right side with constant delivery.

## MATERIALS AND METHODS

### Materials and Animals

Materials for LNC manufacturing include: the lipophilic Labrafac_WL 1349 (caprylic-capric acid triglycerides; European Pharmacopeia, IVth, 2002) which was kindly provided by Gattefossé S.A. (Saint-Priest, France), Lipoïd S75-3 (soybean lecithin with 69% of phosphatidylcholine), and Solutol HS 15 (mixture of free polyethylene glycol 660 and polyethylene glycol 660 hydroxystearate, European Pharmacopeia, IVth, 2002), which were gifts from Lipoïd Gmbh (Ludwigshafen, Germany) and BASF (Ludwigshafen, Germany), respectively. Because of the complex composition of each product, the brand names will be used in the following text. NaCl was obtained from Prolabo (Fontenay-sous-Bois, France). Water was obtained from a Milli RO System (Millipore, Paris, France). Fluorescein-5-isothiocyanate (FITC) was purchased from Fluorescéine IsoThioCyanate (France), Nile Red and 3,3′-Dioctadecyloxacarbovyanine perchlorate (DiO) were purchased from Sigma-Aldrich (USA), and Rhodamine B was purchased from ChemExper Inc. (Belgium). 1,2-Distearoyl-*sn*-Glycero-3-Phosphoethanolamine-*N*-[Amino(PolyethyleneGlycol)2000] (called DSPE-PEG2000-amino in the text) was furnished by Avanti® Polar Lipids, Inc (Alabaster, USA).

Materials for animal testing included elastase (Sigma-Aldrich, USA), collagenase type I (Sigma-Aldrich, USA), trypsin (Sigma-Aldrich, USA), fetal calf serum (Invitrogen, USA), paraformaldehyde (Sigma-Aldrich, USA), FITC-labeled phalloidin (Sigma-Aldrich, USA), rabbit anti-neurofilament 200 polyclonal antibody (Sigma-Aldrich, USA), FITC-labeled goat anti-rabbit IgG (Sigma-Aldrich, USA), 4′,6-Diamidino-2-phenylindole (DAPI) (Sigma-Aldrich, USA), Gel Mount™ Aqueous Mounting Medium (Sigma-Aldrich, USA), O.C.T. (Electron Microscopy Sciences, USA), medetomidine hydrochloride (Orion, Finland), atipamezole hydrochloride (Orion, Finland), Ketamine (Pfizer, USA), L-Polamivet (Intervet, Finland), and ofloxacin (Aventis Pharmacy, Finland).

Nine male Sprague-Dawley rats with normal Pryer's reflex (supplied by the experimental animal unit, University of Tampere) were used in the study in accordance with the local ethics committee of University of Tampere standards (permission no: 985/2003). They were divided into five groups according to their time points (Table 1). All animal experiments were approved by the Ethical Committee of the University of Tampere. Animal care and experimental procedures were conducted in accordance with European legislation.

### LNC Preparation

The first step of the formulation was an emulsion consisting of Labrafac® WL 1349, an oil made of capric and caprylic acid triglycerides (average molecular weight of 512); Lipoid® S75-3, a soybean lecithin made of 69% phosphatidylcholine and other phospholipids; Solutol® HS 15, another surfactant; a mixture of polyethylene glycol 660 hydroxystearate (C18E15); and free polyethylene glycol 660. The optimal amounts of ingredients for preparation of 50 nm LNC were: Labrafac® (1.028 g), Lipoïd® (0.075 g), Solutol® (0.846 g), NaCl (0.089 g) and pure water (2.962 g). This mixture was prepared under magnetic stirring at room temperature to obtain an emulsion of oil in water. After progressive heating at a rate of 4°C/min under magnetic stirring, we observed a short interval of transparency at temperatures close to 70°C, and the inverted phase (water droplets in oil) was obtained at 85°C. Then, three cycles of cooling and heating were applied between 85°C and 60°C at the same rate of 4°C/min (near the phase inversion zone), and finally a fast dilution in cold water at a temperature close to 0°C produced a suspension of nanocapsules.[15,16]

### DSPE-PEG2000-Amino Postinsertion

LNCs were incubated for 90 min with an aqueous micellar solution of DSPE-PEG-amino at 60°C. The suspension was vortexed every 15 min and then quenched in an ice bath for 1 min. The final DSPE-PEG concentration corresponded to 6 mol % of total surface molecules (i.e., Solutol and Lipoïd).[17]

### Nile Red and DiO Encapsulation

A volume of 55 $\mu$L (0.18 $\mu$mol) of a Nile Red in ethanol solution (1 mg/mL) was added to the LNC emulsion, just before diluting the system with cold water. The Nile Red was totally encapsulated in the oily core, with the final concentration of 174 $\mu$mol/L. For DiO encapsulation, Nile Red was replaced by 153 $\mu$g DiO and the final concentration was 174 $\mu$mol/L.

### FITC and Rhodamine B Labeling

After the postinsertion process, 2 mg of FITC isothiocyanate (5.13 $\mu$mol) was added to 2.95 mL of LNC suspension and the pH was increased to 10 by adding of a few drops of 0.1*M* $Na_3PO_4$ solution. The sample was protected from light and placed in a water bath under magnetic stirring at 35°C for 45 min. After the sample was cooled in an ice bath for 3 min in order to stop the reaction, size exclusion chromatography on a sephadex G-15 column was performed to separate free FITC from labelled LNCs. Optical density (FITC detection) as well as turbidity at 680 nm (LNC detection) was measured for each fraction [Figure 1(A)]. Fractions corresponding to the FITC labeled LNCs were analysed by dynamic light scattering. Electrokinetic measurements were performed at a constant conductivity (0.03 $\mu$s $cm^{-1}$). These measurements indicated a hydrodynamic diameter of 52 $\pm$ 5 nm and a zeta potential of $-55 \pm 7$ mV (for non labelled LNCs we obtained $-7 \pm 3$ mV) [Figure 1(B)]. Only fractions with a polydispersity index lower than 0.2 were pooled and used for animal testing [Figure 1(C)]. For Rhodamine B labeling, FITC was replaced by 2 mg Rhodamine B.

### Round Window Membrane Delivery of LNCs

Animals were fully anesthetized with medetomidine hydrochloride (0.5 mg/kg) and ketamine (75 mg/kg). The operation was performed under sterile conditions. After local analgesia with lidocaine, a retro-auricular incision was used to expose the left bulla. A hole was drilled on the bulla with a 2 mm diameter burr. After visualizing the stapes artery, the round window membrane was identified above the artery. A small piece of gelfoam (around 8 $mm^3$) was saturated with LNC and placed on the round window membrane (LNC concentration: 20.5 g/L, stored at 4°C for 3 months). The ears were divided into five groups of 30 min, 60 min, 180 min, 1 day, and 7 days according to the sampling time post-LNC administration (Table 1). For the 1 day and 7 day groups, gelfoam was placed on the left ear for 30 min and then removed, whereas gelfoam was placed on the right ear constantly until the end of the experiment. The hole on the bulla was sealed with muscle and the wound was sutured in the 1 day and 7 day groups. Atipamezole hydrochloride (2 mg/kg) was injected i.p. immediately after the operation to accelerate recovery from anaesthesia of the animals. Saline (2 mL) was administered through subcutaneous injection on the neck. L-Polamivet (0.4 mL/kg) was injected b.i.d. to relieve the pain. Ofloxacin (20 mg/kg) was injected b.i.d. in the 1 day and 7 day groups after operation.

### Whole Mount Sample Preparation

Following i.p. injection of pentobarbital (60 mg/kg), 2–3 mL of air was cardio injected to sacrifice the animals. The bulla was removed and fixed in 4% paraformaldehyde for 1 h. The cochlea was thoroughly washed with tap water for 30 s and then opened by breaking the bony wall under a stero-microscope, and washed again with PBS for 2 $\times$ 5 min. The bulla was counter stained with DAPI (10 $\mu$g/mL) for 10 min, and further washed three times for 5 min each with PBS in a dark room. The middle ear mucosa, stapes artery, round window membrane, lateral wall, and modiolus from the basal turn, cochlear nerve, and ampulla of the semi-circular cannel were taken under a stereo-microscope, placed on glass slide, and mounted with Gel Mount™ Aqueous Mounting Medium for confocal microscopy.

### Cochlear Cell Isolation

To confirm the cellular internalization of LNCs, one small piece of tissue, each from the cochlear modiolus and lateral wall (fixed with 4% paraformaldehyde), was treated with elastase (1 mg/mL), collagenase type I (1 mg/mL) and trypsin (0.5 mg/mL) at 37°C for 15 min. The enzymes were inactivated through incubation with DMEM containing 5% fetal calf serum at room temperature for 5 min. The isolated cells were placed on glass slides and mounted with Gel Mount™ Aqueous Mounting Medium for confocal microscopy.

### Cryosectioning

For clarification of the cellular population in the lateral wall, one piece of the fixed lateral wall was embedded with O.C.T., sectioned by a cryostat (Leica CM3050S, Germany) in 5-$\mu$m sections, and mounted with Gel Mount™ Aqueous Mounting Medium.

### Cellular Specific Staining

To confirm the cell population of the cochlea with regard to the LNCs distribution, immunofluorescent staining was applied to visualize neurofilament in the cochlear nerve tissue, and FITC-labeled phalloidin was used to probe F-actin in the organ of Corti and lateral wall. After fixation and washing as stated above, permeation with 0.3% Triton X-100 PBS for 5 min, and washing again with PBS, lateral wall soft tissue was isolated from the bone and incubated in FITC-labeled phalloidin (50 $\mu$g/mL) for 40 min and then in DAPI for 10 min. After washing with PBS for 2 $\times$ 5 min, stria vascularis was isolated from the spiral ligament and both tissues were mounted as stated above. After incubation with preimmunized goat serum (1:20), the modiolus

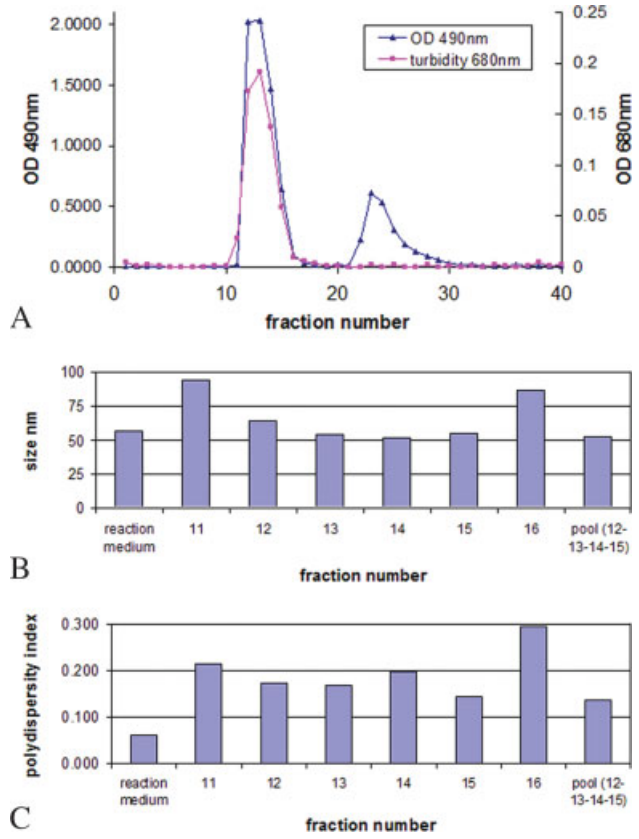


**Figure 1.** Characterization of FITC labeled LNCs. A: Separation of free FITC from labeled LNCs with Sephadex G15. The first peak showed absorbance at both 490 nm and 680 nm, indicating FITC-conjugated LNCs with encapsulated Nile Red. The second peak showed only absorbance at 490 nm, indicating free FITC. B: LNC size for each fraction after chromatography on Sephadex G-15. C: Polydispersity index for each fraction after chromatography on Sephadex G-15. [Color figure can be viewed in the online issue, which is available at www.interscience.wiley.com.]

including basilar membrane was incubated with rabbit anti-neurofilament 200 polyclonal antibody (1:1000) overnight at 4°C, washed with PBS containing 0.2% Tween 20 (PBS-T), and counterstained with DAPI for 10 min; the basilar membrane, together with bony spiral laminar, was isolated from the modiolus and mounted as stated above.

### Confocal Microscopy

The whole mount samples and cryosectioned slices were observed under an Olympus microscope IX70 installed with ANDOR IQ. The excitation filters were 488 nm (blue excitation) and 568 nm (green excitation), with an Ar-Kr laser as the excitation source. The corresponding emission filters were 525/50 (FITC and DiO) and 607/45 (Nile Red and Rhodamine B). DAPI was excited with a 340–380 nm filter and detected using a 500 LP filter. For 3D scanning, the inter slice thickness was 0.5 $\mu$m. The image data was rendered with ImageJ 1.32j software.

## RESULTS

Thirty minutes after administration of the LNC in the tympanic cavity on the round window membrane, abundant LNCs were found in the spiral ganglion cells [Figure 2(A–C)]. LNCs also attached to the outer surface of nerve fibers of the spiral ganglion; this was confirmed by neurofilament staining [Fig. 2(D)]. Nuclear localization was detected in the spiral ganglion, though infrequently [Figure 2(D)]. However, the spiral ganglion distribution intensity of LNCs after thorough treatment including washing with surfactant (Tween-20) during neurofilament staining was much lower than without the staining. LNCs were also visible in the inner hair cells and pillar cells as confirmed by F-actin staining [Figure 2(E–G)]. Again as a result of staining for neurofilament, LNCs were totally invisible in the organ of Corti [Figure 2(H)]. The distribution of LNCs in the lateral wall was found in both the spiral ligament and stria vascularis [Figure 2(I–L)]. The surface appearance of marginal cells of the stria vascularis after F-action staining showed that the intercellular complexes corresponded to the scanning electron microscopy report.[18] LNCs were frequently detected in the intercellular junction area of the marginal cells [Figure 2(K)]. Visualization of LNCs in a single cell isolated from the lateral wall confirmed the internalization of LNCs [Figure 2(N)]. After long incubations with various solutions and many washes during F-actin staining, LNCs disappeared from the spiral ligament while still remaining visible in the stria vascularis. There was also a gradient distribution in the stria vascularis in that more LNCs appeared in the second turn than the basal turn [Figure 2(K,L)]. The amount of LNCs in the cochlea as shown by F-actin staining was much lower than that in the cochlea without the specific staining. These further proved that long time processing swept the extracellular LNC away and the internalization occurred mainly in the stria vascularis rather than the spiral ligament. There was also uptake of LNCs in the stapedial artery, which has been shown to pass by the round window in rats [Figure 2(M)]. The loss of co-localization of Nile Red and FITC indicates the degradation of some LNCs.

One hour postround window membrane delivery, LNCs appeared in the tunnel fibers in the organ of Corti [Fig 3(A)]. LNCs went further distally and were also detectable in the outer hair cells [Figure 3(B,C)]. The internalization of LNCs in the cochlear hair cells was confirmed by isolated single cell imaging [Figure 3(G–I)]. LNCs inside the spiral ligament spread to the type V fibrocytes, which is adjacent to the perilymph of the scala vestibule [Figure 3(D,E)]. LNCs were also found in the spiral prominence and outer sulcus cells [Figure 3(F)].

The possibility of a paracellular pathway for penetration of LNCs through the round window membrane was indicated by the different behavior of LNCs 24 h after transient delivery (LNCs were placed on the round window membrane for 30 min and then removed) and constant administration (LNCs were constantly placed on the round window mem-

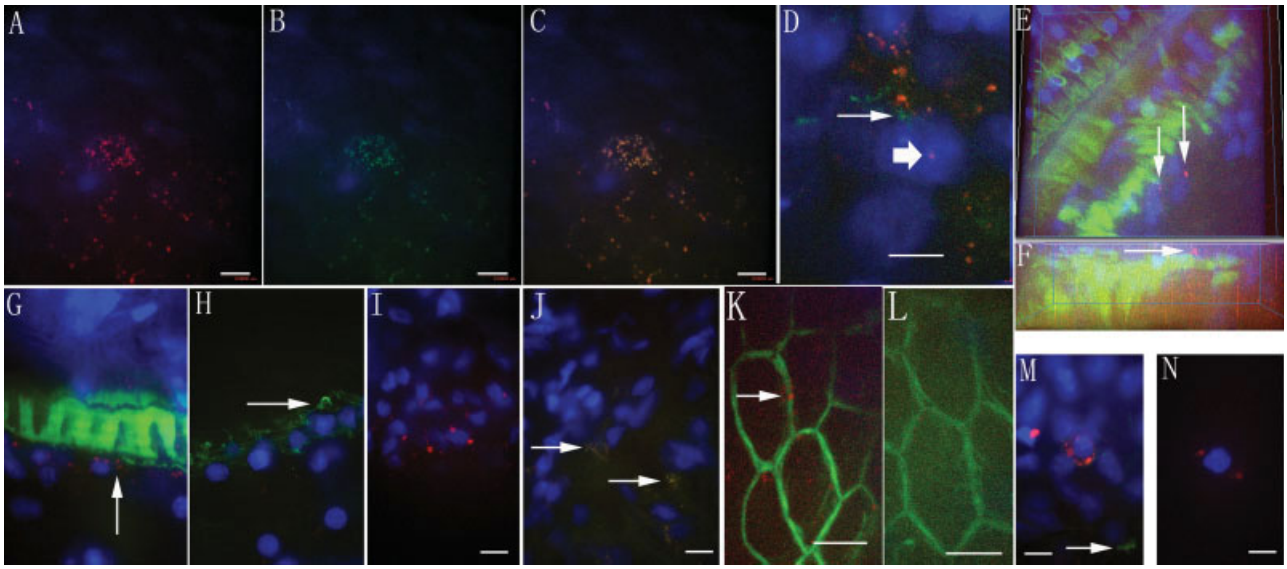


**Figure 2.** Localization of LNCs in different cell populations in the cochlea 30 min post-round window membrane administration. There were abundant nanoparticles in the spiral ganglion cells as shown by whole mount confocal microscopy (A. Nile Red signal; B. FITC signal; C. merged signal). Neurofilament of the spiral ganglion cell was seen with a specific antibody using a whole mounting method (arrow), nuclear localization of LNCs was detected, though infrequently (broad arrow) (D). LNCs reached the inner hair cells as shown by three-dimensional imaging using F-actin staining (arrow) (E, front view; F, lateral view). There was also uptake in the pillar cells as shown by F-actin staining (arrow) (G). However, after neurofilament staining (arrow), LNCs were invisible in the organ of Corti (H). There was also a distribution of LNCs in the lateral wall (I–K). Spiral ligament localization was confirmed by cryosection (arrow) (J); localization in the second turn of stria vascularis, especially intercellular junction site (arrow), was confirmed by F-actin staining (K, whole mount). LNCs were not visible in the basal turn after staining for F-actin (L, whole mount). Coagulated LNCs were detected in the stapes artery (M, whole mount). Only FITC was visible in some places, indicating the degradation of LNCs (arrow). The single cell image proved that the nanoparticles entered the cells (N). Scale bar = 8.5 $\mu$m.

brane until the end of the experiment). The abundant accumulation of LNCs in the round window membrane including the matrix and cytoplasm was detected on the constant delivery side [Figure 4(A)], while only a few LNCs were visible inside the cytoplasm after transient delivery [Figure 4(B)]. Concomitantly, more LNCs reached the hair cells which were continuous with the tunnel fibers [Figure 5(A–D)]. The number of LNCs in the spiral ganglion cells and spiral ligament also increased. Most LNCs accumulated around (but did not enter) the nuclei, although spiral ganglion cells had the quickest uptake during the first 30 min [Figures 2(A–C) and 5(E–H)]. LNCs were also detected in the vestibule, including the semicircular canal and macula utricle.

LNCs remained in the spiral ganglion, including the neuron and nerve fibers, organ of Corti, and lateral wall seven days after round window membrane delivery (Fig 6). Some of the Nile Red and FITC lost co-localization, which indicated degradation of the LNCs.

## DISCUSSION

In the present study, we demonstrate that LNCs pass the round window membrane, penetrate the cochlear membranous partitions, and are incorporated into various cell types within the cochlea. The pathway that the nanoparticles use in passing through the round window membrane could be either via endocytosis or through a nonendocytotic pathway such as those seen in nonviral gene delivery.[19] Our data showed that there was abundant accumulation of LNCs in the round window membrane, including the matrix and cytoplasm on the side of constant delivery [Figure 4(A)], while few LNCs were visible inside the cytoplasm after transient delivery. We suppose that the nonendocytosis pathway, the so-called "paracellular pathway," seems to be the main channel for the LNCs to penetrate the round window membrane. The rapid incorporation of LNCs in the spiral ganglion cells, organ of Corti, and lateral wall upon delivery to the round window membrane can be explained by a paracellular pathway.

The rapid accumulation of LNCs in the spiral ganglion cells indicated that the most likely pathway is directly through the porous modiolar wall of the scala tympani.[20] The uptake of LNCs in the tunnel fibers may originate from either the spiral ganglion or the basilar membrane. The inner and outer hair cells are innervated by afferent nerve fibers that come from spiral ganglion cells and efferent nerve fibers that come from the superior olivary complex. Approximately 90% of the afferent nerve fibers end in synaptic boutons on the inner hair cell bodies (the inner

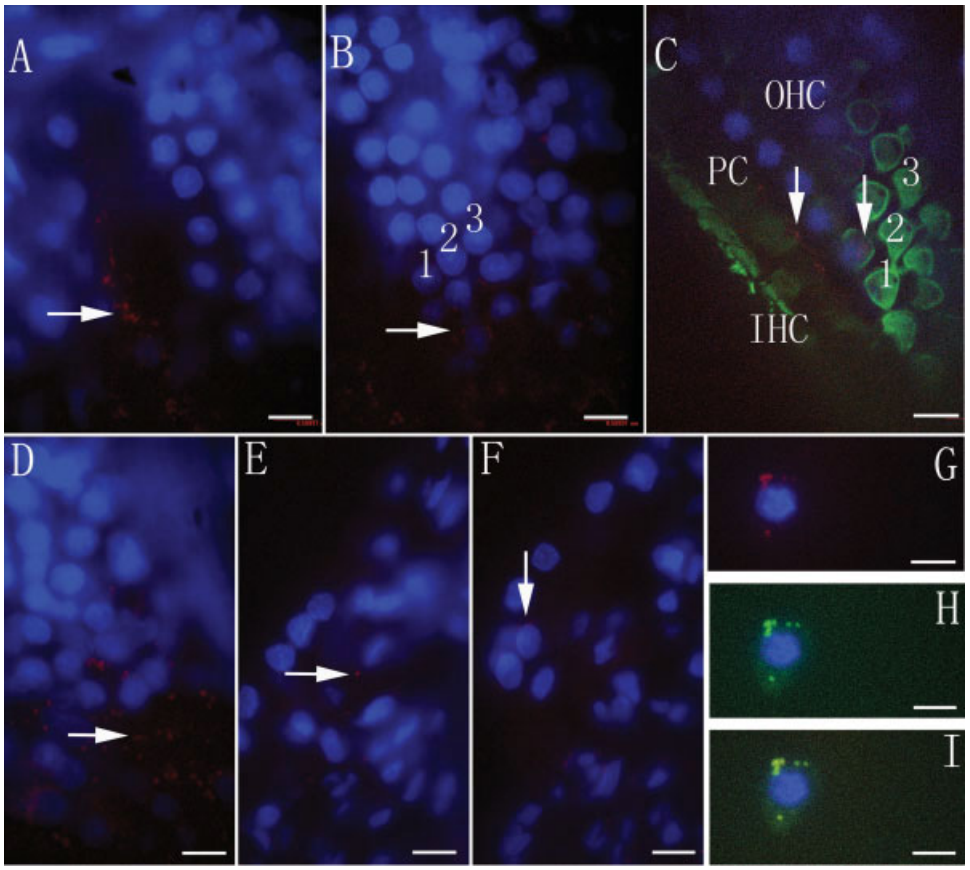


**Figure 3.** Nanoparticles diffused further 1 h after administration. LNCs were visible in the tunnel fibers (arrow) (A), pillar cells (PC) and the outer hair cells (OHC) in the organ of Corti (arrow) (B, C), and lateral wall (D–F). The cell population was confirmed by F-actin staining (C). LNCs were primarily located in the matrix of the lateral wall (arrow) (D). The spiral ligament fibrocytes type V, which are adjacent to the scala vestibuli, showed uptake of nanoparticles (arrow) as demonstrated by cryosection (E). LNCs also diffused to the spiral prominence (arrow) as showed by cryosection (F). The uptake of nanoparticles in the inner hair cells was further demonstrated by isolated single cell imaging (G, Nile Red signal; H, FITC signal; I, merged signal). IHC, inner hair cells; the numbers 1, 2, and 3 refer to the outer hair cells row 1, row 2, and row 3. Scale bar = 8.5 $\mu$m. [Color figure can be viewed in the online issue, which is available at www.interscience.wiley.com.]

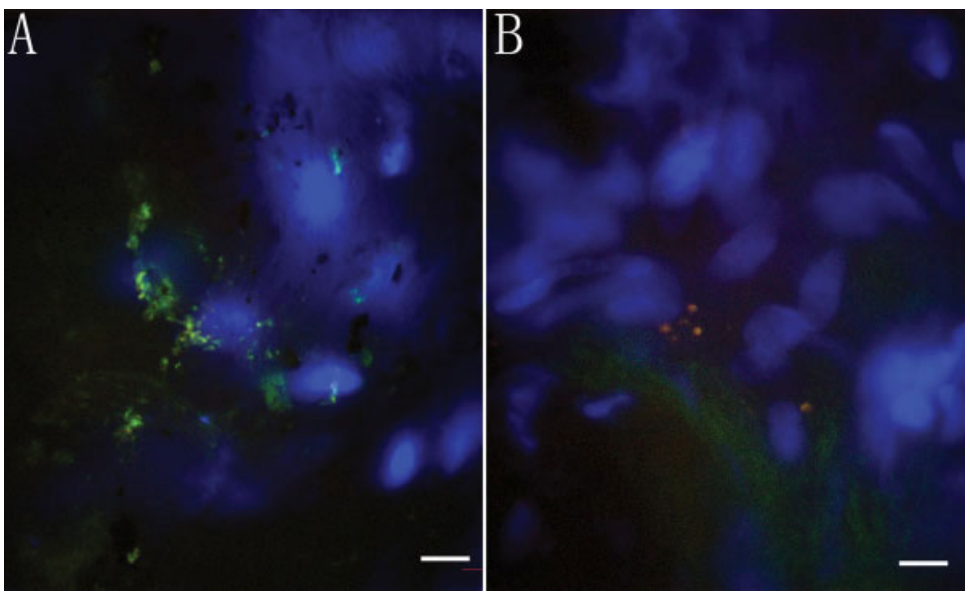


**Figure 4.** Round window membrane permeation of LNCs. Abundant LNCs were present throughout the round window membrane during constant 24 h administration (A). Only a few particles were detectable 24 h after transient delivery (LNCs were placed on the round window membrane for 30 min) (B). Scale bar = 6.8 $\mu$m. [Color figure can be viewed in the online issue, which is available at www.interscience.wiley.com.]

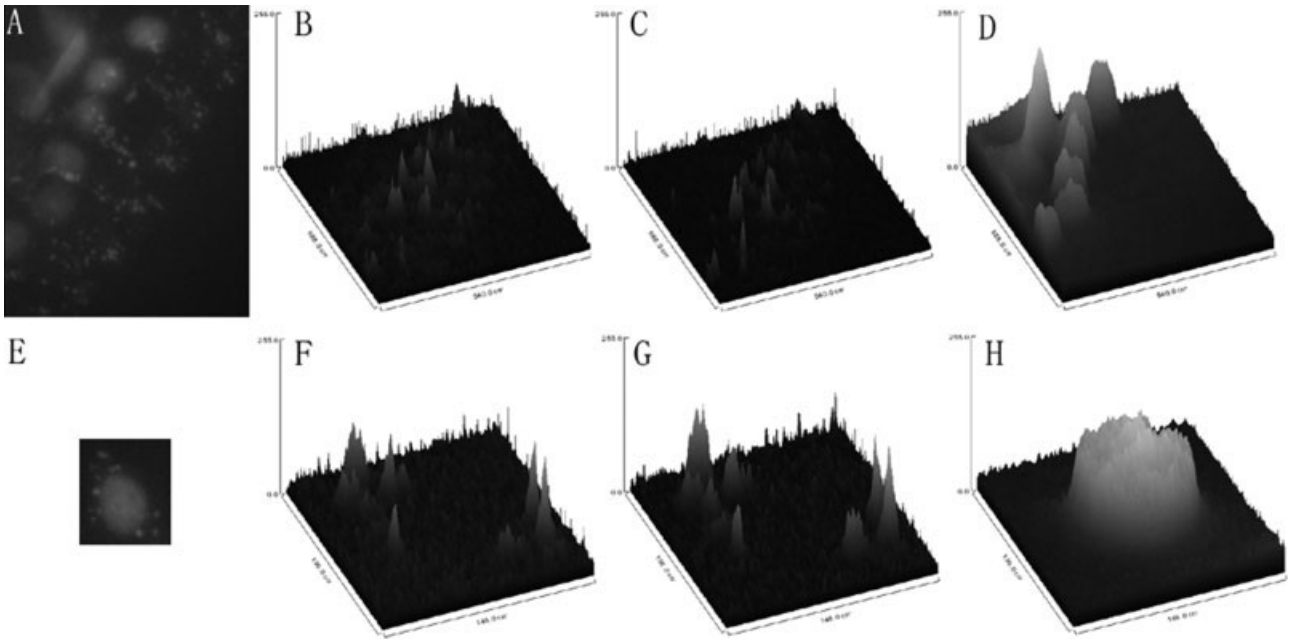


**Figure 5.** Distribution of LNCs in the organ of Corti and spiral ganglion cells was demonstrated by 3D scanning. Continuing through the tunnel fibers, nanoparticles reached the inner hair cells (A). Surface plot from a single slice showed the close spatial relationship between LNCs (B. FITC signal; C. Nile Red signal) and the nuclei of inner hair cells (D. DAPI of the nuclei). The perinuclear localization of LNCs in the spiral ganglion cell (E) was proven by surface plot of a single slice (F, FITC signal; G, Nile Red signal; H, DAPI signal of the nucleus). The samples were taken 24 h post-round window membrane administration of LNCs.

radial bundles). Only 10% of the afferent nerve fibers innervate the outer hair cells (the tunnel radial bundles, tunnel crossing bundles).[21] Efferent innervation of auditory hair cells is provided by the fibers of the lateral olivocochlear bundle to inner hair cells and the medial olivocochlear bundle (also referred to as efferent tunnel fibers) to outer hair cells. Efferent nerve fibers of the lateral system contact the synapses of the radial afferents on the inner hair cells and the medial system the outer hair cells directly (reviewed by Raphael and Altschuler).[22] Because it is hard to verify the different bundles with whole mount material imaging and their role for LNC transport is potentially the same, we can simply call the nerve fibers passing through the inner tunnel of the organ of Corti "tunnel fibers." Tunnel fibers, together with nerve fibers innervating the inner hair cells, pass through Rosenthal's canal. LNCs on the surface of nerve fibers can also freely diffuse between different fibers including afferent and efferent nerve fibers and migrate along the longitude of the nerve fibers. The disappearance of LNCs from the tunnel fibers after long time incubation with solu-

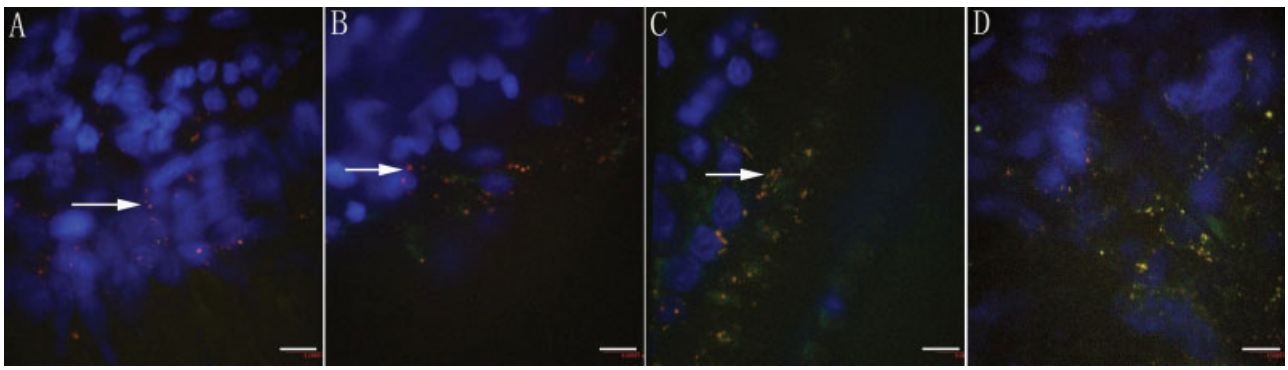


**Figure 6.** LNCs remained in the cochlea 7 days post-transient round window membrane administration. The LNCs were placed on the round window membrane for 30 min and then removed. LNCs presented along the neurofilaments from Rosenthal's canal (arrow) (A) to the tunnel fibers and were in contact with hair cells (arrow) (B, C). There was also rich accumulation of LNCs in the lateral wall (D). Scale bar = 8.5 $\mu$m. [Color figure can be viewed in the online issue, which is available at www.interscience.wiley.com.]

tions indicates their surface location. The delayed distribution of LNCs in the hair cells may come from the spiral ganglion, the tunnel fibers, and the Corti's liquid. The gradient uptake of LNCs from the inner hair cells to the outer hair cells (i.e., quicker and greater uptake in the inner hair cells than that in the outer hair cells) suggests that LNCs chiefly comes from the spiral ganglion area via Rosenthal's canal because of more intense innervation and a shorter distance to the inner hair cells. We call this the "nerve pathway." The recirculation of potassium from hair cells back to endolymph mainly takes a pathway from the supporting cells to the stria vascularis via different channels.[23] LNCs may also travel through the retrograde pathway from the stria vascularis to Corti's liquid because there is a rapid, intense uptake of LNCs in the stria vascularis. This possible pathway seems to be much slower than the "nerve pathway" because we did not find LNCs inside Hensen's cells, Deiter's cells, and outer hair cells, while they appeared in the inner hair cells at the 30-min time point. Our results suggest that LNC is a promising vector to deliver drugs to the spiral ganglion cells and hair cells.

The vestibular distribution of LNCs may originate from the spiral ligament, which was shown in MRI using Gd-DTPA-BMA as a tracer.[6] The uptake of LNCs in the spiral ligament fibrocyte type V, which is in contact with the perilymph in the scala vestibule, provides evidence for this pathway.[24,25] There is a possibility that drugs can also reach the vestibule by applying LNCs to the round window membrane.

A slower communication between different winding was reported in the guinea pig cochlea using Gd-DTPA-BMA enhanced MRI.[6] The present data acquired from rat cochlea using LNCs and confocal microscopy suggests a much faster longitudinal communication. This can be explained by different behaviors of the LNCs and a more sensitive detection by confocal microscopy.

The distribution of LNCs in the middle ear mucosa and stapes artery wall compromises the relative cell population selectivity of our LNCs. This can be further overcome by limiting the LNCs in the area of the round window. It is easier to achieve in humans because the round window area is much larger than that in rats.

## CONCLUSIONS

This study describes the migration of LNCs through the round window membrane and cochlear partitions, finally reaching the inner ear cell populations. LNCs were manufactured by a novel phase inversion-based process. After round window membrane administration, LNCs reached the spiral ganglion, including the neuron and nerve fibers, organ of Corti, and lateral wall, within 30 min. The main pathway for LNCs to reach hair cells was the "nerve pathway," that is, diffusion from perilymph in the scala tympani to the spiral ganglion, continuing with nerve fibers inside Rosenthal's canal to approach the inner hair cells and pillar cells, and finally the outer hair cells. The "paracellular pathway" is the main approach for LNC penetration of the round window membrane. LNCs can also reach the vestibule, middle ear mucosa, and the adjacent artery. This suggested that LNC is a potential vector for delivery of drugs and proteins to the spiral ganglion, hair cells, and the lateral wall.

We are grateful to Mr. Peter Martinsson for his technical support in confocal microscopy.

## REFERENCES

1. El-Hakim H, Abdolell M, Mount RJ, Papsin BC, Harrison RV. Influence of age at implantation and of residual hearing on speech outcome measures after cochlear implantation: binary partitioning analysis. Ann Otol Rhinol Laryngol Suppl 2002;189:102–108.
2. Gantz BJ, Woodworth GG, Knutson JF, Abbas PJ, Tyler RS. Multivariate predictors of audiological success with multichannel cochlear implants. Ann Otol Rhinol Laryngol 1993; 102:909–916.
3. Osberger MJ, Zimmerman-Phillips S, Koch DB. Cochlear implant candidacy and performance trends in children. Ann Otol Rhinol Laryngol Suppl 2002;189:62–65.
4. Geers A, Brenner C, Nicholas J, Uchanski R, Tye-Murray N, Tobey E. Rehabilitation factors contributing to implant benefit in children. Ann Otol Rhinol Laryngol Suppl 2002;189:127–130.
5. Rejali D, Lee VA, Abrashkin KA, Humayun N, Swiderski DL, Raphael Y. Cochlear implants and ex vivo BDNF gene therapy protect spiral ganglion neurons. Hear Res 2007;228(1-2):180–187.
6. Zou J, Pyykko I, Bjelke B, Dastidar P, Toppila E. Communication between the perilymphatic scalae and spiral ligament visualized by *in vivo* MRI. Audiol Neurootol 2005;10:145–152.
7. Salt AN. Pharmacokinetics of drug entry into cochlear fluids. Volta Rev 2005;105:277–298.
8. Jero J, Mhatre AN, Tseng CJ, Stern RE, Coling DE, Goldstein JA, Hong K, Zheng WW, Hoque AT, Lalwani AK. Cochlear gene delivery through an intact round window membrane in mouse. Hum Gene Ther 2001;12:539–548.
9. Maeda Y, Fukushima K, Kawasaki A, Nishizaki K, Smith RJ. Cochlear expression of a dominant-negative GJB2(R75W) construct delivered through the round window membrane in mice. Neurosci Res 2007;58:250–254.
10. Hoffer ME, Balough B, Henderson J, DeCicco M, Wester D, O'Leary MJ, Kopke R. Use of sustained release vehicles in the treatment of Meniere's disease. Otolaryngol Clin North Am 1997;30:1159–1166.
11. Kopke RD, Hoffer ME, Wester D, O'Leary MJ, Jackson RL. Targeted topical steroid therapy in sudden sensorineural hearing loss. Otol Neurotol 2001;22:475–479.
12. Van Wijck F, Staecker H, Lefebvre PP. Topical steroid therapy using the Silverstein Microwicktrade mark in sudden sensorineural hearing loss after failure of conventional treatment. Acta Otolaryngol 2007;127:1–6.
13. Praetorius M, Brunner C, Lehnert B, Klingmann C, Schmidt H, Staecker H, Schick B. Transsynaptic delivery of nanoparticles to the central auditory nervous system. Acta Otolaryngol 2007;127:486–490.
14. Lamprecht A, Bouligand Y, Benoit JP. New lipid nanocapsules exhibit sustained release properties for amiodarone. J Control Release 2002;84(1-2):59–68.

15. Heurtault B, Saulnier P, Pech B, Proust JE, Richard J, Benoit JP. Nanocapsules lipidiques, procédé de préparation et utilisation comme médicament, Patent No. 0002688000, 2000.
16. Heurtault B, Saulnier P, Pech B, Proust JE, Richard J, Benoit J-P. A novel phase inversion-based process for the preparation of lipid nanocarriers. P Pharmaceutical Res 2002;19:875–880.
17. Khalid MN, Simard P, Hoarau D, Dragomir A, Leroux JC. Long circulating poly(ethylene glycol)-decorated lipid nanocapsules deliver docetaxel to solid tumors. Pharm Res 2006;23:752–758.
18. Araki S, Mizuta K, Takeshita T, Morita H, Mineta H, Hoshino T. Degeneration of the stria vascularis during development in melanocyte-deficient mutant rats (Ws/Ws rats). Eur Arch Otorhinolaryngol 2002;259:309–315.
19. Khalil IA, Kogure K, Akita H, Harashima H. Uptake pathways and subsequent intracellular trafficking in nonviral gene delivery. Pharmacol Rev 2006;58:32–45.
20. Rask-Andersen H, Schrott-Fischer A, Pfaller K, Glueckert R. Perilymph/modiolar communication routes in the human cochlea. Ear Hear 2006;27:457–465.
21. Santi PAMP. Cochlear anatomy and central auditory pathways. In: Cummings CW, Fredrickson JM, Harker LA, Krause CJ, Richardson MA, Schuller DE, editors. Otolaryngol Head Neck Surg 1998;4:2803–2830.
22. Raphael Y, Altschuler RA. Structure and innervation of the cochlea. Brain Res Bull 2003;60(5/6):397–422.
23. Hibino H, Kurachi Y. Molecular and physiological bases of the K+ circulation in the mammalian inner ear. Physiol (Bethesda) 2006;21:336–345.
24. Spicer SS, Schulte BA. Differentiation of inner ear fibrocytes according to their ion transport related activity. Hear Res 1991;56(1/2):53–64.
25. Spicer SS, Schulte BA. The fine structure of spiral ligament cells relates to ion return to the stria and varies with place-frequency. Hear Res 1996;100(1/2):80–100.